Master of Science Thesis

Buckling Analysis and Imperfection Sensitivity Study of Scaled Launch-Vehicle Cylindrical Shells

Kevin van Dooren

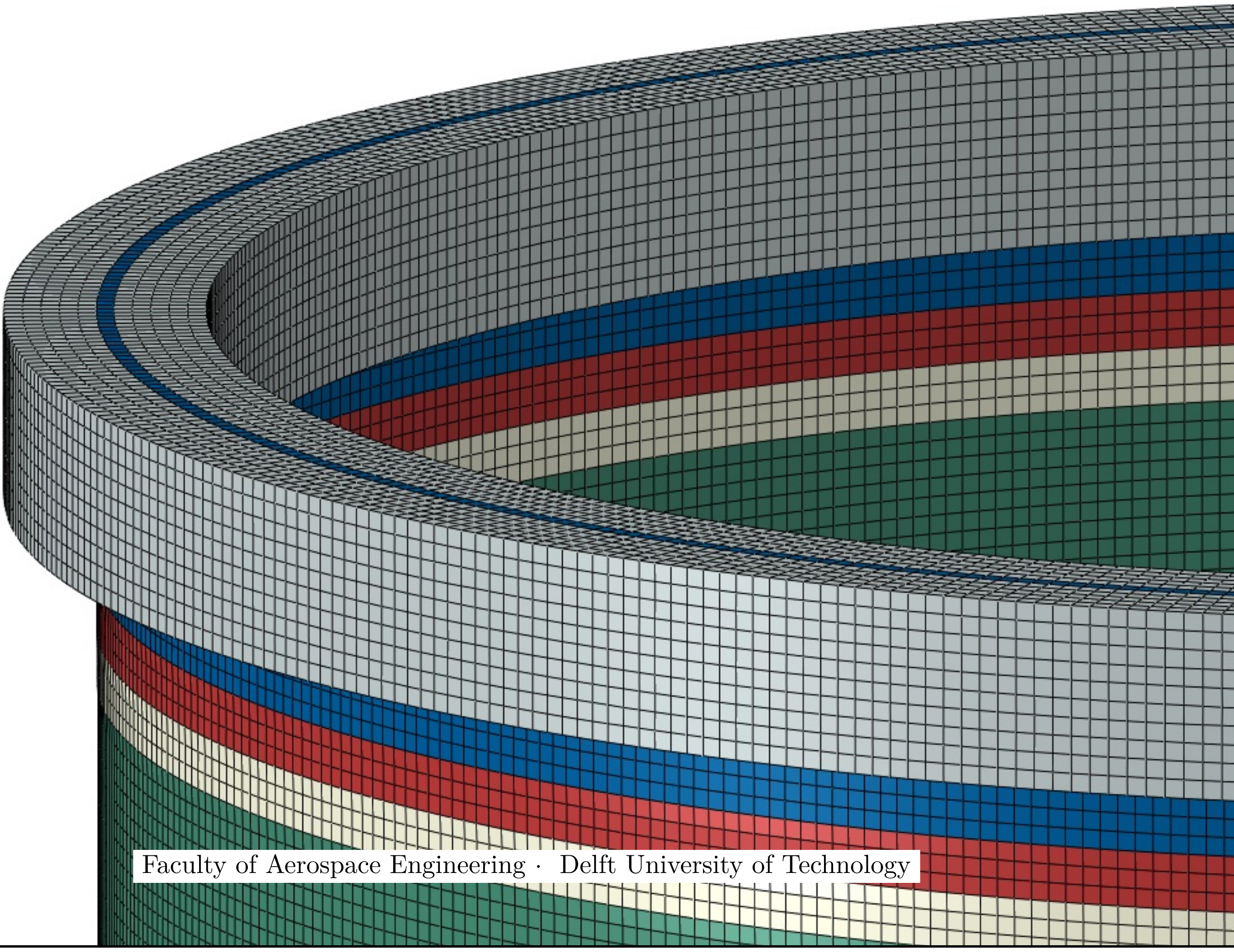

Faculty of Aerospace Engineering · Delft University of Technology

Buckling Analysis and Imperfection Sensitivity Study of Scaled Launch-Vehicle Cylindrical Shells

Master of Science Thesis

For obtaining the degree of Master of Science in Aerospace Engineering at Delft University of Technology

Kevin van Dooren

24-10-18

Faculty of Aerospace Engineering · Delft University of Technology

Delft University of Technology
Faculty of Aerospace Engineering
Department of Aerospace Structures and Materials

GRADUATION COMMITTEE

Dated: 24-10-18

Chair holder:

Prof. Dr. Chiara Bisagni

Committee members:

Prof. Dr. Christos Kassapoglou

Ir. Barry Zandbergen

Dr. Marc R. Schultz

Abstract

A buckling analysis and imperfection sensitivity study of scaled launch-vehicle cylindrical shells have been executed. The emphasis is on scaled cylindrical shells due to the expensive nature of full scale launch-vehicle cylindrical shells and the size constraints of experimental testing equipment. The work as presented in this thesis is part of a framework of a collaboration with NASA Langley. The main objective was to investigate if a scaling method, which is developed as part of this afore mentioned collaboration, results in representative scaled cylindrical composite shells. These scaled cylindrical composite shells will be validated by experimental tests at NASA Langley. The scaling of structures can be a challenging process, as a scaled model which shows full scale representative behaviour is difficult to design due to constraints such as manufacturability. The buckling of cylindrical shells is considered to be a structural problem which is yet to be fully understood. The cylindrical shells show a high imperfection sensitivity, but the exact influence of imperfections caused by different manufacturing processes is a source of uncertainty.

The thesis will focus on two scaled cylindrical shells which resulted from the scaling method, next to the full scale CTA 8.1 cylindrical shell they are based on. The CTA 8.1 is a sandwich cylindrical shell with a honeycomb core which is designed to be representative for a launch-vehicle structure. The first scaled cylindrical shell consists of a solid laminate and the second scaled cylindrical shell consists of a sandwich with foam core. A scaled solid laminate cylindrical shell is of interest, as the core thickness of a scaled sandwich cylindrical shell can become too thin to manufacture.

The scaled solid laminate cylindrical shell was analysed in detail. Multiple elements were compared, of which the SC8R showed the most accurate results and was computational efficient. An imperfection sensitivity study showed that the cylindrical shell was most sensitive to an axisymmetric modeshape imperfection, while it saw a low sensitivity to a measured mandrel imperfection. The loading imperfection that was tested had no effect on the stiffness, while it did lower the buckling load. The scaled solid laminate cylindrical shell did not show failure before buckling, and is deemed to be a valid option for experimental testing purposes.

The scaled sandwich cylindrical shell was analysed with mandrel imperfections only. It did show high strain in pre-buckling, but it did not result in material failure. Multiple element configurations were investigated, where the S4R and SC8R elements showed accurate results for a single element through the thickness.

A comparison was executed between the scaled cylindrical shells and the CTA 8.1 cylindrical shell. The first comparison used nondimensional load and displacement to evaluate

the behaviour. The scaled solid laminate cylindrical shell shows the highest nondimensional stiffness and buckling load. The CTA 8.1 cylindrical shell shows the second highest buckling load, closely followed by the scaled sandwich cylindrical shell. The stiffness of the CTA 8.1 cylindrical shell and the scaled sandwich cylindrical shell are closely matched. The second comparison makes use of strain contour plots, where similar strain patterns are seen. Although differences were observed, the level of similarity that was seen between these scaled structures and their full scale counterpart was not found in literature.

Table of Contents

List of Figures

List of Tables

Preface

The route I have taken to become an Aerospace Engineer might not be the most obvious, I do however not regret any of it. My Mechanical Engineering Bachelor from a University of Applied Sciences have lead to my practical manor of reasoning, which might have made me a sceptic person as well. I tend to not believe technical innovations until I actually see them, though not to the level that I would doubt the moonlanding. During my Bachelor, many opportunities were provided to work with companies, from which I got acquainted with different mindsets and how much the level of precision can vary. Although this might sound obvious, it does open your eyes when u work on an assignment for a company in the semiconductor industry, after finishing an assignment for a foundry the week before.

During my Master of Aerospace Structures & Materials, my interest into stability problems grew due to the stability course as given by my supervisor Prof. Bisagni. This was later combined with courses on the analysis and design of composite structures and non-linear modelling, this set the course for the remaining part of my Master. When I got word the current thesis topic was available, I hurried to the faculty to accept it and sat in an office to get acquainted with the buckling of cylindrical shells the same day. After writing this thesis, I hope I can and have succeeded to transfer the same enthusiasm about the current topic onto the reader, the same enthusiasm I felt that day and still do after researching it. There's however only one way to find out......

Acknowledgements

During both my life and studentship, I've been lucky enough to be supported by a great group of people, who I would like to thank:

- My supervisor Prof. Chiara Bisagni for giving me this opportunity, providing me with her knowledge and advice which have guided me through all the stages of my thesis. She inspired me to work as hard as I possibility could, both by expecting my best and providing me with guidance to reach my goals.
- Inés Uriol Balbin, for the sanity checks, discussions and feedback on my work which have thought me a tremendous amount. She made me feel welcome amongst the PhD candidates, which further inspired me to continue in Delft as a PhD candidate.
- Dr. Marc R. Schultz and Michelle T. Rudd for giving me the opportunity, next to providing me with feedback and tools to improve and expand my work.
- Laura for all the support, talks, smiles and her enjoyment of sweeties. I can't imagine the department without her.
- My father Jan and mother Harriet. The opportunities and support, both financially and emotionally, they've given me which I can not describe by any words. I would not have reached this point without them, and continue to strive to be better because of them and for them.
- My brother Randy. Without him showing the way to Delft, I would probably have not made one of the best decisions of my life. As a brother, former housemate and fellow student, I could and can always count on his support, both in life and when one of the many theories and methods was not making sense.
- My friends from my Master which I had the pleasure to work and learn with: Eva, Tom, Lander, Steven, Linda, Bram, Katleen and especially Guyonne, with whom I also had the pleasure to work and learn with during the Bridging program. During courses, assignments, breaks and drinks, they made me see the bigger picture and help me enjoy my Master period to the fullest.
- Last but foremost, my friend and future joint-owner of Kootte en van Dooren, Luc. I could always count on advise and much needed discussions to see reason, which have broadened my horizon and knowledge for research, engineering and especially FE methods. The discussions kept sparking and increasing my interest into research, these discussions will hopefully continue and help our PhD candidacies become the best period of our lives.

Chapter 1

Introduction

Cylindrical composite shells have their main use in launch vehicles, such as the Saturn, Atlas and Ariane, where buckling under the axial compression loadcase is a major consideration because of the thin walled construction. Recent years has seen several research groups do extensive research on the buckling of composite cylindrical shells, as its generally considered to be one of the structural problems yet to be fully understood. The largest source of uncertainty is the influence of imperfections caused by the manufacturing process of the shells, which is a popular topic for composite materials in general as well. Cylindrical shells have shown to be highly sensitive to these imperfections, as it can lower the buckling load by a considerable amount, which was researched quite extensively [1]. Creating a higher understanding of the influence of the imperfections will enable designers to use the full potential of composite materials. The cylindrical shells can then be designed for a limit load closer to the buckling load, offering considerable weight reductions. Buckling is seen as one of the primary limiting design phenomena, as the ability to carry load by the structure is highly reduced after buckling. Besides the load carrying abilities, the large deflections afterwards can cause further failure modes and ultimately collapse will occur.

A common design guideline being used for the design of cylindrical shells, is the NASA SP-8007 [2] technical report, which originates from the 1960s and is based on experimental tests from as far back as the 1920s. This design guideline was not meant to be used for composite materials, which is one of the reasons why new alternatives are needed. The basic idea of this design guideline is that the imperfections cause a load reduction, and that for a cylindrical shell design a knockdown factor (KDF) can be calculated. This KDF consists of the buckling load of the perfect cylindrical shell divided by the buckling load of the imperfect cylindrical shell. This design guideline is considered to be highly conservative [3], and thus new guidelines are needed.

The second topic of the literature review is the scaling of structures. The need for scaled structures comes from experimental size constraints which are in most cases determined by the size of testing equipment. Besides size constrains, testing on scaled models will also have financial benefits compared to the testing of full scaled structures as less material is needed and the manufacturing of smaller parts is less expensive in general. These scaled models are used to predict the structural behaviour of the full-scale structure or system, mostly called the prototype or full scale structure, as accurately as possible. The scaling process itself can be challenging, to create a scaled model which is a good representation of the full scaled model with certain constraints such as manufacturability taken into account. Furthermore, the general validity of results obtained from scaled model compared to full scale testing is yet to be fully understood.

A scaling method has been developed by Uriol Balbin et al. [4] which was published in 2018. This scaling method has resulted in two scaled cylindrical shells, which are based on a cylindrical shell designed by NASA named the CTA 8.1. The objective is to research if these scaled cylindrical shells can be used for experimental testing while showing representative behaviour in comparison to the full scale cylindrical shell. The work as presented in this thesis is in a framework of a collaboration with NASA Langley. The thesis will focus on the FE modelling of cylindrical shells, in combination with methods to compare the results of these FE models. Firstly a preliminary analysis of a cylindrical shell will be executed to become acquainted with the software package used, next to providing preliminary research for the effect of type of elements and mesh properties. The cylindrical shell for the preliminary analysis will be modelled for both an isotropic and composite material.

This is followed by the analysis of the first scaled cylindrical shell. This cylindrical shell is constructed of a solid laminate, whereas the CTA 8.1 is constructed of a sandwich composite. The analysis of the scaled solid laminate cylindrical shell will include a comparison of element types, for both linear and non-linear analyses. The scaled solid laminate cylindrical shell will furthermore be used for the analysis of different types of imperfections, in combination with an investigation into the imperfection sensitivity to these imperfection types. The imperfections that will be modelled are: modeshape imperfection, loading imperfection and measured imperfections. The analysis of the scaled solid laminate cylindrical shell is followed by the analysis of the scaled sandwich cylindrical shell. This analysis will start with a element configuration comparison, as modelling a sandwich composite with different elements through the thickness can be of interest. This is followed by the analysis of the scaled sandwich cylindrical shell in combination with mandrel imperfections.

The last chapter will focus on the analysis of the CTA 8.1 cylindrical shell, with measured imperfection, after which a comparison with the scaled cylindrical shells will follow. Different aspects of the structural behaviour of these cylindrical shells will be compared, next to an investigation into the relation between imperfection amplitude and knockdown factor between the analysed cylindrical shells.

Chapter 2

Literature Review

2.1 Buckling of Cylindrical Shells

The first paragraph of this chapter will consist of the introduction of a past research group in Europe named New Robust DESIgn Guideline for Imperfection Sensitive COmposite Launcher Structures (DESICOS) and a current research group in the US at NASA named Shell Buckling Knockdown Factor (SBKF) Project. The second paragraph will go in depth about statistical methods for the inclusion of imperfections and according buckling behaviour. The third paragraph shows the possibilities with perturbation methods, such as perturbation loads and perturbation displacements applied to the cylindrical shell in the lateral direction. The fourth paragraph goes in depth about methods using results of experimental tests for the validation of FE or analytical models. The last paragraph is on the determination of structural behaviour of shells by nondimensional parameters, which is one of the methods used for the SBKF project.

2.1.1 Recent Research Projects

In 2007 a new project was started at NASA named the SBKF project, with the goal of developing a new design guideline for shell buckling. A detailed goal, history summary and the development approach of the project was described by Hilburger [3] in 2012 which gives good insight for why this project was needed. The design guideline currently being used dates back to the 1960s by Peterson et al. [2] which is mostly referred to as NASA SP-8007 and is not developed with the current composite materials in mind. The guideline was established by using a lowerbound method in combination with experimental test data, this lowerbound was then determined to be the KDF to be used in combination with bifurcation buckling analyses, see Figure 2.1. As the bifurcation analyses itself does not take any imperfections into account and thus resulted in unconservative buckling values. Furthermore, the guideline has not been updated since the original publishing and the guideline is considered to be overly conservative, resulting in heavy designs. There are several causes for it to be overly conservative: the extra precision that current manufacturing methods have achieved since and the extra material tailoring possibilities of composite materials are not taken into consideration among other reasons. More recent research groups have also indicated that the KDFs used in the aerospace industry are conservative, with test results supporting these claims. Although new analysis based KDFs are a goal for the SBKF project, it's also meant to develop a new design method for cylindrical composite shells which brings several new challenges. This requires more understanding on the buckling behaviour and imperfection sensitivity of the cylindrical shells, as this is also considered one of the reason for the previous method to consist of a lowerbound method combined with test data. The phenomena that were seen during testing were not always understood and even the quality of a few of the test reports is questionable although still providing proper information. The design space of the method will first be focused on launch-vehicles and later be expanded to a larger design space to accommodate a larger portion of applications. The approach of the project is divided into four parts. Starting with a study into the sensitivities of the performance to properties of the structure such as material and type of joints. The second part consists of numerical and experimental testing with a focus on different failure modes besides global buckling, to ensure a new less conservative method does not cause other critical failure modes. Next is the development of new analytical methods to determine the KDFs in combination with recommendations for structural approaches. And as last is developing a implementation approach, which can be quite challenging as the design process has been practically the same since the 1960s. Although the paper then goes into more detail about the intended methods of the analytical KDFs, these details will be spared as these research topics have been published in separate papers in the mean time and these will be highlighted further on in the literature study.

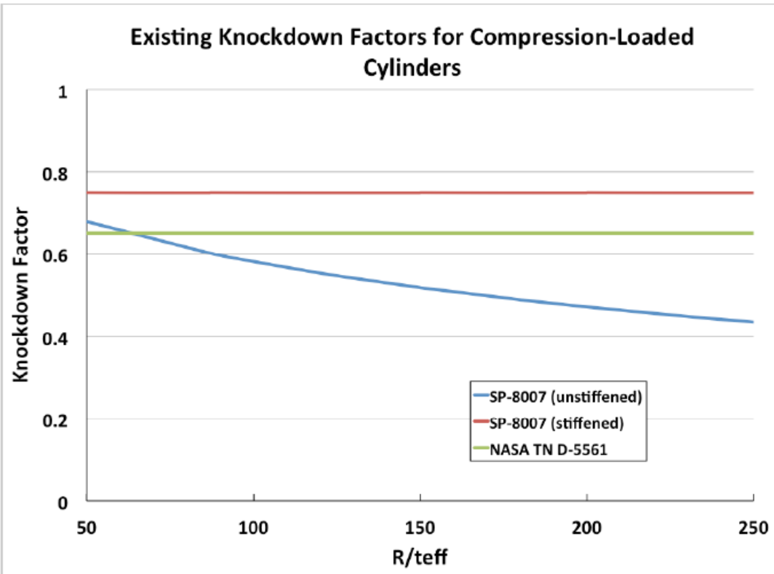

Figure 2.1: Buckling KDF as specified by NASA SP-8007 [3].

A more recent published paper concerning the SBKF project goes more in depth in general and on the application of sandwich composites, which is the type of construction that will be used in the thesis for which this literature study is intended, by Schultz et al. [5]. Sandwich composites have a high structural efficiency combined with acceptable manufacturing cost, therefore the priority is gaining knowledge of the behaviour of this kind of structure for both strength and stability. As the primary load case for launch-vehicles is axial compression, buckling is the phenomena of interest. Furthermore, the imperfection sensitivity of shell structures is considered to be relatively high and is therefore a popular topic of research. The imperfection sensitivity of a sandwich composite structure, also considered a shell if it's thin enough, has not been researched extensively but it has gained attention in recent years as seen in the SBKF project and others. Although manufacturing processes become more accurate, there is no such thing as a perfect part (or cylindrical shell in this case), accounting for imperfections will remain important. The interest lies in the method of accounting for these imperfections, especially as it can greatly reduce costs if an extensive amount of experimental testing is not required. As was mentioned before, the SBKF project is also focusing on analysis based KDFs. The main reasoning, besides cost reduction compared to empirical methods, is that a lot of the theories, and or tools, involved to develop these analytical methods have gained considerable improvements. Examples of these theories are the available nonlinear structural analysis tools, Abaqus for example, and the general understanding of buckling behaviour of cylindrical shells combined with imperfection sensitivity. The paper also includes a study to define a relationship between the KDF and the areal mass. For this study launch-vehicle components were used from recent NASA projects. The study starts with a buckling design sensitivity analyses of these components, for which several structural optimization software packages are used. This is followed by a buckling imperfection sensitivity analyses for which imperfection characteristics of certain manufacturing processes can be used, as it is considered that a manufacturing process will create similar imperfections for different parts. A wide variety of results are shown for design parameters as part of the optimization process. It is therefore concluded that the areal mass can be reduced by 4 to 19 % dependent on the type of structure by updating the design guidelines as they are used today. The last set of results consist of the normalized buckling load compared for 3 different designs and imperfection amount, see Figure 2.2. In general it can thus be concluded that the SBKF project shows good prospects, with considerable weight decrease possibilities combined with less experimental testing needed.

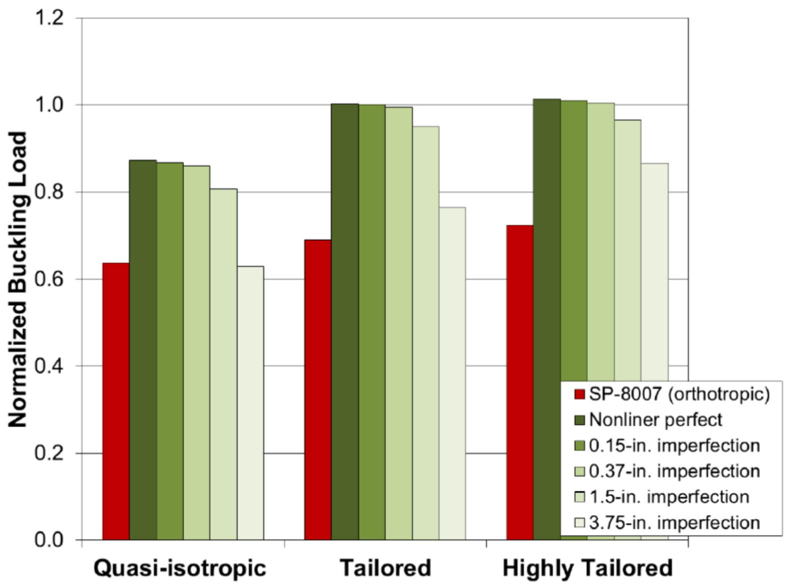

Figure 2.2: Normalized buckling load vs design options and imperfection amplitudes [5].

A similar project was ongoing in Europe, from 2012 until 2015, named DESICOS. This project was based around approximating imperfections by using a single perturbation load approach, which is seen as a worst case scenario and could guarantee robust designs, combined with a stochastic approach. A overview of this project and its goals were published by Degenhardt [6]. The project went in-depth on the imperfection sensitivity of cylindrical composite shells, where the sensitivity is influenced by a large variation of design parameters for a composite laminate and is therefore seen as an important aspect of the research. The loading imperfection was examined as well, as previous research showed that imperfect loading will influence the buckling behaviour greatly. During the project real imperfections were measured and included in the testing of several test shells. Of one specific test cylindrical shell with a high imperfection sensitivity, 10 samples were manufactured and experimentally tested for which the results can be seen in [7] by Degenhardt et al. From these results an improvement of 45% was reached for the design buckling load with respect to NASA SP-8007.

2.1.2 Statistical Methods

Statistical methods have a wide variety of applications within the field of engineering. There are several steps within the design process were statistical methods have its place. It goes from using statistics on experimental results to determine design guidelines, to using probabilistic methods to determine a KDF accounting for imperfections and using Monte Carlo simulations to determine imperfection variations.

A study by the European Space Agency (ESA) which was executed at DLR, lead to the publication by Degenhardt et al. [7] with the focus on determining imperfection sensitivity and possible KDFs. For the research, 10 composite cylindrical shells were manufactured according to the same design. Measurements were executed for both thickness imperfections and geometric imperfections, which could be used for the FE analyses later on. For the FEA, Abaqus was used and a investigation was executed for both mesh convergence and solver comparison after which a Newton Raphson method with artificial damping is chosen. It's not stated which element was used or why the Newton Raphson method was preferred above the other possibilities available in Abaqus. When comparing the results from the experimental tests and the numerical results, it is be seen that the numerical results show a 39 % higher buckling load which is considerable. This is most likely caused by loading imperfections not being taken into account as stated by the authors. A probabilistic analysis is then executed, by the use of a Monte Carlo simulation. The results of the Monte Carlo simulation, a distribution of inclination angles for the loading platform, were applied to the FE model. This once again confirmed the sensitivity to loading imperfections, as the buckling load drops considerably for small inclination angles. The main reason to include this paper, is that the test data from the cylindrical shells is used in another project a few years later which will be shown here after. This new project is a good indication of the progress that has been made since the tests were actually conducted.

As a part of the DESICOS project, a stochastic analysis was published by Kepple et al. [8] which makes use of real imperfection data. This data was gathered by a previous DLR-ESA program, for which 8 cylindrical composite shells were manufactured and scanned for imperfections. Furthermore, experimental test data was acquired as well by axial compression tests on these same cylindrical shells. A stochastic method was used to incorporate the material imperfections and thickness variations. These imperfections were approximated by applying a variable distribution of matrix and plies to the FE model. The stochastic method consists of several techniques: A Hough Transform for variations in the resin distribution and imperfections in ply placement, a 2D Short Time Fourier Transform was applied to create an estimation of the 2D matrix imperfections spectrum, a Monte Carlo analysis was executed for the ply placement imperfections and lastly a moving average technique was used to apply the thickness variations to the FE elements. The paper then continues with load imperfections and how to implement them, as previous research showed that the loading imperfections can have a considerable impact on the buckling load. There were no boundary imperfections measurements taken from the aforementioned cylindrical shells, so assumptions are made based on previous research and according to a numerical analysis of the cylindrical shells. In this numerical analysis, a comparison was made between buckling loads for varying bending angles and circumferential variation angles and the buckling load measured during the previous DLR-ESA program. According to this comparison, a range for the bending angle could be determined for the statistical analyses after which a Monte Carlo simulation was executed. For the final results, the FE solver ANSYS was used. The cylindrical shells were modelled under axial compression, for both with and without imperfections. The imperfections were implanted by type of imperfection, and afterwards all imperfections were implanted at once to be able to compare the impact of each type of imperfection and the combinations. The result of the numerical analysis can be seen in Figure 2.3 and Figure 2.4. It can be seen that the loading imperfections has the largest influence on the buckling load, with the KDF being 0.64, and also showing the largest spread. When all imperfections are included, the total KDF would be 0.55. A comparison is then being made with the KDF according to NASA SP-8007, which would be 0.32. The large difference could be caused by NASA SP-8007 being conservative in general, next to the improved manufacturing methods used for the cylindrical shells. This study thus proves that a large improvement can be achieved by this new method.

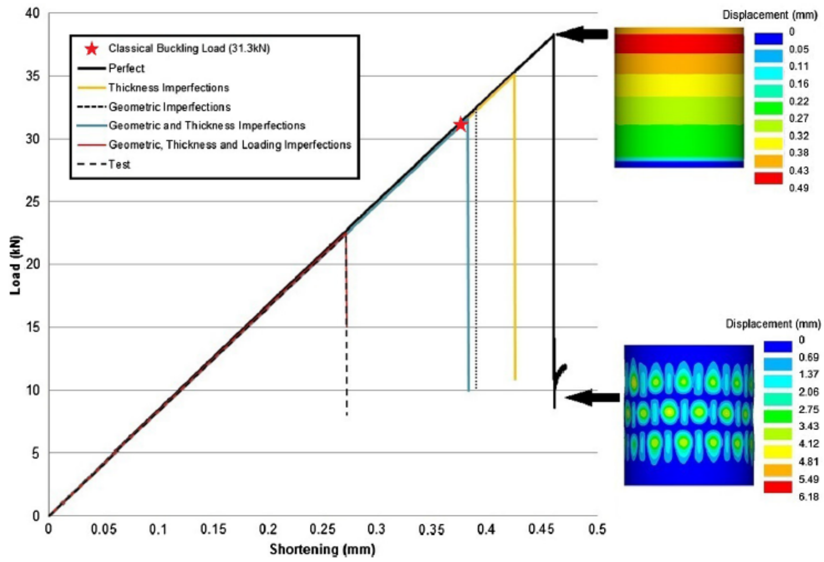

Figure 2.3: Load vs axial shortening to compare influence of imperfections [8].

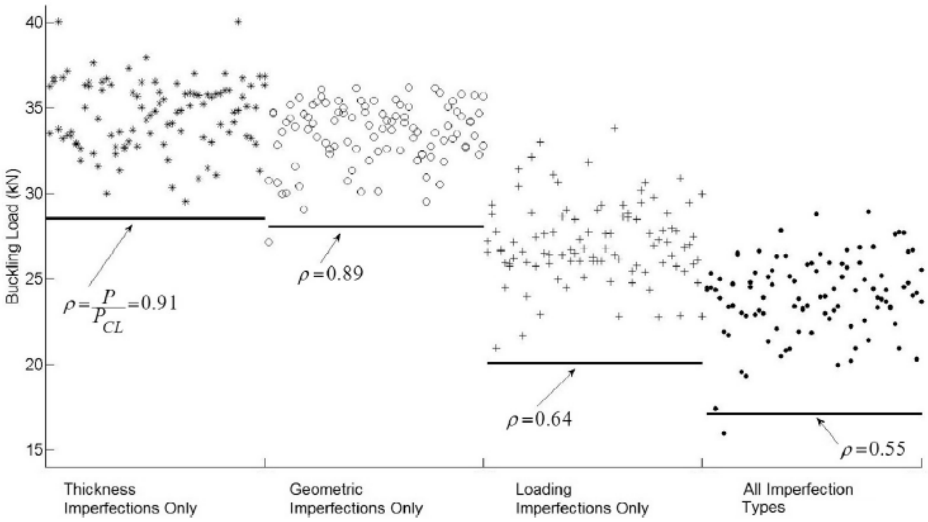

Figure 2.4: KDFs comparison per imperfection [8].

A statistical analysis for KDFs was published by Takano [9] in 2012, which includes a large amount of experimental data from a wide variety of researchers. The goal was to provide designers with a solution for the designing of cylindrical shells, which might not be perfect but should at least be practical. For the comparison with the different test data sets, a proposed solution which is based on the Green-Lagrange strain theory is used. The author chose this theory as he considers it to be the most precise compared to other linear bifurcation theories, as it contains the lowest amount of simplifications. The first step in the determination of the KDFs is to determine the validity of a number of experimental results. As from the comparison between the experimental results, it can be seen that there are several outliers which are circled in the comparison graph, see Figure 2.5. A stress analyses was executed by using the Tsai-Wu criteria, from which was concluded that some of the experimental results contained material failure before buckling and thus lowering the buckling load or even leading to collapse before buckling. Furthermore, there were test samples containing residual thermal stresses due to the curing process and test samples with improper bonds to the end plates, which were excluded as well. With the outliers excluded, the results seem to lose the dependency on the radius over thickness ratio which results in the assumption of no dependency on this ratio. The further determination of the statistical KDFs, is based on determining the A and B basis values of the buckling loads as measured during the experimental tests in combination with the buckling loads obtained from the proposed solution. This includes steps as determining if all the data can be seen as one sample, which was not the case, a study of the cause of variations among others and lead to an A-basis value of 47.9% and a B-basis value of 62.6%. As can be seen in Figure 2.5, the A and B-basis are on the conservative side, besides that the upper range of the radius over thickness ratio is determined by a single data source which lowers the certainty of the factors. In comparison to the widely used NASA SP-8007 design guideline, the determined KDFs are more reliable while being less conservative. The KDFs can be further improved, but this will require more experimental data. The statistical method is shown and explained in detail and could thus be applied when new experimental data becomes available.

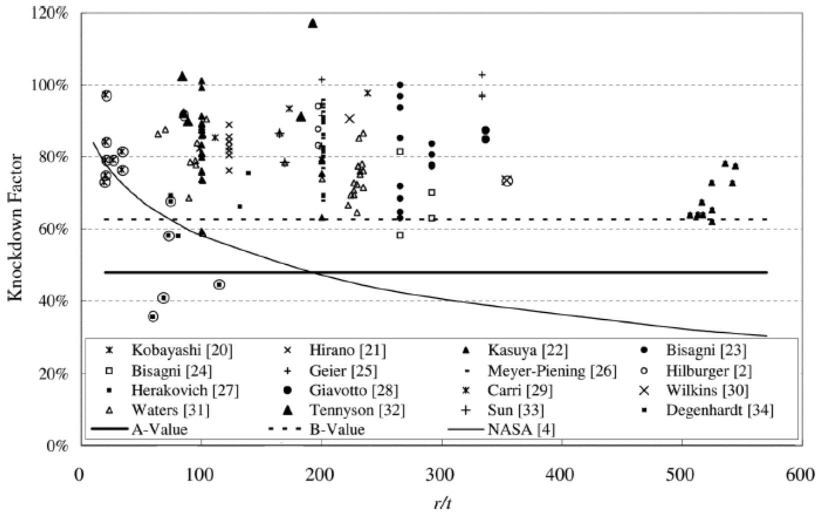

Figure 2.5: Comparison of experimental data [9], with circles around outliers.

Imperfections can be included in the buckling analysis by a large variety of methods, one of which is a probabilistic analysis. As a part of the DESICOS project, Bisagni and Alfano [10] published a probabilistic analysis, for which measured imperfections are used. The probabilistic analysis makes use of a combination of two methods, namely the Stress-Strength Interference Method and the Latin Hypercube Method, where the probability is considered for the cylindrical shell to endure the loading without buckling. From the analysis, a probabilistic buckling factor is determined which is dependant on the imperfections. This buckling factor is the ratio between the buckling load of the perfect cylindrical shell, which is determined by linear eigenvalue buckling analysis, and the imperfect cylindrical shell. The test subject consists of a scaled sandwich composite cylindrical shell of SYLDA, which was designed by Airbus Defence and Space. The test subject itself was manufactured during the Desicos project for use in experimental testing and imperfection measurements, both geometric imperfections and thickness variations, and was furthermore modelled in Abaqus, see Figure 2.6. First the buckling load without any imperfections is determined, then the imperfections are implanted into the model. For a worst case scenario with both geometric imperfections and thickness variations implanted, the KDF would be 0.85. For the probabilistic analysis, boundary imperfections and ply misalignment are also included. When the worst case scenario is analysed by the probabilistic method, the probabilistic buckling factor would be equal to 0.75. It should be noted though, that the boundary imperfections alone would equal a probabilistic buckling factor of 0.79, which is not taken into account in the Abaqus model. A comparison is then being made with the KDF according to NASA SP-8007, which would be 0.57, which is considerably lower. At first sight the determined KDF would be a large improvement, but it should be said that the geometric imperfections and thickness variations are now defined by a single shell. The imperfections are thus not yet statistically determined, for which a larger imperfection database is needed, which would be crucial for this method to be used for design purposes.

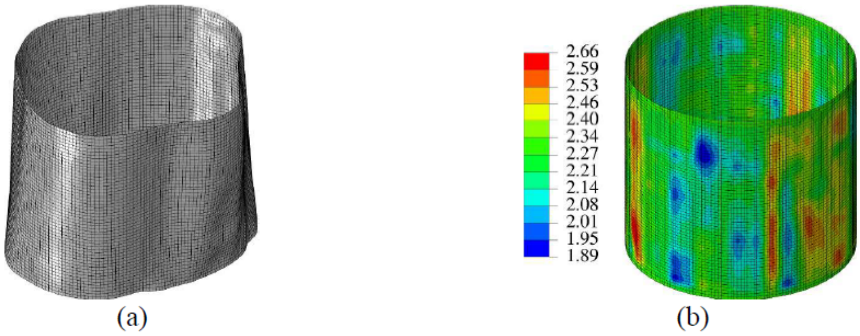

Figure 2.6: Geometric imperfections (a), Thickness variation(b) [10].

2.1.3 Perturbation Methods

The use of perturbation methods to approximate the behaviour of imperfect cylindrical shells has been a popular research topic in the last 10 years. Several types of perturbations have been researched and have shown considerable promise for the use in design guidelines. Perturbation methods are based on the principle, that applying a perturbation can be seen as a worst case scenario. For example by applying a dimple which would approximate the worst imperfection due to manufacturing or approximate a dimple as seen in the pre-buckling phase. Some of the possible perturbations are: radial perturbation load, radial perturbation displacement, edge loading perturbation etc. The advantage of a perturbation method lies in less experimental testing needed, which saves considerable expenses for the design of structures.

In a technical report published in 2013 by Cha and Schultz [11] a buckling analysis for a composite cylindrical shell was shown. It used a different method for including initial geometric imperfections, as it approximated the influence of these imperfections by applying a radial perturbation load, also called the Single Perturbation Load Approach (SPLA). This method of applying a geometric imperfection was chosen as it influences the buckling load without having a large influence on the axial stiffness of the cylindrical shell. This was shown in a research executed by Haynie and Hilburger [12] where 3 different methods were compared. The predictions are based on a FE analyses, somewhat similar to the model as used in [13], and a closed form analyses. The results from the FE analyses consist of axial shortening vs load, normalized buckling load vs radial perturbation load and radial displacement vs axial shortening. The normalized buckling load vs radial perturbation shows a bilinear graph, where the intersection of both lines is the start of a lower bound plateau as one of the lines has almost zero slope. Although there are results below this lower bound, in the results shown by [13] these were local buckling events at the perturbation location instead of global buckling. This is most likely the reason why this intersection point is deemed an indication for the lower bound buckling load. This method does provide a new way of determining a lower bound but it is questionable if it's representative of geometric imperfections found in real structures as there's no comparison with experimental findings in this publication.

The SPLA method was also used in a study published by Orifici and Bisagni [14] in 2013. This paper focused on both monolithic composite and sandwich composite construction for the cylindrical shells. It includes both cylindrical shells with and without cutouts. The numerical analysis is executed in Abaqus and S4R elements were used. The analyses were executed by applying the perturbation load with a constant loading rate, after which the perturbation load is kept constant and a axial displacement is applied. The buckling load was considered to be the maximum load, after which the load carrying capability lowers considerably. These analyses lead to the results shown in Figure 2.7. Although it can be seen that the behaviour of all test configurations is bilinear, the quasi-isotropic shows it in a more extreme matter in comparison to the other configurations which indicates a higher imperfection sensitivity. This behaviour of the quasi-isotropic cylindrical shell was caused by local buckling caused by the perturbation load before final buckling. From the buckling patterns, it is concluded that the lower perturbation loads cause normal buckling patterns as seen without perturbation loads. However, the higher perturbation loads cause buckling modes which aren't seen in normal buckling behaviour and thus it can be considered unrealistic. The results from the sandwich composite cylindrical shell showed similar behaviour compared to the monolithic constructed cylindrical shells, but the increase in core thickness resulted in the buckling pattern consisting of a lower amount of half waves. Furthermore influences of the cylindrical shell length were seen which prevented the normal buckling shape, as without perturbations, to occur. An investigation was executed to determine if material failure could happen, it showed that for most configurations there would be no material failure when the perturbation displacements does not exceed twice the thickness, but for sandwich constructions occurrences of both core failure and ply failure were seen for perturbation displacements equal or larger than the thickness. The next step was an analyses which included eigen-mode shapes as imperfections. This lead to a similar graph as shown for the SPLA analyses, see Figure 2.8.

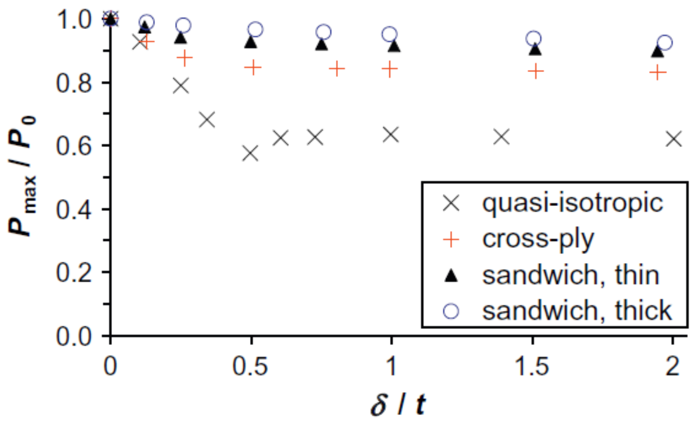

Figure 2.7: Normalized load vs perturbation displacement over thickness [14].

The single perturbation load approach is also a method used during the DESICOS project. During this project, a comparison was made between the SPLA method and four other common methods by Castro et al. [15]. The other methods of the comparison consist of: linear buckling mode-shaped imperfection (LBMI), measured geometric imperfections also called Mid-Surface Imperfections (MSI), Axisymmetric imperfections (ASI) and Geometric Dimple-shaped Imperfection (GDI). LBMI consist of buckling modes determined from the perfect cylindrical shell, which are then multiplied by a scaling factor and applied to the perfect model to create an imperfect cylindrical shell.

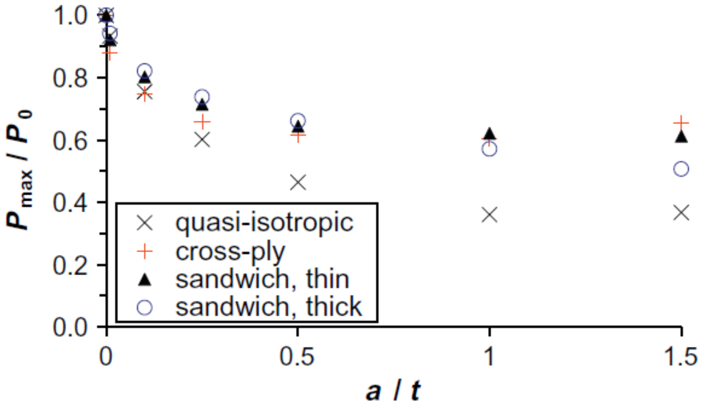

Figure 2.8: Normalized load vs imperfection magnitude [14].

The GDI imperfection method, consist of applying one wavelength of a cosine in the circumference direction and one wavelength of a cosine in the length direction of the cylindrical shell, which together form a dimple. The ASI method is somewhat similar to the GDI method, but now there is only one or multiple wavelengths in the length direction around the whole circumference. The MSI approach makes use of imperfection measurement data from a previous research project, which are then combined with a scaling factor to create a realistic representation of quality of the manufacturing process. The different methods were compared by applying them to two composite cylindrical shells that are similar to cylindrical shells used in previous research projects. The FE package Abaqus was used, in combination with Python code to apply the imperfections in the Python API of Abaqus. A set of comparison KDFs were determined, for which the NASA SP-8007 lowerbound guideline and a Reduced Energy Method (REM) was used, the latter being in combination with Abaqus. It showed however, that the REM method was dependant on the eigenmode and was unable to produce a lower-bound KDF as intended for the comparison. A wide variety of results were plotted, mainly end shortening vs applied load for different modes and measured imperfections for the two test cylindrical shells. The results indicated that the SPLI and ASI methods gave lower KDFs compared to the MSI method, with some of the GDI cases giving a higher KDF which was dependent on the shape parameter. In general, the LBMI method gave the lowest KDFs with the downside of this method being the large dependency on the eigenmode. The ASI turned out to be the preferred method, as it resulted in KDFs close to the most critical LBMI. The SPLA method was preferred over the GDI method, as it is a simple method in comparison but it does still require further development to determine the perturbation load value to be used.

In 2017 a paper was published by Wagner et al. [16] which consist of both development and validation of KDFs, with a claim that the load capability of cylindrical shells can be up to 40% more efficient compared to previous methods. The development stage will consist of comparisons between methods to determine KDFs, which are Single Perturbation Displacement Approach (SPDA) and Single Boundary Perturbation Approach (SBPA), see Figure 2.9, with the methods being applied to 3 different composite cylindrical shells. SPDA approximates the influence of geometric imperfections and the SBPA method combines geometric imperfections with loading imperfections. The SBPA method consists of applying a local loading imperfection with a certain height and width, which induces a single dimple as the geometric imperfection and local bending, and thus combines two imperfections with one adjustment to the model. The SPDA method is executed by creating a single dimple, by applying a radial displacement to a node. These methods are based around the concept, that the buckling load is dependent on the forming of a single dimple just before the cylindrical shell buckles. There is also an interaction to consider, between the forming of this single dimple and pre-buckling patterns. For the FE analyses the software package Abaqus was used, where the models consisted of S4R elements. For the analyses with the SBPA method, different FEA were executed using different heights of the loading imperfection. This resulted in a boundary perturbation height which consequently results in a minimum local buckling load, which would correspond to results of experimental tests as validated by previous research. The buckling load was then determined for this perturbation height, which resulted in the KDFs as seen in Figure 2.10. It can be seen that the experimental testing results are considerably higher compared to the SBPA results, which is caused by the accurate manufacturing of the test cylindrical shells according to the authors. The next step would be to apply the SPDA method. The radial displacement for which the buckling load is considered representative for a imperfect cylindrical shell was determined by gradually increasing the displacement, until a maximum perturbation force is reached as seen in Figure 2.9. The corresponding buckling loads and KDFs can be seen in Figure 2.11. It is seen that for cylindrical shell C1, the SPDA buckling load is higher compared to the empirical results and the method is thus unconservative for this specific cylindrical shell as this is not the case for cylindrical shell C2 and C3. A comparison was also being made with results from previous research using the SPLA method, which is conservative in comparison. For the determination of the KDF design guideline, the SBPA method is used, as it is seen as more robust. One of the test specimens, named C3, showed the highest buckling loads for both perfect and imperfect state. As this specimen used a quasi-isotropic layup, it is considered by the authors that cylindrical shells for launch-vehicles should only be constructed of quasi-isotropic laminates. As previous research showed that the KDFs for isotropic and quasi-isotropic cylindrical shells are similar, determination of the knockdown guideline is focused on isotropic cylindrical shells. A large amount of isotropic shells were modelled in combination with the SBPA method. The resulting KDFs were then fitted with power laws. The end result are two sets of equations, the first set calculates the KDF which only accounts for geometric imperfections and the second set accounts for both geometric imperfections and loading imperfections. One of the comparisons between the KDF accounting for both imperfections (designated TH) and previous experimental results can be seen in Figure 2.12. It can be seen that the method is capable of showing great results, but it does limit the tailorability of the composite material, which is ultimately one of the benefits of a composite material in the first place.

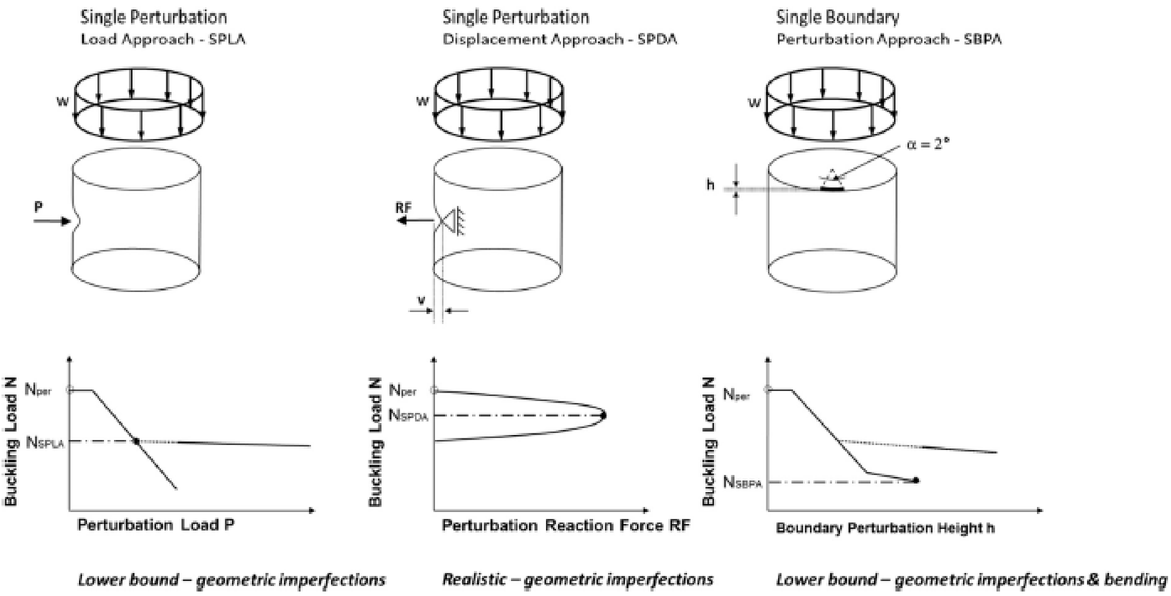

Figure 2.9: Comparison of perturbation methods [16].

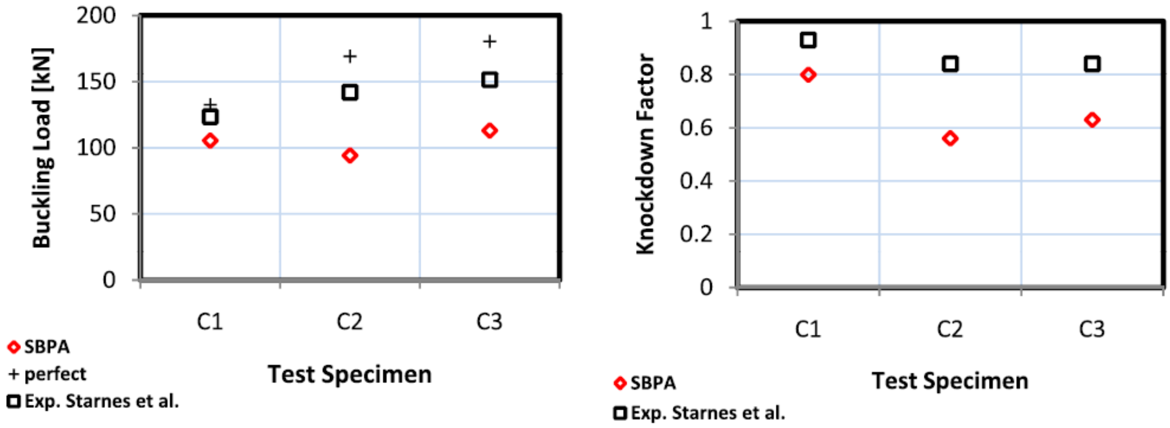

Figure 2.10: SBPA buckling load (left) and KDF (right) comparison [16].

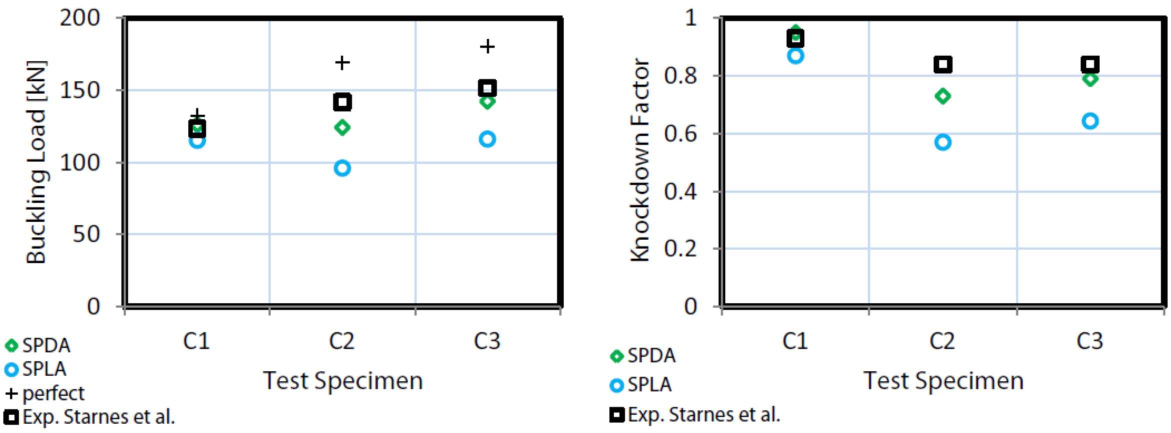

Figure 2.11: SPDA buckling load (left) and KDF (right) comparison [16].

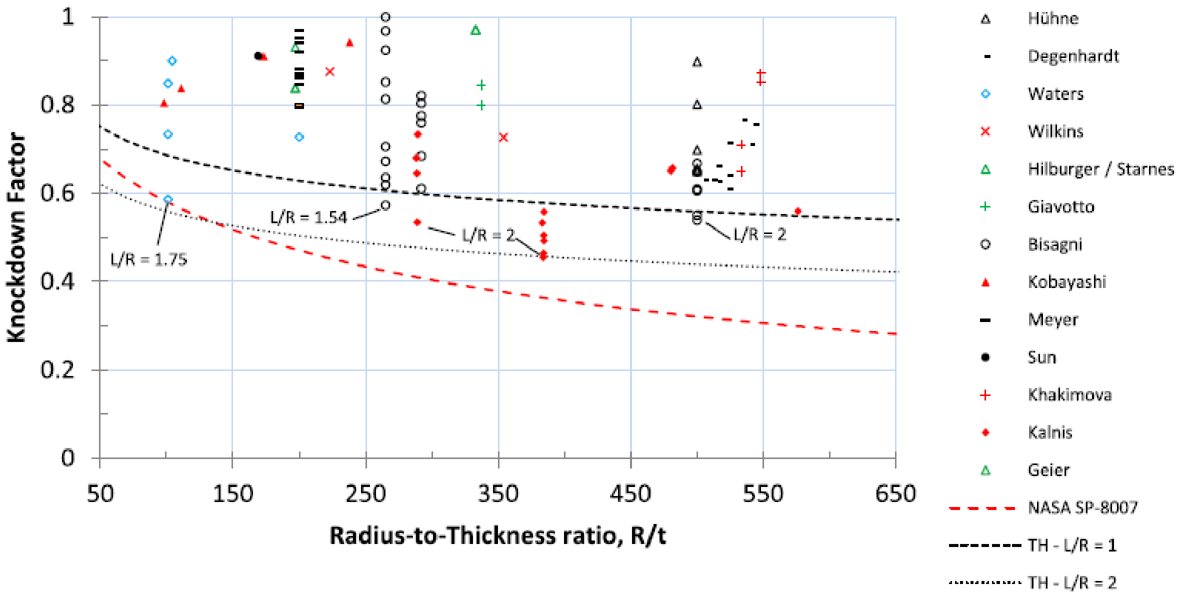

Figure 2.12: Comparison between TH KDFs and experimental results [16].

2.1.4 Experimental Validation

The main reason behind the increasing popularity of FE methods comes down to the costs of experimental tests. These tests are very expensive and are therefore executed as least as possible. The experimental tests are thus mainly for validating purposes, instead of a general design tool. Research into approximations of experimental results, by simulating or approximating the real life circumstances and imperfections in the widest sense, has been a field that gained popularity partially because of the wide development of FE methods for which the possibilities can seem endless. The inclusion of all types of imperfections and other influences on the behaviour of test samples, from the effects of the experimental setup to material and manufacturing imperfections, have increased the accuracy and realistic behaviour of the theoretical methods. Furthermore, experimental tests are a wealthy resource for the determination of the behaviour of structures in general, to validate design guidelines of common structures and research behaviour of new types of structures.

The inclusion of measured imperfections for numerical analyses is not necessarily a new method. In 2000 a combined experimental and numerical effort for the buckling and post-buckling of cylindrical shells was published by Bisagni [1]. The numerical analyses makes use of three different types, linear eigenvalue buckling analysis, nonlinear Riks method and dynamic analyses. Furthermore, two cylindrical shells were modelled to determine the influence of the imperfections and the sensitivity to these imperfections per cylindrical shell was examined. The two cylindrical shells consist of different layup but are further geometrically equal. The numerical analyses were executed by using Abaqus in combination with the conventional shell element S4R, which is still a popular combination for the FE modelling of cylindrical shells currently. The buckling load resulting from the linear eigenvalue analysis turns out to be highly dependent on the mesh, which requires a mesh convergence study to reach accurate results, but is in good agreement with the analytical solution. The nonlinear analysis, which uses a modified Riks method as available in Abaqus, also shows good agreement. The dynamic analyses in combination with the expliecit method is computational more efficient compared to implicit, while still showing good agreement with the analytical solution. Especially when it is considered that the buckling load of a cylindrical shell is highly sensitive to imperfections, an error of 3-4% is more then adequate. The analyses of imperfection starts off with imperfections which are based on the linear buckling modes in combination with a variable for the amplitude, with the first FE model utilising an axisymmetrical mode. Varying this imperfection amplitude results in imperfection vs buckling load curves, from which is concluded that the reduction of the buckling load for the same amplitude differs between cylindrical shells with different layups. This is already an indication of the imperfection sensitivity, as seen before in this literature study. Furthermore, both nonlinear methods, the Riks method and dynamic analysis, show good agreement with the dynamic analyses showing higher buckling loads in general. For a second comparison a different buckling mode is used as imperfection, now considering a diamond shape buckling mode. It turns out that the cylindrical shell which shows a diamond shape while buckled, shows equal behaviour for both imperfection shapes, while the cylindrical shell showing an axisymmetric shape while buckling shows more critical behaviour for the axisymmetric imperfection shape. This effect of the imperfection shape, is clearly visible for high imperfection amplitudes, but becomes obsolete for lower amplitudes. The final FE model incorporates the measured imperfections, for which the imperfections of a zone in the centre of the cylindrical shell is used. The imperfections between this zone and the edge, is linearly interpolated from the measured imperfection to zero imperfection at the edge. Boundary imperfections or loading imperfections were not taken into account. However, it has been concluded by more recent research to be of considerable influence. When the results of the measured imperfection FE model are compared to the experimental results, it is seen that the FE model shows higher buckling loads in the range of 15-20%. It is mentioned by the author that this difference, could also be explained by the thermal expansion of the mandrel which is used for the manufacturing process, which can cause reduction in bending stiffness as the fibers tend to concentrate towards the inside, while not affecting membrane stiffness. When comparing the Riks method to the Dynamic analyses, the Riks method shows equal behaviour as analytical solutions, when the Dynamic analyses follows the behaviour which is comparable to the experimental test, see Figure 2.13. This also leads to the Dynamic analyses being able to capture the different buckling shapes past the first buckling mode.

Although the previously mentioned SBKF project started in 2007, there was already extensive research going on in the years prior. In 2004 a paper was published by Hilburger and Starnes [17] which focuses on the effect of imperfections on the buckling behaviour of cylindrical shells. The publication consists of both experimental work and numerical analysis. The numerical models include a wide variety of imperfections, stated as traditional and non traditional imperfections. These consist of geometric imperfections, thickness variations, ply placement imperfections, edge imperfections with loading imperfections and at last the effect of elastic boundary conditions. The analyses include both a nonlinear static analysis and a nonlinear transient analysis, in combination with a analyses for material failure. The FE software package of choice was STAGS, in which the 410 quadrilateral element was used. It is noted that the implantation of the imperfections could lead to some side effects. As the thickness variations are applied in steps, dependent on the spacing between integration points, which can lead to larger imperfections than was intended.

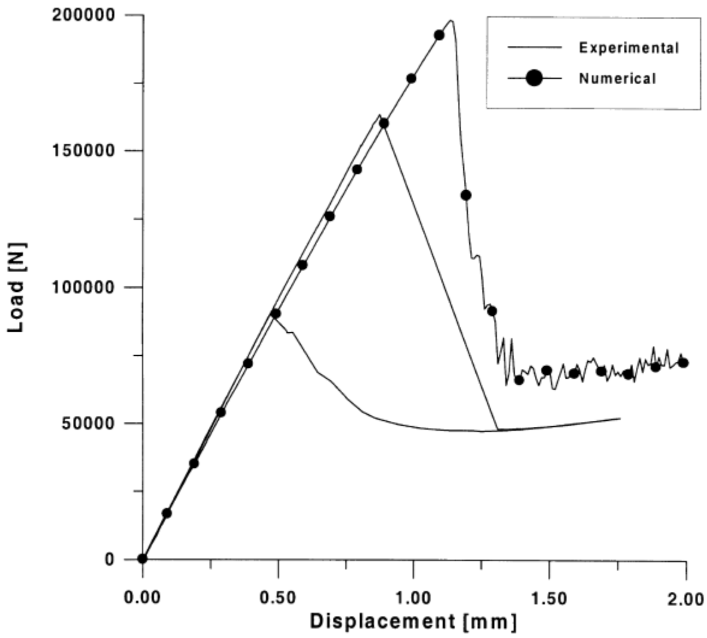

Figure 2.13: Comparison between experimental and numerical load vs displacement for dynamic analyses [1].

Furthermore, the combination of the mesh size and spacing between integration points can lead to problems with the ply imperfections, causing an artificial increase in bending stiffness. Ultimately it does indicate that the implementation of imperfections into a FE model is not straight forward and should be handled with care. As the side effects can result in an increase of the buckling load, causing an error compared to experimental results. Although STAGS will not be used for the thesis this literature study is intended for, the detailed explanation of the imperfection implementation can still be of great value as the procedure to implement imperfections isn't always shown in details in other papers. The test samples for this study consisted of six cylindrical shells, all varying in layup with three samples consisting of an 8 ply layup with a radius over thickness ratio of 200 and the other three consisting of a 16 ply layup with a radius over thickness ratio of 100. The laminates used for the test samples consisted of both quasi-isotropic layups and orthotropic layups. The buckling load of the 8 ply cylindrical shells determined by the numerical model, showed an error ranging from 8 to 18% compared to the experimental test results. Further failure predictions of the numerical model showed good correspondence with what was observed during testing. The numerical model of the 16 ply cylindrical shell resulted in a buckling load ranging from 17 to 18% higher compared to the experimental testing for 2 of the test samples, while one test sample collapsed at a load 44% lower compared to the predicted buckling load of the numerical model. The early collapse of the cylindrical shell was most likely caused by a material failure, induced by a ply gap imperfection. This ply gap can lead to considerable stress concentrations and thus exceed the material allowables at low loads. The error between the numerical model and the testing results is most likely caused by variations in shell properties, such as fiber volume fraction and the accuracy of the measured imperfections. The numerical models furthermore showed nonlinear behaviour due to the imperfections, such as a nonlinear coupling between the compressive stress and the shell response such as local buckling. The author further concludes that this research shows good promise for further research on determining imperfection signatures.

The six test samples as mentioned in the previous paper were used for further research on imperfection signatures by Hilburger et al. [18]. If such a signature for imperfections can be developed, it could be of great importance in the general development of design guidelines. As this could be of use in preliminary design as well, instead of just using the imperfections for validations afterwards. A lot of the projects on the development of design guidelines focus on worst case scenario which could lead to more conservative designs compared to designs based on real imperfections. The numerical analyses is again executed by using STAGS, similar to the numerical analyses as seen in the previous paper by Hilburger [17] but with less imperfection types included. The imperfections will be restricted to the geometrical imperfections at first. The determination of the manufacturing imperfection signature was based on representing the actual imperfections by a Fourier series. A mean imperfection shape and standard deviation are then established for the measured imperfections after which a coefficient of variation is determined for each imperfection. The imperfections, determined by the using the mean deviation and the minus deviation minus or plus the standard deviation, are then implemented into the numerical model which leads to Figure 2.14. It can be seen that this method thus leads to a bounded range of the predicted buckling load. Furthermore, the results correlate well with the numerical models which include the measured imperfections, and thus shows great promise for this method, and showing a maximum error of 10% compared to the buckling loads determined by the experimental tests. Especially when it is considered that only the geometrical imperfections are used in the determination of the imperfection signature, which could thus be expanded by imperfections such as thickness variations which have shown to greatly influence the buckling load as well. The behaviour of the shells as seen in the numerical analyses, both with measured imperfections and the imperfection signature, was in correspondence with the behaviour as seen during the experimental testing.

In 2015, as part of the DAEDALOS project, another paper was published by Bisagni [19] which focuses on both static and dynamic axial loading of composite cylindrical shells. The same auther also published on the topic of dynamic buckling in 2005 [20]. The inclusion of dynamic load cases creates possibilities to determine dynamic buckling behaviour, damping characteristics and hysteresis among others. While current design guidelines are mostly based on static loading, as seen in this literature study, aerospace structures are most often dynamically loaded which leads to its own set of problems which should be taken into account. Three test samples were manufactured at DLR and were subjected to both static and dynamic loading, the dynamic testing consisted of both modal tests at a variety of load levels and dynamic buckling tests. The static tests were executed on two different test setups. The static experimental tests showed an average difference of the buckling load of 5,7% between the test setups, which is most likely caused by imperfections related to boundary conditions and loading. The numerical analyses was executed using Abaqus in combination with S4R elements. The linear eigenvalue buckling analyses shows considerable higher buckling loads, as expected, but when the measured imperfections were added to the numerical model the buckling load is approximately 22% higher. This remaining difference is most likely caused by imperfections at the boundary of the shells. The dynamic testing showed a consistent trend, with the dynamic buckling loads being 5% higher compared to the static buckling loads. It should be said though, that this is based on three test samples and the range of 5% falls within the range of scatter.

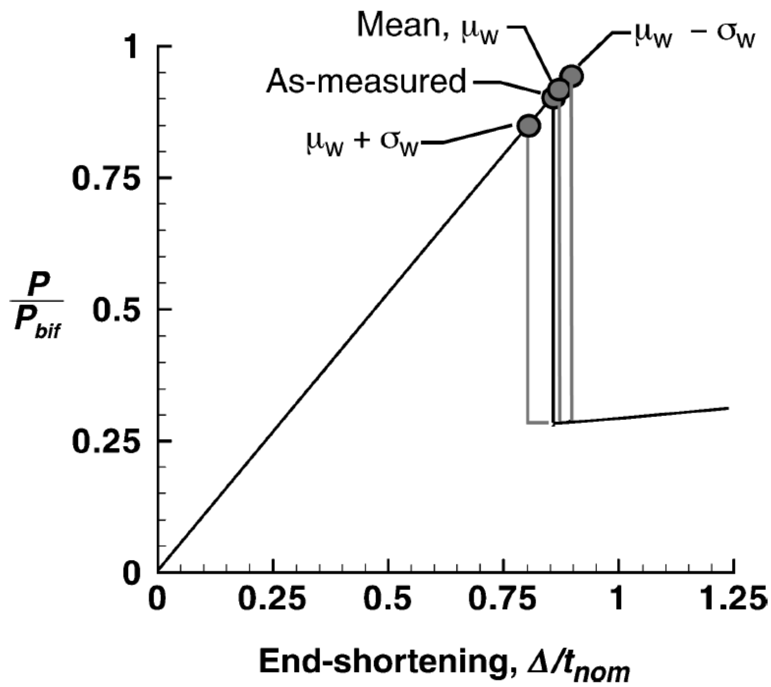

Figure 2.14: Normalized load versus end shortening for imperfection signatures and measured imperfections [18].

The difference could also be related to the modes of excitation as was concluded by other researchers. The modal analysis resulted of a wide spectrum of modes and damping values under 4 different load cases. The natural frequencies showed a decrease for an increase of axial load and a corresponding higher damping value. The final test was a test until final failure for one of the test samples. It showed a large post-buckling zone, which showed a load carrying ability of 40-30% compared to the buckling load, with final failure at a total shortening of 26 times the shortening for buckling. This final failure test also gave the opportunity to photograph several buckling shapes, which require going till final failure. More papers on the postbuckling range were published by Bisagni and Cordisco [21] [22] [23], both for combined loading cases and stiffened cylindrical shells.

The results of both the experimental testing and analysis of a NASA test article named CTA8.1, was published in 2018 by Schultz et al. [13]. The test article was tested at a purpose built testing facility for buckling at NASA Marshall Space Flight Center. The testing facility is capable of up to 1.5 * 10^6 lb in pure axial compression next to combined axial and bending loads and tension loads. For the manufacturing of the cylindrical shell which consisted of a sandwich composite, an out of autoclave process was used. The process consisted of manual layup in several steps, with curing in an oven under atmospheric pressure by using a vacuum bag. After all intermediate steps were completed, the cylindrical shell was post cured in an oven. Several non-destructive tests were executed to find any imperfections. The imperfections, or flaws, consisted of dry fibers, a large delamination and voids. Furthermore, testing methods were used to assess the thickness variations and radial imperfections which can be used in the finite element model. Several steps in the repair process were required, with some being successful but the voids in the padup could not be fixed and required further steps. Before the experimental test was executed, a finite element model was made to be able to make a prediction of the structural behaviour. The model consisted of both the cylindrical shell and the test setup itself to include influences of the test structure, see Figure 2.15. The cylindrical shell itself was modelled by using S4 shell elements and the test structure consisted of B31 shear-flexible beam elements. The imperfections as measured before were applied as a radial displacement of the mid surface and thickness variations of the core material. A static nonlinear analyses was used in combination with a transient nonlinear analyses. As material properties tests were delayed, the properties used for the first model consisted of assumed properties and data from the material vendor. When the test article was loaded till a safe margin before buckling, it was determined that the FE model showed different results and the material properties were adjusted. Specifically, the stiffness in in-plane directions were adjusted. When the test article was loaded until buckling, the buckling load was within 1% but the experimental results showed a slight nonlinearity. Further results such as radial displacements were also considered and analysed in detail. After the test, test samples were taken from the cylindrical shell to determine the material properties more accurately. These new material properties were then used in a new FE model, for which a user subroutine function was used to approximate the nonlinear behaviour of the material. This resulted in an even closer approximation of the experimental results, but it is noted by the authors that existing differences are most likely caused by loading imperfections. In general great results were achieved when comparing the FEA results to the experimental test, which is a great indication of the progress that has been made to approximate the structural behaviour without considerable experimental testing.

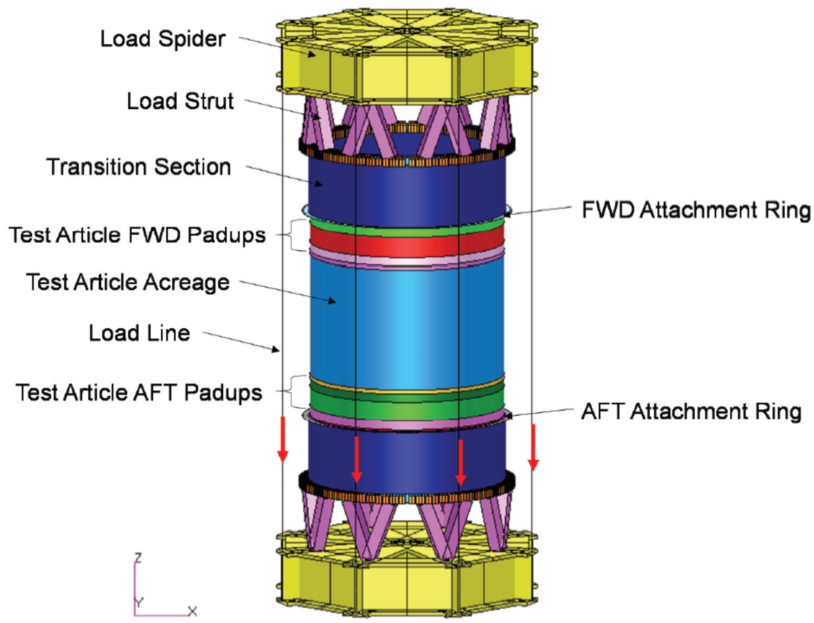

Figure 2.15: CTA8.1 test setup FE model [13].

2.1.5 Nondimensional Parameters

During the 1990s the buckling behaviour of composite materials was gaining popularity and new methods were needed. In 1991 Nemeth [24] published research about a method to parameterize the bifurcation buckling behaviour of shells in the elastic region. These parameters can be very useful in the aerospace industry, where weight is a priority and less conservative design methods are an ongoing topic for research studies. The design goal is to take advantage of the anisotropy of the material, to tailor the material to the structural needs. The focus of this research is on double-curved panels under combined loading, as these have a wide range of applications in the aerospace industry, with a symmetric layup. The parameters developed could also lead to new methods for the scaling of structures. As the parameters were made nondimensional and thus could parameterize the behaviour without having a direct link to the size, material and boundary conditions of the structure of interest. This creates possibilities to compare structures, and thus also previous or new experimental results, without them necessarily being in the same range of sizing or manufactured from the exact same material. This could be of great help, especially in early design phases, and limits the need for experimental testing which is expensive. The method was build around equations for nonlinear deformation. The strain displacement relations, nonlinear equilibrium equations, compatibility equation,constitutive equations and buckling equations were used in the analyses. Furthermore, the analyses also include a form of the Batdorf Z parameter and an example problem is presented. The analyses and included derivations are shown and explained in detail, these will however not be shown in this literature study as these are quite extensive. After the derivations, it is noted by the author that the parameters can also be used to determine the sensitivity of the buckling behaviour to each structural property. This could be useful for scaling purposes, as it can be a good indication for what structural properties to scale without losing all similarity with the full-scale prototype.

In 2010 Nemeth [25] published another technical report which continues on and expands his previous work about nondimensional parameters. The analyses will now include composite quasi-shallow shells with the inclusion of possible initial geometric imperfections. It furthermore deems to develop design tools that are able to determine the effect of structure properties, such as material properties and layup configurations, on the imperfection sensitivity of the mentioned shells under loading conditions. The sensitivity for each type of imperfection can also be helpful in determining the viability of manufacturing methods, as the variations, or accuracy, for structural properties can differ between each method. With these design tools it is then possible to produce examples of the nondimensional parameters as a function of these properties, which can be used as a guideline of sorts during preliminary design. As in the previous work of this author, the derivations are explained and shown in detail. The end results/values of the nondimensional parameters are produced for cases of angle-ply laminates, quasi-isotropic laminates and unbalanced unsymmetric laminates for a large range of configurations to create a large but usable design space. This makes the research applicable for a wide field of structural designers.

Further development of the nondimensional parameters, to tailor them to the specific case of cylindrical shells under axial compression, was published by Schultz and Nemeth [26] with emphasis on the imperfection sensitivity. It is has been shown by several research projects, that cylindrical shells are susceptible to being sensitive to imperfections with the buckling load being reduced considerably. The effect of the shell anisotropy on the imperfection sensitivity was studied in detail, for the case of a sandwich composite cylindrical shell. The parameters that were developed, offer insight into the behaviour of cylindrical structures while reducing the amount of design variables. This provides a method to maneuver through the design options and simplify preliminary design stages. The study does not feature applied measured imperfections for the buckling analyses, but makes use of buckling modes to approximate realistic imperfections. For the analytical model, Donnell's equations will be used to determine the nondimensional parameters and related equations. The Donnell's equations are limited to thin shells, as the transverse shear flexibility is neglected. As this study is also focusing on sandwich composite cylindrical shells, it is noted that the radius over thickness ratio might be higher compared to isotropic cylindrical shells, as the composites in general have low transverse shear stiffness. The analytical part of the project starts off with the derivations for the bifurcation buckling equations for a perfect cylindrical shell. After which the analyses continues with the nonlinear deformations of a imperfect cylindrical shell. The imperfections are included by introducing a imperfection function which determines the radial displacement from the middle surface of a perfect cylindrical shell. As noted earlier, the imperfections consist of buckling modes, as during the design stages the actual imperfections are still unknown and these buckling modes should lead to conservative results. The first set of results are shown for the isotropic cylindrical shell, the results were obtained by using a symbolic solver in combination with the analytical model. The results consist of end shortening vs load curves, for different imperfection amplitudes, see Figure 2.16. It can be seen that after a certain imperfection amplitude, the nodge in the curve almost disappears. The next step was the FE model, which was constructed by using the FE software STAGS. The FE analyses consist of both linear eigenvalue analyses and a geometrically nonlinear analyses. The model consisted of a E410 element, which is a four node quadrilateral shell element without transverse shear flexibility. Then a combined graph is shown, for the imperfection sensitivity factors vs imperfection amplitude, for both the analytical and FE model, see Figure 2.17. The next step is a comparison between 3 sandwich composite cylindrical shells which were structurally optimized by the software package PANDA2. The same procedure as used for the isotropic cylindrical shell is applied to the composite cylindrical shells. The results of the composite cylindrical shells were compared to the isotropic cylindrical shell, for both the analytical and STAGS model, see Figure 2.18. It is seen that the highly tailored composites show the highest imperfection sensitivity factor, thus having a buckling load closest to the bifurcation buckling load of a perfect cylindrical shell.

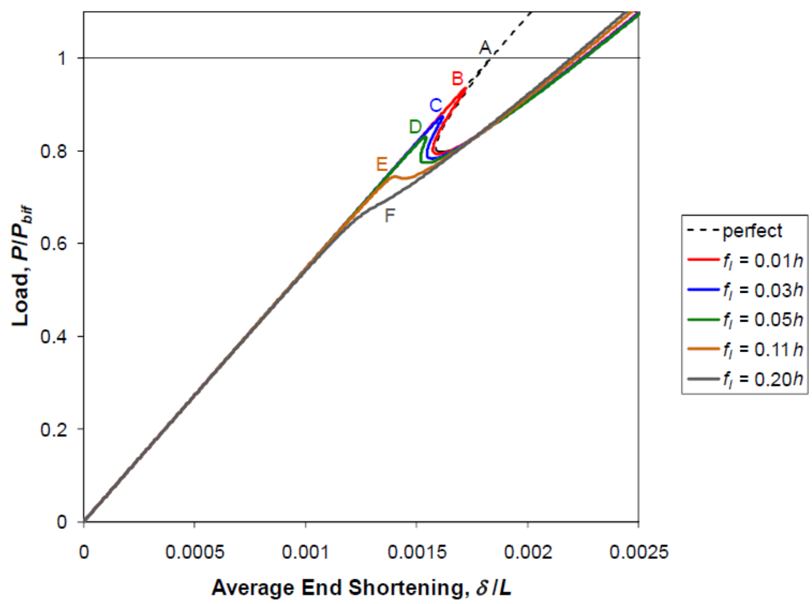

Figure 2.16: Average end shortening vs normalized Load for the analytical model [26].

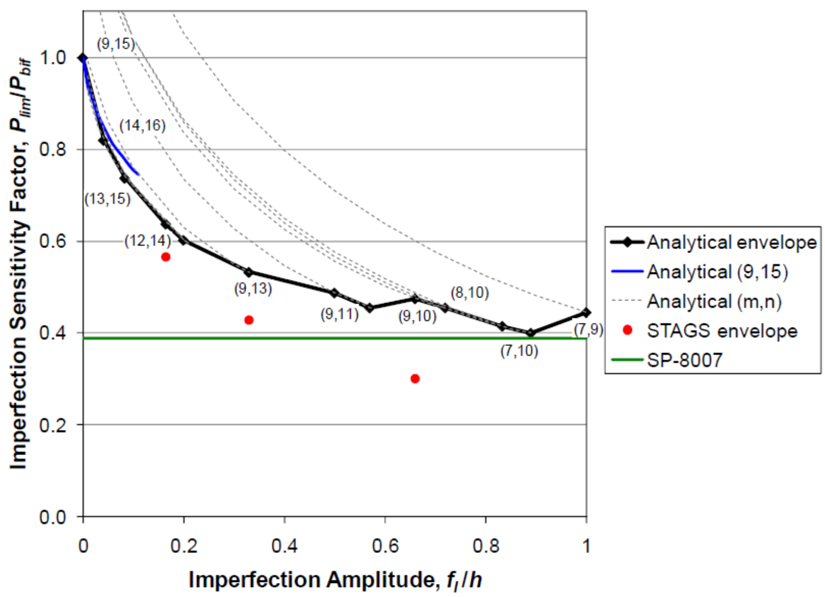

Figure 2.17: Imperfection sensitivity factors vs imperfection amplitude [26].

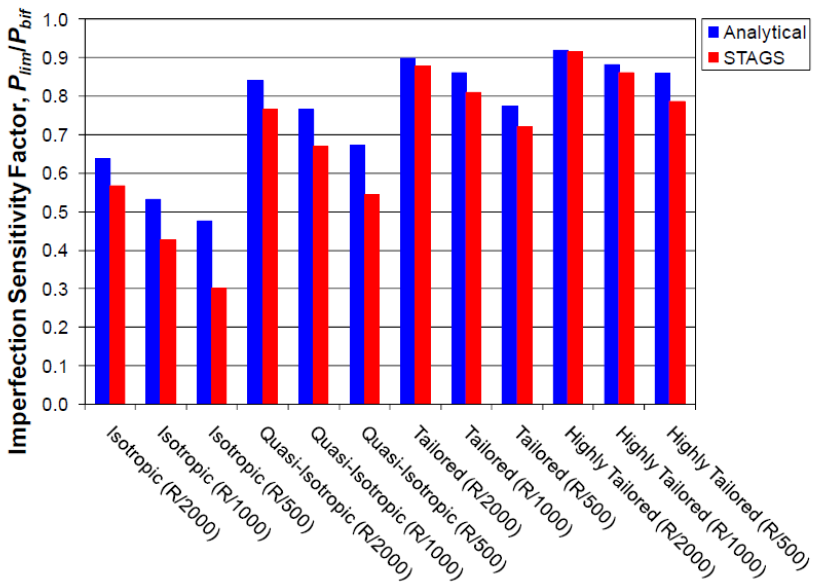

Figure 2.18: Imperfection sensitivity factor for different materials and imperfection amplitudes [26].

2.1.6 Remarks for Buckling Analysis

Several different methods for the determination of buckling behaviour have been presented. The emphasize was on the inclusion of imperfections, and also the imperfection sensitivity of the cylindrical shells. This imperfection sensitivity was shown per type of imperfection and with a combination of imperfection types. Depending on the type of loading imperfections, loading imperfections can have a large influence on the buckling load. While it was not always included in the research shown, loading imperfections should thus be considered next to other types of imperfections which are more commonly seen in FE analysis. For the buckling analyses in combination with a scaling method, using real measured imperfections which are then scaled for the cylindrical shell of interest would be ideal. As including real imperfections has been shown to lead to great results, and is off course the most direct representation of the real imperfect cylindrical shell. The first step to include scaled imperfections could be approximating the imperfections by a imperfection signature, which could simplify the scaling process and has already been shown by one of the cited authors. It should be noted however, that determining imperfection signatures, is a topic of its own which requires intensive research and also a database of real imperfections.

2.2 Scaling of Structures

In this section several methods for the scaling of structures will be explained. Different theories and their application will be examined. This section will be purely about scaling and the effects of scaling. Not to be confused with size effects, which is about strength and stiffness properties of the material and the dependency of these properties on product size. The first paragraph will go into detail on similitude theory for which governing differential equations are used, in which Simitses and Rezaeepazhand [27] have done extensive research. The second paragraph is about dimensional analyses, which focuses on expressing variables in base units from which scaling laws are derived by using the Buckingham Pi theorem. The following paragraph goes in depth about the scaling by using nondimensional parameters, which is ongoing research as part of the SBKF project. The last paragraph is a short summary of the methods in a comparative matter, combined with first insight on how the methods might be used for the following thesis.

In 2016 Coutinho et al. [28] published a review about similitude theory based reduced scale models which provides a good overview of scaling of structures in general. It explains the basic definition of the similitude theory method and its use, next to a time line of the research field starting since 1915. The timeline and accompanying research are explained in detail and it's a wealthy resource of references in this research field. The review shows the difference methods within similitude theory, from dimensional analysis to governing differential equations and energy equations. The areas of research are then elaborated on, which includes impacted structures, rapid prototyping and empirical methods. This review is a preparation on further research by the same authors, which will be shown in the suitable paragraph.

2.2.1 Similitude Theory by Governing Differential Equations

Similitude theory is a widely used theory for several scaling problems. It can be used for structural strength and stiffness, vibrations and impact problems. For this literature study the main focus will be on the scaling of structural strength and stiffness. The majority of recent work for structural similarity is based on the work by Simitses and Rezaeepazhand [27, 29, 30] from the 1990s. Both authors The theory is based on the principle that the prototype and the model are two different systems, but consist of similar parameters. These parameters determine the structural behaviour or response to applied loads, both dynamical and static loads. By developing similarity conditions, also called scaling laws, the mathematical system of the scale model can be mapped, or transformed, onto the system of the prototype to determine its behaviour. The system is defined by the governing differential equations for the particular situation that is being modelled.

In 1996 Rezaeepazhand et al. [31] published a paper specifically focusing on the scaling of laminated cylindrical shells under axial compression. The material is assumed to be linear elastic. Furthermore, it is assumed that there are no imperfections or that the imperfections have equal effect on both model and prototype. For the buckling analysis, Donnell-type equations are used for circular cylindrical shells under uni-axial compression. Combining these equations with an ABD-matrix formulation and Donnell kinematic relations, results in a simplified form of the governing differential equations. Three shape functions u,v and w are assumed. By substituting the displacement equations into the buckling equations, multiple sets of homogeneous algebraic equations are determined. From these equations, the critical buckling load can be determined. By applying similitude theory, a set of scaling laws are determined. When complete similarity is achieved by using ply-level scaling it produces excellent results as seen in previous papers. From these results it's also apparent that the critical buckling load is linearly dependent on the number of plies used for the prototype. If not mentioned otherwise, models are geometrically scaled next to the mentioned variable to retain similarity of the curvature parameter Z. The next model makes use of different amount of plies compared to the prototype, outside of a certain range the accuracy drops but there's still a wide range. There is a underestimation but it declines fast when the number of plies increases. In previous papers the stacking sequence had always been equal for model and prototype. Using a different stacking sequence for model and prototype, the accuracy of the scaling laws is still retained. When both stacking sequence and number of plies differ between prototype and model, there is an underestimation seen at lower number of plies but this declines at higher ply numbers, see Figure 2.19. It can be concluded that a cylindrical shell under axial compression is not sensitive to a stacking sequence distortion. The next step is the distortion in length. For the following results, only the length is changed between model and prototype. This also results in a different curvature parameter Z compared to the prototype. The curvature parameter can be associated with the imperfection sensitivity of a cylindrical shell, it is thus an important design rule to design a model with the equal or close to curvature parameter and thus equal or close to imperfection sensitivity. If this design rule can't be satisfied, and the curvature parameter differs between prototype and model, one of the two might be more sensitive to imperfections. Which direct effect the imperfections might have is not reported. The distortion in length does not produce an inaccurate result. The authors even report that extreme values of the model length that showed different mode shapes, result in accurate predictions. The radius of the cylindrical shell is the next distortion to be tested with further properties of the model and prototype being equal. This distortion turns out to have a large effect on the accuracy of the scaling method. It should also be noted that the resulting curvature parameter Z range of this graph is smaller compared to the distortion in length. The last distortion of this paper, of which it shows results, consists of different thicknesses. This distortion caused an inconsistent accuracy which is caused by the different wave numbers as a result of thickness changes. It is still possible to design an accurate model but the wave numbers should be taken into account. The distortion in material properties was also mentioned. This distortion resulted in a model which did not predict the behaviour of the prototype accurate. The results of this distortion are unfortunately not shown or graphed in the paper.

Both Rezaeepazhand and Simitses kept publishing work about similitude theory in co-operation with other researchers which will be shortly mentioned hereafter. In 1997 Tabiei and Simitses [32] executed an analysis which includes the imperfection sensitivity of scaled models. In 2002 Frostig and Simitses [33] published a paper which focused on the similitude of sandwich beams. In 2004 Frostig and Simitses [34] published a paper about the buckling of sandwich panels with a soft core.In 2011 Rezaeepazhand and Yazdi [35] published a paper about the use of similitude theory focused on the prediction of flutter for angle-ply composite plates.

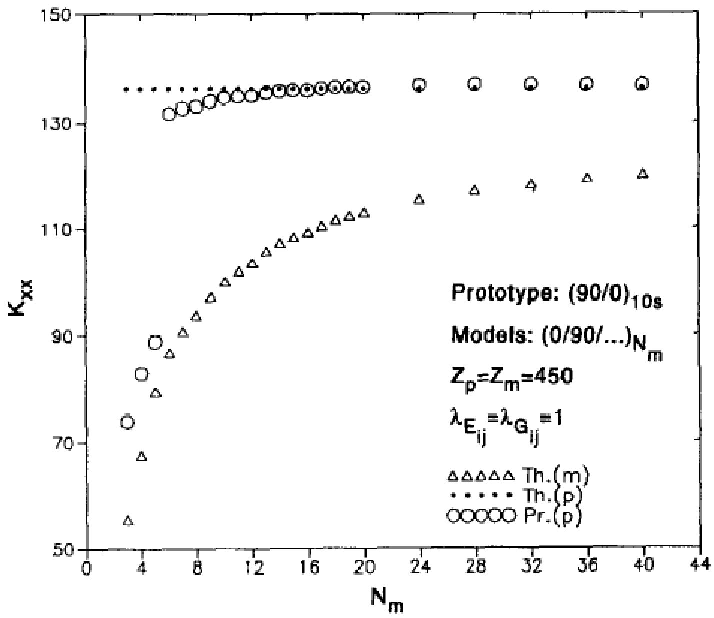

Figure 2.19: Accuracy comparison for models which differ in number of plies and stacking sequence[31].

In 2017 Coutinho et al. [36] published a research focusing on a modular approach to structural similitude. The method was based around several relationships which are kept as general as possible, which were then subdivided into different modules. The relationships, or equations, that are being used to derive the scaling laws are:

- Governing differential equations, with plane-stress assumption.
- Stress-strain relations.
- Strain-displacement relations.
- Force and moment resultants.
- Displacement field.

For each of these modulus scaling laws are then derived for the case of a generalized plate. The next step is to combine these scaling laws for complete similarity, partial similarity is not yet considered and is outside of the scope of this paper. There is no mention of a load case, as it is kept as general as possible. In the following case the scaling laws for the generalized beam were derived. Some of the scaling laws of the generalized plate were applied to the beam as well. In the strain-displacement, displacement field and force and moment modules a difference is being made between loadcases. The loadcases considered were uniaxial bending, biaxial bending and torsion. The paper continues with a case study of a stiffened plate which combines both plate and beam scaling laws. The plate was pinned along all edges and the loadcase consists of uniform pressure on the skin side. A selection of scaling laws was then made and later applied to a prototype and the 1/10 scale model. The results are shown in the form of transverse displacement in the model under three different load levels, see Figure 2.20. These transverse displacements are then scaled to the prototype, which results in Figure 2.21.

As can be seen from this graph, the results form the model scale very accurately. For all three loading options he results match. The authors conclude that this modular method can thus be very accurate, next to the benefit of having less limitations compared to other methods. These limitations were prevented through the combination of different scaling methods, as the sub-systems were scaled and combined into one scaled system.

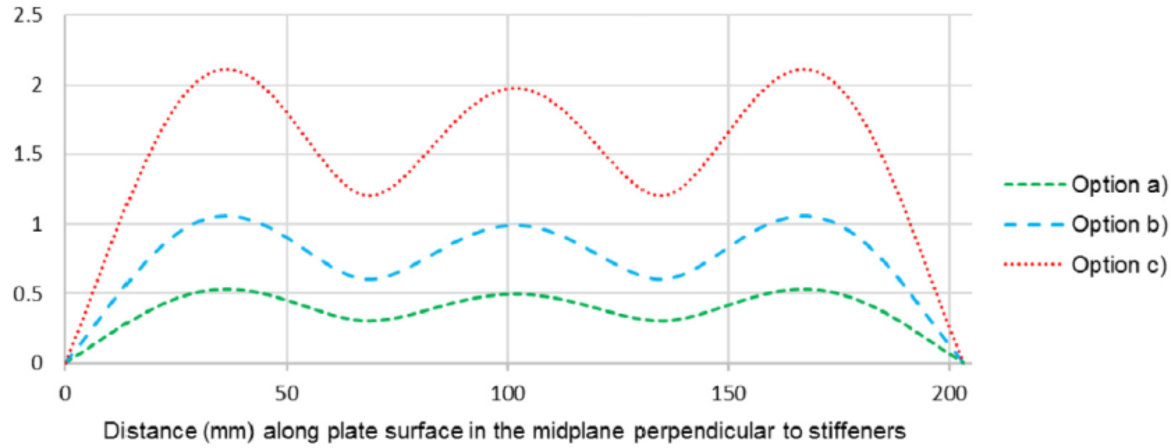

Figure 2.20: Transverse displacement for 3 different scaled loadings [36].

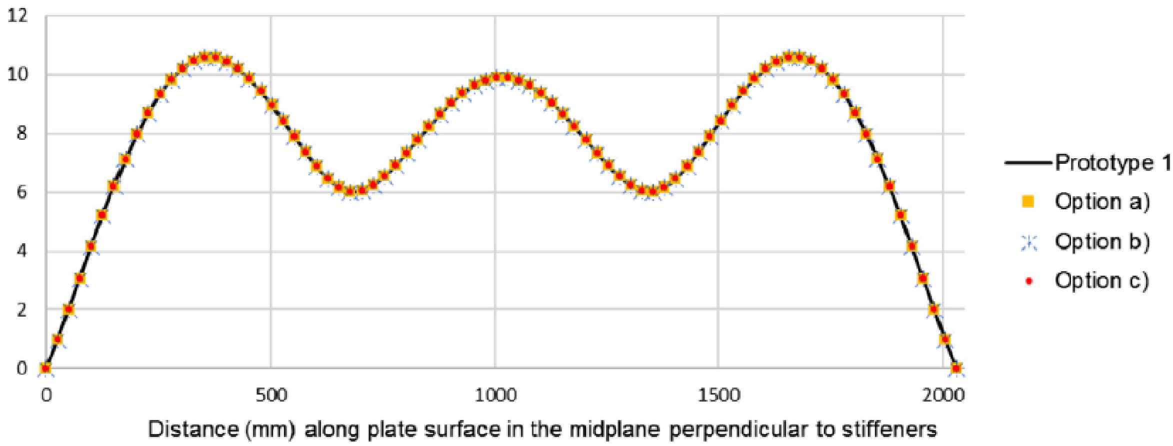

Figure 2.21: Transverse displacement of prototype with scaled predictions [36].

The majority of recent work which uses governing differential equations for the similitude theory is mostly focused on vibration studies. In 2014 Luo et al. [37] presented a research about distorted scaling laws used for dynamic cases. In 2015 Zhu et al. [38] published a paper about designing a dynamic similitude method for thin walled cylindrical shells which makes use of strength requirements. The derivation of the scaling laws was very detailed and includes the scaling of strength. In 2017 Zhu et al. [39] published a review which focused on plates and shells and their design by dynamic similitude. It includes both dimensional analyses and governing equation analysis next to examples for applications of similitude. It shows an approach for distorted models and explains the need for more research next to it being a wealthy resource of references. For more papers from recent research see: Luo et al. [40], Luo et al. [41], Eydani Asl et al. [42], Asl et al. [43]. Similitude theory has also been applied to impact problems of which the work of Morton [44] is an example. It is however less popular compared to strength, stiffness and dynamic purposes.

2.2.2 Dimensional Analyses

Another method for scaling is dimensional analysis, which can be done by using the Buckingham Pi Theorem, Simitses and Rezaeepazhand [45]. This method is based around the similitude of the physical dimensions of the system. One of the benefits of this method compared to using governing differential equations, is the ability to use this method for systems of which the governing differential equations are complex and difficult to determine. The shortcomings of this method lie in the amount of similarity equations or conditions it can determine for the scaling factors for certain systems, especially when distorted models are used. This problem mainly occurs for structural strength and stiffness problems, while it's not a common problem for dynamic or vibration problems where it's widely being used.

In the 60s and 70s a considerable amount of testing of scaled models is done by NASA. This included mostly vibration analyses of launch vehicles. In 1964 a technical report was published by Mixson and Catherine [46] which focuses on the vibration properties of a 1/5 scale model and a full scale model of the Saturn SA-1. The scaling analyses were based on the scaling of general dimensions and the material properties were kept constant between the models. It was concluded that the method resulted in accurate similarity between scaled model and full-scale prototype. In 1967 a technical report was published by Brock Jr et al. [47] which focused on a 1/10 scale model of the Apollo/Saturn V, for which Leadbetter [48] published another technical report in 1970 that went more in depth about the analysis part. In 1968 Catherines [49] published a technical report focusing on a 1/40 scale model of the Saturn V and its launch tower for use in experimental tests. It presents detailed results of these experimental tests, but no comparison was made to the full-scale model. Another group of papers was published around a 1/8 scale model for the shuttle solid rocket booster (SRB), by Levy et al. [50] in 1975, Leadbetter et al. [51] in 1976 and Blanchard [52] in 1977. The papers don't show a detailed scaling process, the paper from 1975 focuses on a finite element model of the SRB , the paper dating from 1976 goes more in depth on the construction of the scale model and the paper dating from 1977 shows the full list of scaling relationships that were used. Although the methods used in these technical reports might not be applicable for the structural scaling that this literature study is focusing on, it does however show that scaling has been widely used with success.

2.2.3 Scaling by Nondimensional Parameters

The nondimensional parameters as published by Nemeth [24] [25] can also be used for the scaling of structures. As these parameters are seen as a way to determine the behaviour of a structure in general, without necessarily taking the size of the structure into account. With the added complexity of composite structures, where the tailoring possibilities can be overwhelming especially in early design stages, simplifying the structural behaviour can be crucial to determine scaled models which are representative of the full scaled prototype without having full similarity. Applicable research will be shown and explained.

In 2001 Hilburger et al. [53] published a paper which includes scaling by using nondimensional parameters. The research is focused around a multi-cell non-circular composite structure with a combined loadcase of mechanical load and internal pressure loading. The nondimensional parameters are derived from a first order shear deformation plate theory, which follows the method published by Nemeth [24]. The nondimensional parameters used consist of:

- Membrane parameters
- Bending parameters
- Ratios of transverse shear stiffnesses
- Plate aspect ratio
- In-plane displacement
- Normal displacement
- In-plane loading
- Pressure loading

The structure for this research consists of several subcomponents. For complete similarity each model subcomponent has to satisfy complete similarity, and thus have equal coefficients in the governing partial differential equations, with the same subcomponent from the prototype. This equals the nondimensional parameters being equal for the corresponding subcomponents of model and prototype. As the structure consists of several subcomponents, the intersection of these subcomponents need to satisfy continuity conditions. Which consist of displacement and moment compatibility conditions. The displacement compatibility condition result in the same parameters mentioned before, but the moment compatibility condition results in an extra nondimensional parameter. To test the method, three configurations are designed. A prototype, complete similar sub-scale model and a partial similar sub-scale model. The first two models consists of sandwich panels, were the partial similar model consists of monolithic-laminates. Results for these configurations were determined by FEM-models after which the responses from the sub-scale models were scaled to full-scale responses. The complete similarity case showed accurate results, the partial model showed less accurate results. For example, the displacement results showed an error between 30 and 40%. The partial similarity and the effect on the parameters is further explained and the sensitivity of the parameters is examined. It is shown that the behaviour of the parameters, and their influence on the resulting displacement, differs per parameter and that there even is a slight dependency on the loadcase.

In 2018 Uriol Balbin et al. [4] published a research using nondimensional parameters for the scaling of cylindrical sandwich composites. The nondimensional parameters are as published by Nemeth [24] and are tailored for the structure and loadcase of interest by Schultz and Nemeth [26]. Both the prototype, or baseline cylindrical shell, and the model were constructed from the same materials which are carbon fiber epoxy and aluminium honeycomb core. Two baseline cylindrical shells, which are simplified sub scale launch-vehicle designs, were scaled. The assumptions for the buckling equations consist of small strains and the neglect of flexural anisotropy, transverse-shear deformations, initial geometric imperfections and it is noted that the last two assumptions might not be valid for every case. The analysis starts with defining the compatiblity and equilibrium equations after which the nondimensional parameters are specified. The similarity conditions, or scaling laws as named in previous papers, are equal to the nondimensional parameters itself. The advantage of the presented methodology is that the parameters are decoupled and can thus be calculated in a certain order. The first nondimensional parameters to be calculated are the membrane orthotropy parameter and the flexural orthotropy parameter. For this research two stacking sequences were considered, which includes one variable for the fibre orientation. With the material properties being constant and the influence of the core being negligible, the dependency being left is the dependency on the fibre orientation. Both parameters match the baseline value for practically the same fibre orientation. With two baseline cylindrical shells and two matches per parameter, this resulted in a total of 4 fibre orientation and stacking sequence combos for the scaled cylindrical shells, see Figure 2.22. The next step in the analyses is to compare the parameters which define the relation between the radius to length ratio and membrane compliance, and the same ratio and the bending stiffnesses, see Figure 2.23. With the stacking sequence and fibre orientation already determined and the core influences being negligible, the dependency that is left is the radius over length ratio which is linear. As with the previous two parameters, the ratio for matching parameters between scaled models and baseline cylindrical shells is practically equal for both parameters, which ultimately lead to a single solution for each scaled cylindrical shell. The nondimensional parameter that is left is the Batdorf-Stein parameter. The dependencies that are left after previous calculations are the radius and core thickness. As the radius of the cylindrical shell is limited by the testing equipment as an upperbound, only the core thickness is left to be determined which is limited by the manufacturability, see Figure 2.24.

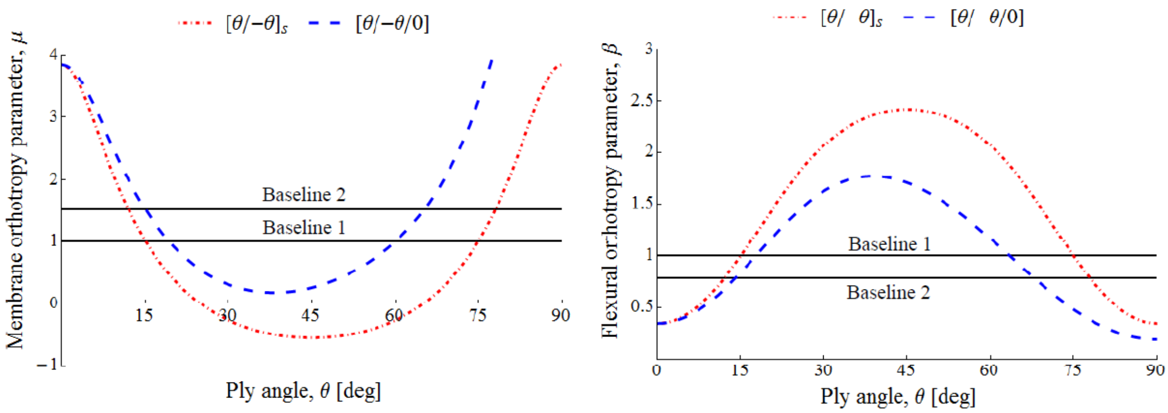

(a) Membrane orthotropy parameter, μ (b) Flexural orthotropy parameter, β

Figure 2.22: Membrane and flexural orthotropy nondimensional parameter [4].

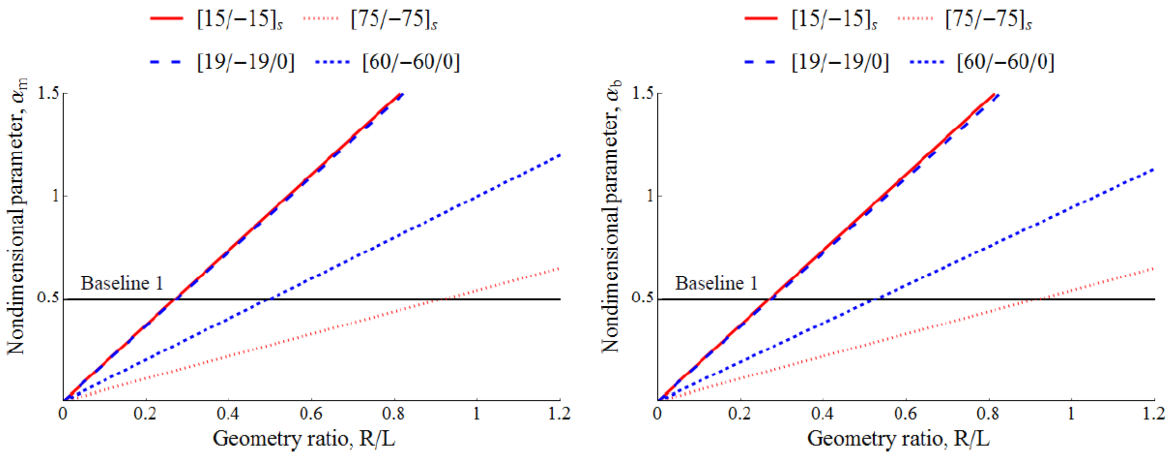

(a) Nondimensional parameter, α_m (b) Nondimensional parameter, α_b

Figure 2.23: Radius over length dependency for baseline 1 configurations [4].

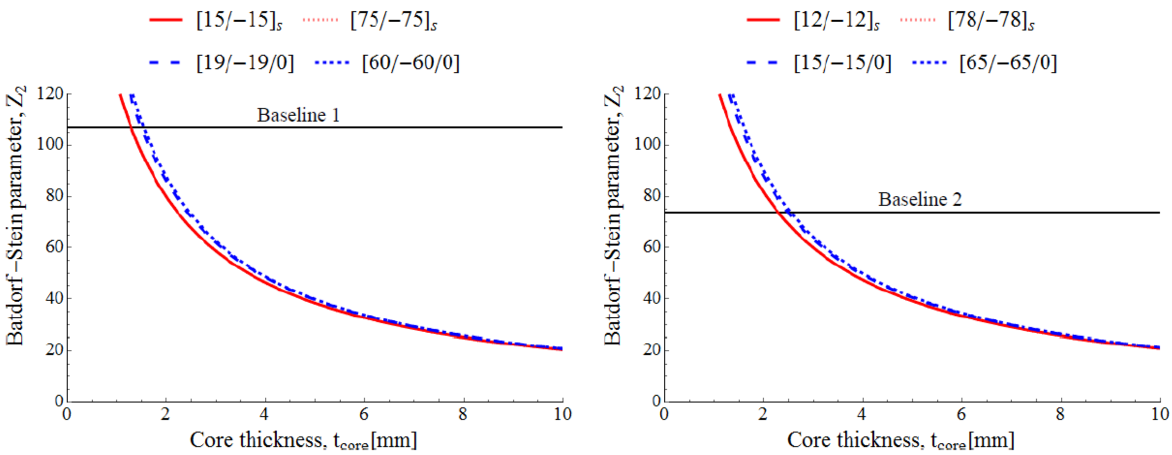

(a) Batdorf-Stein parameter, Z_2 for Baseline 1 scaled configurations (b) Batdorf-Stein parameter, Z_2 for Baseline 2 scaled configurations

Figure 2.24: The Batdorf-Stein parameter [4].

The core thicknesses were then determined. With all the variables determined for the resulting eight scaled cylindrical shells, the nondimensional parameters are then calculated. When comparing the nondimensional parameters for the baseline and scaled cylindrical shells, it can be seen that there were some deviations. Especially the flexural orthotropy parameter shows substantial deviation, up to 20% for one of the configurations. Next an evaluation is done to determine the effect of the flexural anisotropy as this was neglected during the formulation of the nondimensional parameters. These effects can be determined by comparing elements of the constitutive relations that relate moment elements to curvature elements. It was seen that one of the stacking sequences as used for the analyses part, showed a large influence by the flexural anisotropy and was therefore discarded. The last step is the verification of the methodology. The buckling mode and buckling load is first compared for the baseline and scaled cylindrical shells. This consists of the axial half waves, circumferential full waves, nondimensional load parameter and the buckling load itself. It can be seen that the buckling modes are a match, and that the nondimensional load parameter only shows a small deviation of less then 1 %. The buckling load is then determined by the method of Schultz and Nemeth [26] and another method which is based on different assumptions and formulations. This comparison is deemed to be a good indication whether the flexural anisotropy can be neglected or not. It is then shown that there is a considerable difference in buckling loads, especially for two of the four scaled cylindrical shells which are then also disregarded leaving two scaled cylindrical shells for the last test by finite element. The finite element analyses were executed by using the software package Abaqus. The model consisted of S4R elements, as the core of the sandwich was deemed thin enough to be modelled as a ply in the layup. The buckling loads for the four models are then determined by explicit nonlinear dynamic analyses and compared to the analytical solutions. The difference in loads is quite small, ranging from 1.1 % to 8.82 %, and is considered to be caused by the assumptions of neglecting anisotropy effects and transverse shear compliance. The last comparison is that of the buckling modes. The modes of both the baseline and scaled cylindrical shell FE models match, but are different compared to the buckling modes resulting from the analytical analyses. This methodology thus showed great results, it is however noted by the authors that the range of the method can be improved by including the flexural anisotropy and transverse shear.

In 2018 Przekop et al. [54] published a paper which is part of the SBKF project. Buckling critical cylindrical composite test articles were designed from real launch vehicle data. The scaled designs are called sub-scale. Analytical design methods were developed as part of this project, but these methods still have to be validated by experimental methods. These experimental tests were accompanied by Finite Element Models (FEM) for which Abaqus is being used. The method to determine the design of the test article, was described as being a practical engineering approach. Several nondimensional parameters were used, of which geometry and sandwich stiffness ratios, for the design. It is noted that the parameters as published by Nemeth [24] were calculated and considered, but are not a direct part of the design process. The geometric parameters consist of the radius over effective thickness ratio, which is a indication of the thinness of the cylindrical shell, next to the length over diameter ratio. The buckling response of cylindrical shells is highly affected by the membrane and bending stiffnesses and is thus an important factor in determining the design of the scaled models. The parameters used for the design are based on these stiffnesses, in particular the ratios between these stiffnesses. For the case of a sandwich composite, the buckling response is primarily affected by the bending stiffness, and the membrane stiffness is therefore left out. The first step was to calculate these nondimensional parameters for existing launch-vehicle cylindrical-shell designs which consist of real,proposed and other designs determined by the SBKF project. The next step was to determine loads for several failure modes, to ensure that the test article had global buckling as failure. These steps generated over 100000 designs, which were then reduced by limiting the buckling loads, a safe margin below the maximum of the testing facilities, and strain at the critical buckling load. Further reduction was reached by selected designs that assured a large range of the nondimensional parameters, which ultimately resulted in 5 test article designs. The analysis and experimental test of the first article, named CTA8.1, was published by Schultz et al. [13] in a separate paper. The second test article is then designed in detail and a FE model is created. The detailed design focuses on the manufacturing method and the buildup of the facesheet at the edge of the cylindrical shell for load introduction. The FEM model was introduced to include more elements from the experimental test setup. The attachment rings were included and the pad-ups were added as well. The cylindrical shell and included parts of the test setup were modelled using a S4R element, where the sandwich cylindrical shell was modelled as a laminate with the core being seen as a single ply. After the design of the test article was modified according to the FE results, the rest of the test setup was included in the model as well. The extra additions included the steel load introduction frame among other parts. These were included to properly model the influence of the test fixture on the structural behaviour. Then the results of the FE analysis are presented and graphed. The results consist of a stability comparison, displacement, strains and buckling loads for both eigenvalue and nonlinear transient methods which are then compared to closed-form solutions. Furthermore the influence of imperfections was researched, by using the imperfections from a previously manufactured cylindrical shell which resulted in a bucking load reduction of 13.8%. At first a uniform mesh was used, from the first analyses it was seen that there was a load plateau after buckling. A random perturbed mesh was then used and prevented this previous numerical phenomena from happening again. The comparison between both FE methods and closed-form analyses, showed that both the buckling loads and strain values varied between methods up to 30 or even 50 % depending on the test article. Two of the designs were also altered, as they showed large strains at the corresponding buckling loads. It can be concluded that the design of test articles according to this method is quite extensive, as that it requires several steps and design alterations when problems occur. It does have its advantages though, as it has a higher degree of certainty that the test articles will show similar structural behaviour compared to the full-scale cylindrical shells, and still has a high cost advantage compared to full-scale testing.

2.2.4 Remarks for Scaling Methods

The scaling methods as shown have a wide variety of what is actually being scaled. From scaling the geometry and dimensions to scaling of structural behaviour. It is noteworthy to say that scaling for structural behaviour and strength by using similitude theory seems to be hardly used in the aerospace industry in recent years, which might be an indication that its disadvantages prevent it from being used more often. The demands on the scaled structure for complete similarity can make the scaled model almost impossible to manufacture or constraint the scaling factor, while distorted models can result in large inaccuracies when multiple scaling laws can't be satisfied. The scaling method of using nondimensional parameters is very recent, and while scaled models have been created and modelled with success, it's still the question what the test results of these scaled cylindrical shells mean for the full scale cylindrical shell. As the effect of the imperfections on different scales might still vary. The test results from these scaled cylindrical shells are most ideal for validating FE models and methods, as the behaviour should be as close as possible to the behaviour of the full scale cylindrical shell without actually testing the full scale cylindrical shell.

2.3 Concluding Remarks Literature Review

The research as shown in this literature review just touches the surface of the amount of research that has been done concerning buckling of cylindrical shells, let alone for general shell buckling. While extensive research has been done, there are still critical questions to be answered, especially for the case of a composite material. The inclusion of imperfections, and especially the imperfection sensitivity, increases the complexity of both the analytical and numerical solutions for buckling load calculations. The statistical methods come into play when scatter signatures need to be determined for all the different types of imperfections, each having a different effect on the buckling load [9, 10]. Although the general goal of a large portion of the research groups is to minimize the experimental testing due to costs [3, 6], these tests are still needed to validate new methods, next to establishing a database for imperfections and their signatures. Considering that a large portion of test data used till this day, originates from as far back as the 50s and might thus not be representative for the current manufacturing accuracy and materials.

The cost of experimental testing is also one of the reasons for renewed interest in scaled models. Smaller test specimens lead to lower costs, caused by both lower material and manufacturing costs and lower testing equipment requirements. Although, not as popular compared to the topic on buckling of shells, scale models have been a topic of interest since the 60s [46] and have picked up renewed interest with research groups suchs as the SBKF project group [4, 54]. It's unfortunate however, that this hasn't lead to a definite answer on what information a scaled model can provide to predict the full scale behaviour. Several scaling theories and methods have been shown, even specifically for buckling of cylindrical composite shells [31, 32]. It seems that the relation between scaled model and full scale prototype is partially unknown because of three main issues. The first consists of problems with distorted models causing inaccuracies, for example similitude theory by governing differential equations focusses on the scaling of the buckling load, but multiple distortions can cause a scaled model to be non representative. Secondly, the methods that focus on scaling the behaviour, such as the nondimensional parameters method [4], these studies do not have an answer yet on what test results of these scaled models tell about the full scale model, next to that these scaled models should be ideal for numerical validation. This method has lead to test specimens which are manufacturable, and shows thus great promise in the practical sense compared to similitude theory. The third and final problem are the imperfections and how these could be scaled or not. The different scales of a structures could have different imperfection signatures and imperfection sensitivity, which is still a large unknown. It would be ideal if imperfections, as measured from a scaled model, could be scaled to a full scale prototype by using dimensional analyses with respect to the geometry in combination with a statistical method for the determination of the scatter for the use in numerical simulations. The problem however is that this will require a database of imperfections combined with a separate research that only focusses on imperfections.

To increase the general understanding of the relation between scaled models and a full scale prototype, a step-by-step approach seems most logical to distinguish the different influences on the structural behaviour. Starting with numerical simulations of both the scaled model and full scale prototype [4] to determine similarities and dissimilar behaviour. After which the imperfections can be included by scaling them to the full scale prototype, to see the different behaviour as a function of the imperfections and their scale. The downside of the last step is that it incorporates two factors of influence, the scalability of imperfections and the imperfection sensitivity of the different scales of cylindrical shells. It might be of interest to come up with a method to separate these two influences by, for example, using an imperfection amplitude [32], which can be varied and applied to cylindrical shells of different scales.

2.4 Research Question, Aims and Objectives

The main objective of the literature review was to acquire knowledge on buckling of cylindrical shells and scaling of structures. There are **no** recent results of the scaling of cylindrical shells and how representative these cylindrical shells are in comparison to the full scale cylindrical shell. The most recent scaling method for cylindrical composite shells, published in 2018 by Uriol Balbin et al. [4], has resulted in scaled configurations of a full-scale cylindrical shell developed by NASA. However, these scaled cylindrical shells have not been studied yet, and the validity of the scaling method is still unknown, although showing good promise. From this unknown the following research objectives and questions are defined.

2.4.1 Research Objective

The main objective of the thesis is to investigate if the scaling method by Uriol Balbin et al. [4] results in representative scaled cylindrical composite shells, which will be validated by experimental tests at NASA Langley. This research will consist of a numerical investigation with the main focus on two scaled cylindrical shells.

Due to the cylindrical shell being an imperfection sensitive structure, the numerical modelling can be challenging. Therefore, the research is divided into three sub-objectives. The first sub-objective is to get a greater understanding of the general modelling of a cylindrical shell. Using different elements and material configurations to compare results, and determine how an accurate FE model can be developed. The second sub-objective is to accurately model both the full scale and scaled cylindrical shells. This includes investigating the imperfection sensitivity of these cylindrical shells to different imperfection types, next to an investigation into the influence of numerical parameters on the buckling behaviour of cylindrical shells. The last sub-objective is to create a comparison for the full scale and scaled cylindrical shells to determine how representative the scaled cylindrical shells actually are. It is thus both the method to reach the understanding of the relation between scaled and full-scaled cylindrical shell, and the gained knowledge on scaled cylindrical shells which are goals for the following thesis.

2.4.2 Research Questions

From the research objective as stated, a research question with accompanying sub questions will be formulated.

- What methodology can assess if a scaled cylindrical shell can show full scale representative behaviour?
  - What is the most accurate method of modelling a cylindrical shell numerically?
  - How does each type of imperfection influence the buckling behaviour of both scaled and full scaled cylindrical shells?
  - What is the influence of the scale of the cylindrical composite shell to the imperfection sensitivity?
  - What method can be used to compare results from cylindrical shells of different scales?

Chapter 3

Preliminary Analysis of a Cylindrical Shell

This chapter will describe the preliminary analyses on a cylindrical shell, 800 mm diameter and 800 mm length. The 800 mm diameter was chosen as it is the maximum diameter possible for testing equipment intended to be used later on in the project, this diameter is also a constraint for the development of a scaled cylindrical shell. The analyses that were executed were done according a step by step process. This was partially done to get acquainted with the software package Abaqus, in combination with the modelling of a cylindrical structure and its challenges. It also gave a good knowledge base for more detailed and time consuming analyses later on in the thesis. Both isotropic and composite materials were used. Starting with an isotropic material, in order to focus on the modelling of the structure itself, without having to deal with the challenges of modelling a composite material from the beginning. After a basis is established for the modelling of this cylindrical shell, further analyses will focus on the modelling of a composite cylindrical shell. All cylindrical shells considered in this chapter do not include imperfections.

3.1 Aluminium Cylindrical shell

The first cylindrical shell to be modelled will have a diameter and length of 800 mm and 800 mm respectively, in combination with a shell thickness of 1 mm and 2 mm. It will make use of a commonly used aluminium alloy namely 2024 T4, of which the properties are reported in Table 3.1. The buckling loads resulting from the FE analyses were compared with analytical buckling loads according to NASA SP-8007 [2]. The analytical buckling loads can be seen in Table 3.2. The analytical buckling load calculations require operations of the classical laminate theory, for which Kassapoglou [55] was used. First the modelling technique used for the structure type of interest was explained. After which a mesh size sensitivity investigation was executed, by comparing buckling load, stiffness and modeshape. This is followed by an element comparison for two different mesh sizes.

Table 3.1: Aluminium 2024 T4 Material Properties.

E [MPa]	ν
73100	0.33

Table 3.2: Analytical buckling loads for the aluminium cylindrical shell without imperfection according to NASA SP-8007 [2].

Shell Thickness [mm]	1	3
Buckling load [kN]	280.91	2528.23

3.1.1 Modelling Technique

This section will focus on the FE models used for the following sections. The meshes used will always be regular. This is a convenient way of meshing when the meshes need to be comparable for all elements. Otherwise the results may depend more on the mesh itself, instead of the general mesh size and element type. A comparison between a non-structured and structured mesh can be seen in Figure 3.1. A non-structured mesh could be of interest when certain zones need a finer mesh, while zones which are not of interest can be meshed coarser to increase the computational efficiency. A convenient way of applying boundary conditions is to use reference points. These reference points are tied to each side of the structure by a rigid body tie, which transfers the boundary condition applied to the reference point to the appointed edge. The boundary conditions used are: clamped on one side and clamped except for the longitudinal direction on the opposing side. The type of loading might differ between displacement and force based through the chapter, but will always be in axial direction. The use of reference points furthermore simplifies the output for a load-displacement graph, as the reference point where the load is applied, will output the total load and corresponding displacement without having to sum the reaction force of all the nodes on the edge.

3.1.2 Mesh Sensitivity Analysis

For the mesh sensitivity analysis, the S4R element was used. This is a 4 noded conventional shell element, which has both displacement and rotational degrees of freedom. A shell thickness of 1 mm is used in combination with mesh sizes of: 20 mm, 10 mm and 5 mm. The type of analyses used are eigenvalue analysis and linear static analysis, where the applied load for the linear static analysis is equal to the analytical buckling load. This will result in a comparison for buckling load and modeshape as a result of the eigenvalue analysis, and a comparison for stiffness resulting from the linear static analyses. This resulted in the data reported in Table 3.3 and the modeshapes shown in Figure 3.3.

The table reporting the results consist of the buckling load of the first five eigenmodes resulting from the eigenvalue analyses, next to the resulting displacement from the applied load of the linear static analyses. Both the buckling load values and displacement values are within 1% for all mesh sizes, with the largest change seen between the 20 mm and 10 mm mesh. The buckling load shows a maximum difference with respect to the analytical buckling load of 1.2% for the 20 mm mesh, which can already be considered accurate enough. The 20 mm mesh is too coarse which leads to some of the half waves being irregular. The 5 mm mesh results in a different modeshape in comparison to the 10 mm and 20 mm mesh.

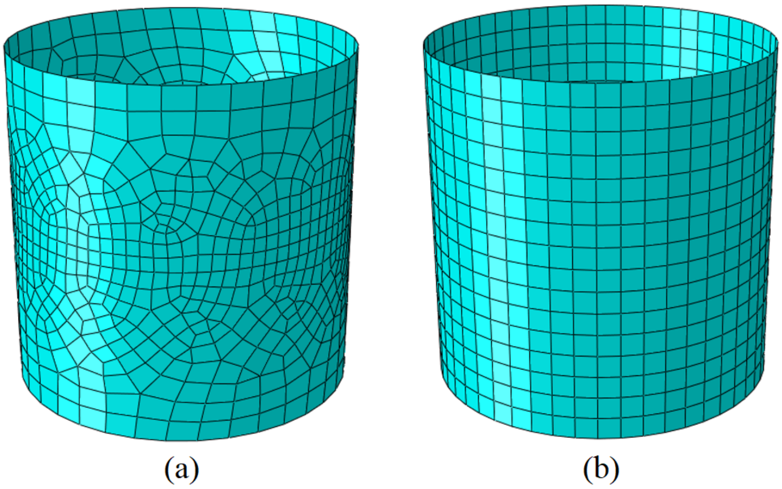

Figure 3.1: Comparison of a non-structured (a) and (b) structured mesh.

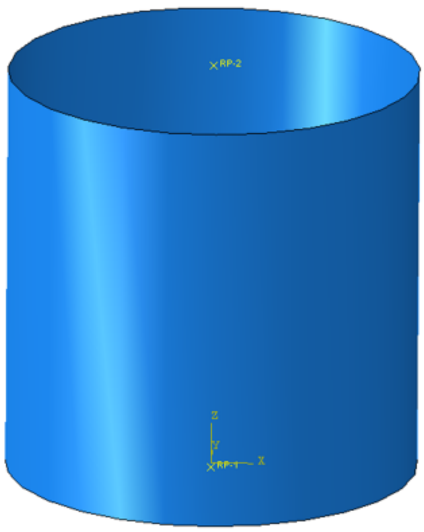

Figure 3.2: FE model of the 800 mm x 800 mm cylindrical shell.

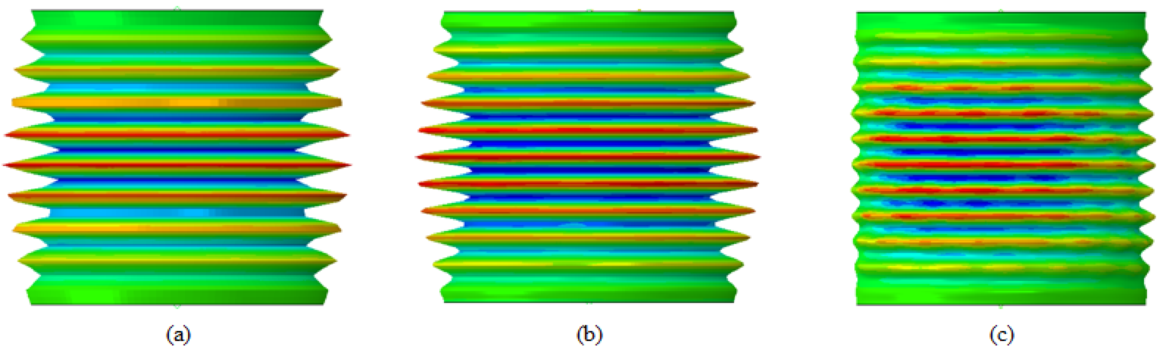

Figure 3.3: Modeshape comparison for the aluminium cylindrical shell, showing radial displacement for mesh sizes: (a) 20 mm, (b) 10 mm and (c) 5 mm.

Table 3.3: Mesh size sensitivity result data for the aluminium cylindrical shell.

Alu. 2024 T4 1 mm thickness			
Element	S4R	S4R	S4R
Mesh size [mm]	20	10	5
Eigenvalue Analyses			
CPU time [s]	77.50	1202.10	9062.80
Force eigenmode 1 [kN]	284.32	282.20	281.80
Force eigenmode 2 [kN]	284.49	282.24	281.80
Force eigenmode 3 [kN]	284.49	282.24	281.81
Force eigenmode 4 [kN]	284.58	282.29	281.82
Force eigenmode 5 [kN]	284.75	282.33	281.83
Linear Static Analyses, Force of 280.91kN			
CPU time [s]	1	7.8	40
Displacement [mm]	1.218	1.220	1.220

The 5 mm mesh shows an asymmetric modeshape and some irregularities of the half waves as well. It seems that these irregularities are not caused by the mesh being too coarse, but just being part of the modeshape. The increase in CPU time is substitutional, especially if the CPU time between the 20 mm and 5 mm mesh is compared. Finer meshes than 5 mm could be considered when looking at the modeshape alone. However, the buckling load shows convergence and a finer mesh would increase the CPU time. It was therefore decided that finer meshes were unnecessary. Especially when it is considered that these are linear analyses, the increase in CPU time for an even finer mesh would become a problem for non-linear analyses further on during the thesis.

3.1.3 Element Comparison

For the element comparison, 4 elements were considered: the S4R element as previously mentioned, the 8 noded continuum shell SC8R element, the 8 noded continuum solid shell CSS8 element and the 8 noded classical brick C3D8R element. All of these elements, except for the S4R element, uses only displacement degrees of freedom, while the S4R element uses both rotational as displacement degrees of freedom. The CSS8 element is new in the 2017 version of Abaqus, and is said to show superior bending behaviour for a solid element and suitable for both solid composites and 3D material models. For the CSS8 and C3D8R element, both 1 and 3 elements through the thickness (T-t-T) were compared, and for the S4R and SC8R element 1 element through the thickness was used. Both a shell thickness of 1 mm and 3 mm was used, as each type of element might react differently to the thickness. For the comparison an eigenvalue analysis was used, next to linear static analysis. As this results in a large amount of analyses, a mesh size of 10 mm was chosen to somewhat limit total CPU time for the first part of the comparison, after which a fine mesh of 5 mm is used for the final comparison.

1 mm Shell Thickness

The results for a shell thickness of 1 mm are reported in Table 3.4. The results consist of the buckling loads for the first five eigenmodes resulting from the eigenvalue analyses for all element combinations, next to the resulting displacement from the linear static analyses. The CPU time of each analysis is also reported, as a relative comparison. The corresponding modeshapes of the eigenvalue analyses are shown in Figure 3.4. The first thing to notice is that the results of the C3D8R element with 1 element through the thickness are inaccurate and the modeshape shows irregularities as well. When 3 elements through the thickness are used with the C3D8R element, the results improve drastically, but are not on the level of the results from the other elements. The results of the S4R element are then used as the main comparison for the other element combinations, for which the percentage difference was calculated.

With the results of the C3D8R element out of consideration, the maximum error for both buckling load and displacement w.r.t. the S4R element is 3.3%, see Table 3.5. The maximum error for the displacement is 0.2%. This level of agreement can be considered sufficient, but it should be said that the buckling load resulting from the S4R element is closest to the analytical buckling load of 280.91kN. The modeshape of the S4R and SC8R elements show agreement, while the modeshape of the CSS8 element is different for both configurations. This might be caused by the CSS8 element can be considered both a shell and solid element, while the S4R and SC8R elements are shells. The S4R and SC8R element show a axisymmetric modeshape, while the CSS8 with 1 element through the thickness shows a asymmetric modeshape with wrinkling of the waves. The CSS8 element with three elements through the thickness, shows a diamond modeshape. The difference between the two configurations using the CSS8 element might be caused due to the difference in degrees of freedom, due to the increase in nodes. When comparing CPU time, the S4R and SC8R element are close, but the CSS8 element is computationally less efficient. Using 3 elements through the thickness for the CSS8 element is also unnecessary, as the difference between the results is negligible and the CPU time increasing considerably.

Table 3.4: Result data aluminium cylindrical shell thickness of 1 mm and mesh size of 10 mm.

2024 T4 1 mm Thickness						
Element Elements through thickn.	S4R 1	SC8R 1	CSS8 1	CSS8 3	C3D8R 1	C3D8R 3
Eigenvalue Analyses						
CPU time [s]	1202.10	1247.50	4267.60	21840.00	125.30	312.00
Force eigenmode 1 [kN]	282.20	289.23	291.30	291.52	29.82	286.87
Force eigenmode 2 [kN]	282.24	289.26	291.31	291.54	29.82	286.93
Force eigenmode 3 [kN]	282.24	289.26	291.34	291.57	30.11	290.96
Force eigenmode 4 [kN]	282.29	289.30	291.34	291.59	30.12	291.23
Force eigenmode 5 [kN]	282.33	289.33	291.35	292.08	30.59	297.78
Linear Static Analyses, Applied Force of 280.91kN						
CPU time [s]	7.8	8.8	23.8	75.1	8.3	35.7
Displacement [mm]	1.220	1.217	1.222	1.222	1.224	1.227

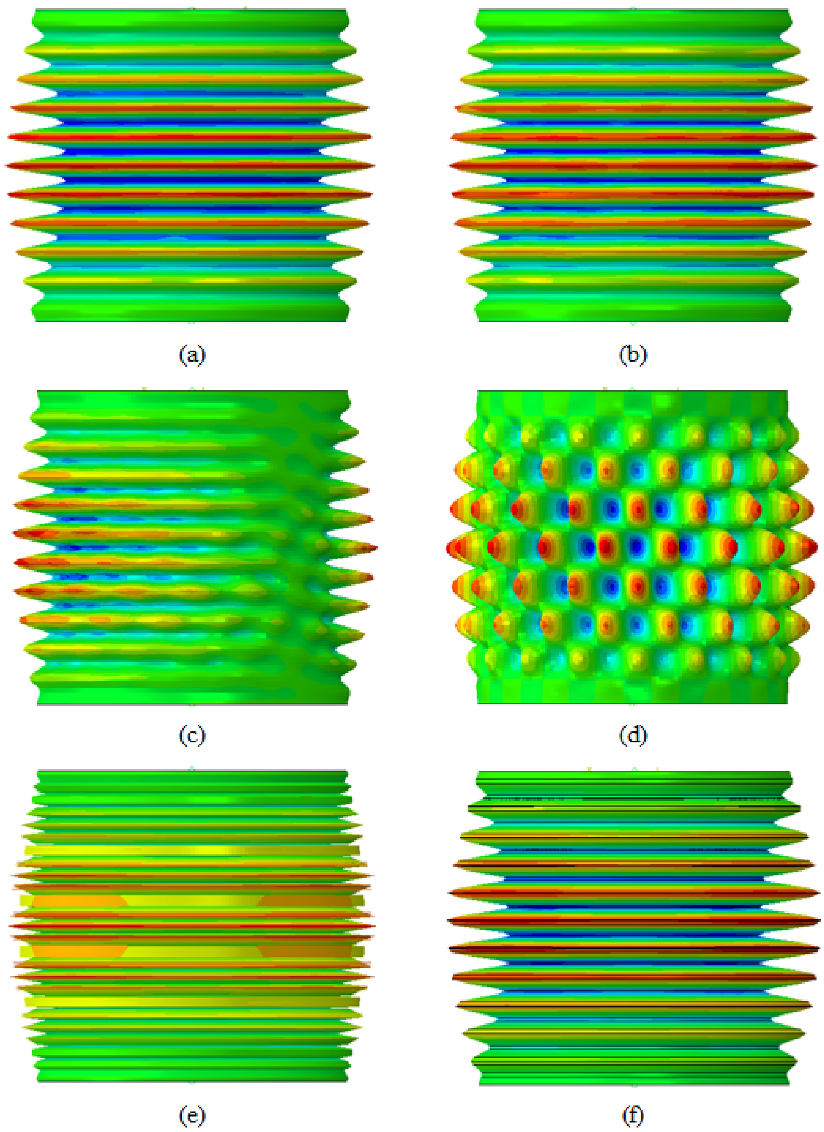

Figure 3.4: Modeshape comparison 1 mm shell thickness and a mesh size of 10 mm, showing radial displacement for 6 different configurations: (a) S4R, (b) SC8R, (c) CSS8 1 T-t-T, (d) CSS8 3 T-t-T, (e) C3D8R 1 T-t-T, (f) C3D8R 3 T-t-T.

Table 3.5: Result data comparison w.r.t. S4R aluminium cylindrical 1 mm shell thickness and mesh size of 10 mm.

2024 T4 1 mm Thickness					
Element Elements through thickn.	SC8R 1	CSS8 1	CSS8 3	C3D8R 1	C3D8R 3
Eigenvalue Analyses					
CPU time	3.8%	255.0%	1716.8%	-89.6%	-74.0%
Force eigenmode 1	2.5%	3.2%	3.3%	-89.4%	1.7%
Force eigenmode 2	2.5%	3.2%	3.3%	-89.4%	1.7%
Force eigenmode 3	2.5%	3.2%	3.3%	-89.3%	3.1%
Force eigenmode 4	2.5%	3.2%	3.3%	-89.3%	3.2%
Force eigenmode 5	2.5%	3.2%	3.5%	-89.2%	5.5%
Linear Static Analyses, Applied Force of 280.91kN					
CPU time	12.8%	205.1%	862.8%	6.4%	357.7%
Displacement	-0.2%	0.2%	0.2%	0.4%	0.6%

3 mm Shell Thickness

The results for a shell thickness of 3 mm are reported in Table 3.6, with the corresponding modeshapes of the eigenvalue analyses shown in Figure 3.5. The results consist of the buckling loads for the first five eigenmodes, with corresponding CPU times as a relative comparison, and the displacement as a result from the linear static analyses. The applied force used for the linear analyses is equal to the analytical buckling load. When reviewing the results, the C3D8R element shows the same problems as for the shell thickness of 1 mm, and is not considered for further analyses or discussions. The most noticeable difference w.r.t. the 1 mm shell thickness results ,is the level of agreement for the modeshapes. As the 4 configurations all show a diamond modeshape which is very similar. The results of the S4R element are again used as the main comparison for the other element combinations, for which the percentage difference was calculated. These percentage differences are reported in Table 3.7. The maximum error is only 0.7% and 0.5% for the buckling load and displacement, respectively. The CSS8 element results in a buckling load closest to the analytical buckling load and again results in the highest CPU times. These results are all very close, and these elements all thus show promising results for this kind of structure.

5 mm Mesh Comparison

The highest error seen in previous comparison of this chapter was for the 1 mm shell thickness. The comparison for the finer mesh will therefore be made with a 1 mm shell thickness. The results of the 5 mm mesh are reported in Table 3.8 and corresponding modeshapes shown in Figure 3.6.

Due to the lower amount of element configurations, both the results of the three element configurations and the difference w.r.t. to the S4R results are reported in the same table. The level of agreement between the resulting buckling load and displacement is more then sufficient and the results from the different elements seem to convergence for finer meshes.

Table 3.6: Result data aluminium cylindrical shell thickness of 3 mm and mesh size of 10 mm.

2024 T4 3 mm Thickness						
Element	S4R	SC8R	CSS8	CSS8	C3D8R	C3D8R
Elements through thickn.	1	1	1	3	1	3
Eigenvalue Analyses						
CPU time [s]	1236.50	1298.40	2543.50	7225.70	344.10	655.60
Force eigenmode 1 [kN]	2548.23	2559.42	2530.49	2530.35	247.77	2414.62
Force eigenmode 2 [kN]	2548.25	2559.43	2530.54	2530.36	247.79	2417.42
Force eigenmode 3 [kN]	2548.72	2560.01	2531.05	2530.91	250.10	2436.46
Force eigenmode 4 [kN]	2548.74	2560.03	2531.07	2530.97	250.14	2436.46
Force eigenmode 5 [kN]	2551.94	2571.07	2541.85	2541.96	250.43	2439.17
Linear Static Analyses, Applied Force of 2528.23kN						
CPU time [s]	7.6	8.7	22	73.6	8.5	35.4
Displacement [mm]	3.657	3.637	3.651	3.651	3.675	3.657

Table 3.7: Result data comparison w.r.t. S4R aluminium cylindrical 3 mm shell thickness and mesh size of 10 mm.

2024 T4 3 mm Thickness					
Element	SC8R	CSS8	CSS8	C3D8R	C3D8R
Elements through thickn.	1	1	3	1	3
Eigenvalue Analyses					
CPU time	5.0%	105.7%	484.4%	-72.2%	-47.0%
Force eigenmode 1	0.4%	-0.7%	-0.7%	-90.3%	-5.2%
Force eigenmode 2	0.4%	-0.7%	-0.7%	-90.3%	-5.1%
Force eigenmode 3	0.4%	-0.7%	-0.7%	-90.2%	-4.4%
Force eigenmode 4	0.4%	-0.7%	-0.7%	-90.2%	-4.4%
Force eigenmode 5	0.7%	-0.4%	-0.4%	-90.2%	-4.4%
Linear Static Analyses, Applied Force of 280.91kN					
CPU time	14.5%	189.5%	868.4%	11.8%	365.8%
Displacement	-0.5%	-0.1%	-0.2%	0.5%	0.0%

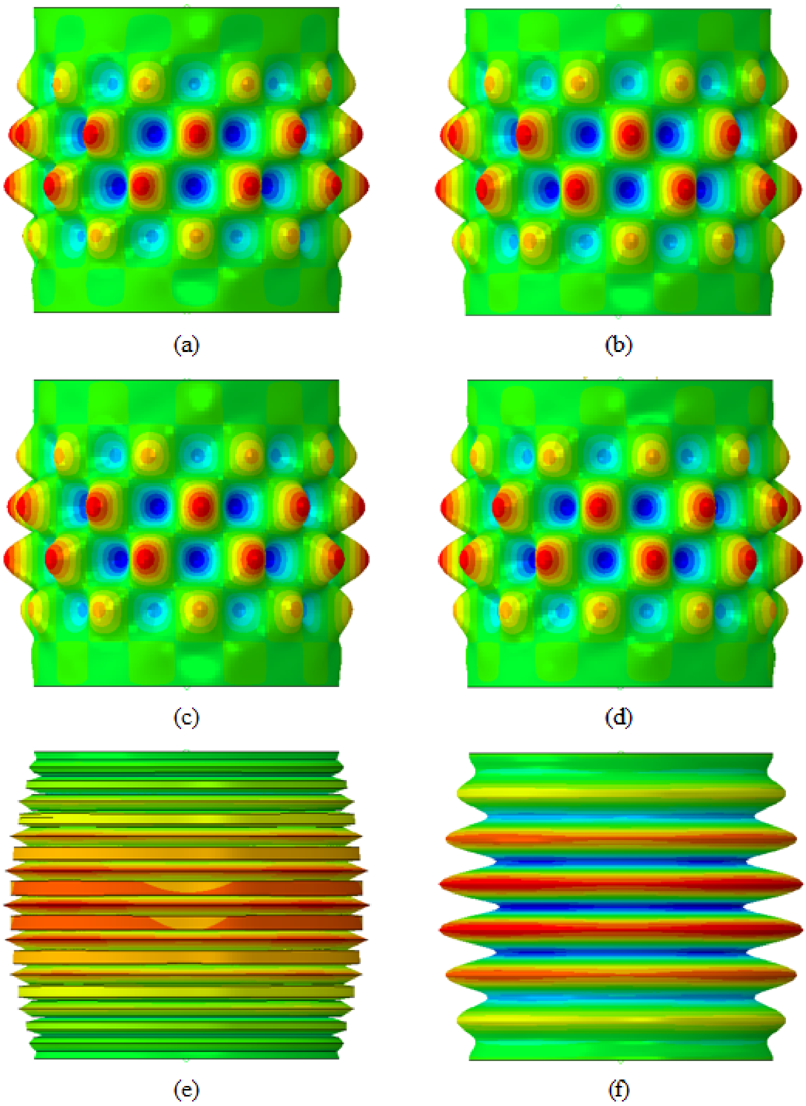

Figure 3.5: Modeshape comparison 3 mm shell thickness and a mesh size of 10 mm, showing radial displacement for 6 different configurations: (a) S4R, (b) SC8R, (c) CSS8 1 T-t-T, (d) CSS8 3 T-t-T, (e) C3D8R 1 T-t-T, (f) C3D8R 3 T-t-T.

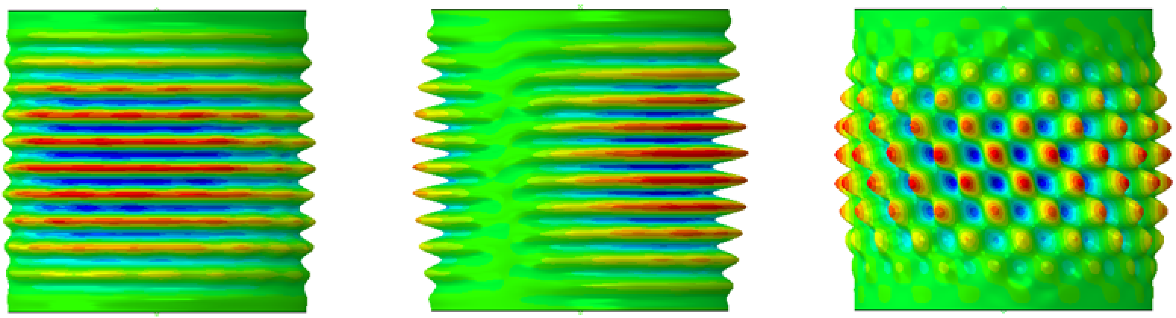

(a) (b) (c)

Figure 3.6: Modeshape comparison for a shell thickness of 1 mm using a mesh size of 5 mm, showing radial displacement for 3 different configurations: (a) S4R, (b) SC8R, (c) CSS8 1 T-t-T.

The modeshape of the S4R and SC8R are in agreement, with the modeshape of the SC8R only rotated around the longitudinal axis. The modeshape of the CSS8 is again different, but now equal to the modeshape previously it showed with a mesh size of 10 mm and 3 elements through the thickness. The modeshapes of the S4R and SC8R element are now similar to the modeshape showed by the CSS8 element with 1 element through the thickness for a mesh size of 10 mm. The difference in CPU time is lower compared to previous analyses, but is still considerably in favour of the S4R and SC8R element.

Table 3.8: Results of the 5 mm mesh for a shell thickness of 1 mm, error w.r.t. S4R shown in shaded columns.

2024 T4 1 mm Shell Thickness					
Element Elements T-t-T	S4R 1	SC8R 1		CSS8 1	
Eigenvalue Analyses					
CPU time [s]	9062.80	8991.30	-0.8%	34242.00	277.8%
Force eigenmode 1 [kN]	281.80	283.96	0.8%	282.53	0.3%
Force eigenmode 2 [kN]	281.80	283.96	0.8%	282.54	0.3%
Force eigenmode 3 [kN]	281.81	283.97	0.8%	282.54	0.3%
Force eigenmode 4 [kN]	281.82	284.00	0.8%	282.56	0.3%
Force eigenmode 5 [kN]	281.83	284.01	0.8%	282.78	0.3%
Linear Static Analyses, Applied Force of 280.91kN					
CPU time [s]	40	46.6	16.5%	96.3	140.8%
Displacement [mm]	1.220	1.216	-0.3%	1.219	-0.1%

3.2 Composite Cylindrical Shell

The next step is to model a composite cylindrical shell which was used for a comparison between the S4R, SC8R and CSS8 element using 4 different layups. The cylindrical shell will have the same dimensions, of 800 mm diameter and 800 mm length. The material used is IM7/8552, see Table 3.9. The layups consist of a 0 layup, a 90 layup, a quasi-isotropic layup and lastly a random generated layup. These layups are chosen to be able to test a wide range of effects, as these layups contain high and low stiffness differences between longitudinal and circumferential direction, and coupling. The layups combined with the corresponding analytical buckling load are shown in Table 3.10. For the comparison, both a force and displacement eigenvalue analyses was used, next to a linear static analysis. For the eigenvalue analyses the first four eigenmodes are requested, instead of the first five in previous comparisons to save computational time. The force eigenvalue analyses is used as it can be compared to the previous results of the aluminium cylindrical shell, while the displacement eigenvalue analyses is used due to next chapters using applied displacement instead of applied force. The linear static analyses are therefore also displacement based.

Table 3.9: IM7/8552 Material Properties.

E_{11} [MPa]	E_{22} [MPa]	ν [-]	G_{12} [MPa]	t_p [mm]
153960	10066	0.3	5930	0.132

Table 3.10: Analytical buckling load for the composite cylindrical shell without imperfection according to NASA SP-8007 [2].

Layup	Buckling load [kN]
$[0]_8$	91.14
$[90]_8$	91.11
$[0, 45, -45, 90]_s$	171.53
$[36, 54 - 14, 31, -44, 83, 41, -34]$	192.34

3.2.1 Material Orientation

The use of a composite layup in combination with 3 types of elements and a cylindrical structure does provide some challenges. The software package Abaqus handles the material orientation for each type element slightly different. For the S4R and SC8R element it is defined by a cylindrical coordinate system, which ensures the stacking direction and the rotation around the stacking direction is consistent for the whole cylindrical shell. For a solid element such as the CSS8 element a different method was chosen. When a cylindrical coordinate system is defined for a structure using a solid element, the 1 direction of the material is applied to the radial direction. This is caused by the fact that a solid element uses a 3D material model and directly uses the radial coordinate system for the material model and not just for the stacking direction and rotation as it would for a shell. One could change the material model itself, to convert the material properties to this cylindrical coordinate system. It was decided to not convert the material properties, as using the same set of material properties for all elements during the comparison was preferred. The second and last possibility that was considered, was to use a discrete definition for the orientation of the material. This is done by defining a surface of the cylindrical shell, which is used for the stacking direction and rotational axis of the plies, combined with defining a primary axis which is in the axial direction of the cylindrical shell. This method defines the material orientation for each element in the input file, which does increase the size of the input file, but it was still the preferred option instead of converting the material properties.

3.2.2 Element Comparison

For each element and layup combination, a force and displacement based eigenvalue analysis was executed next to a linear eigenvalue analysis, all using a mesh size of 5 mm. This results in buckling loads and displacements and a resulting force due to the applied displacement. The displacement for the linear static analyses was chosen so that it would result in a force that was in the same order of magnitude as the eigenvalue results. The results of the linear static analyses are used to compare the stiffness, which is why the resulting force value in itself is not the main interest. The results of the FE analyses are shown in Table 3.11, Table 3.12, Table 3.13 and Table 3.14.

The results do vary slightly, all elements are within 8% for all configurations, and the random generated layup shows the largest spread. This spread is most likely caused due to coupling effects, as the random generated layup is the only layup in this test with considerable coupling. The SC8R and CSS8 results are close for the random generated layup, while the S4R results are showing an offset. This might be due to the S4R element having problems with the coupling effects, while these effects do add stiffness for the SC8R and CSS8 element.

This coupling effect might also be the cause of the CPU time relative differences shown for this layup. In general, S4R has the lowest CPU time. The exception is the random generated layup, where the S4R shows a CPU time which is close to the CSS8 CPU time and considerably higher compared to the SC8R element. The CPU time of the CSS8 element is the highest for all analyses, which was seen for previous FE analyses as well. The CSS8 is computational far less efficient, which is something to take into account for more complex analyses.

When comparing the buckling loads to the analytical buckling loads, it can be seen that the FE analyses show buckling loads within 2% of the analytical solution for the first three layups. For the random generated layup, the difference between analytical and FE results ranges from 6% to 13%, which is most likely also caused by the coupling effects.

The modeshapes resulting from the S4R analyses for the 4 different layups are shown in Figure 3.7. All 3 elements resulted in exactly the same modeshapes for all layups except for the quasi-isotropic layup. Therefore the modeshapes for each element are only shown for the quasi-isotropic layup in Figure 3.8. The 0 and 90 layup both show a diamond modeshape, with the 90 layup showing a much finer diamond pattern in comparison to the 0 layup. The quasi-isotropic and random generated layup show a slightly twisted pattern, with a higher amount of waves in the circumferential direction. The two twisted modeshapes are mirrored, and the random generated layup shows more twist in comparison the quasi-isotropic layup. When comparing the modeshapes for the quasi-isotropic element for each layup, it can be seen that the S4R element results in the modeshape being mirrored compared to the SC8R and CSS8 element. This might be caused by the S4R not having a finite thickness, in comparison of the SC8R and CSS8 element having a finite thickness. When comparing these results to the results of the aluminium cylindrical shell, there are far less differences in modeshapes. This is most likely caused by the modeshape being more pronounced due to the anisotropy of the material, while an isotropic material can results in modeshapes which vary significantly shape wise but are close together for their corresponding load. This is also supported by the fact that the first four modeshapes, looked visually exactly the same for each element for each layup, while the first four modeshapes could vary slightly for the aluminium cylindrical shell.

Table 3.11: Eigenvalue and linear static analyses results for layup: $[0]_8$, difference w.r.t. S4R results are shown in the shaded columns.

Element	S4R	SC8R		CSS8	
Elements T-t-T	1	1		1	
Eigenvalue Analyses, Applied Force					
CPU time [s]	1600.60	1977.40	23.5%	4094.50	155.8%
Force eigenmode 1 [kN]	93.19	93.29	0.1%	92.15	-1.1%
Force eigenmode 2 [kN]	93.19	93.29	0.1%	92.15	-1.1%
Force eigenmode 3 [kN]	93.43	93.54	0.1%	92.31	-1.2%
Force eigenmode 4 [kN]	93.43	93.54	0.1%	92.31	-1.2%
Eigenvalue Analyses, Applied Disp.					
CPU time [s]	1522.80	1893.60	24.3%	3994.60	162.3%
Disp. eigenmode 1 [mm]	0.18	0.18	0.2%	0.18	-1.0%
Disp. eigenmode 2 [mm]	0.18	0.18	0.2%	0.18	-1.0%
Disp. eigenmode 3 [mm]	0.18	0.18	0.2%	0.18	-1.1%
Disp. eigenmode 4 [mm]	0.18	0.18	0.2%	0.18	-1.1%
Linear Static Analyses, Applied Disp. of 0.25 mm					
CPU time [s]	29.4	42.7	45.2%	168	471.4%
Force [kN]	127.748	127.63	-0.1%	127.58	-0.1%

Table 3.12: Eigenvalue and linear static analyses results for layup: $[90]_8$, difference w.r.t. S4R results are shown in the shaded columns.

Element	S4R	SC8R		CSS8	
Elements T-t-T	1	1		1	
Eigenvalue Analyses, Applied Force					
CPU time [s]	3967.30	4416.60	11.3%	9748.50	145.7%
Force eigenmode 1 [kN]	91.66	92.03	0.4%	90.82	-0.9%
Force eigenmode 2 [kN]	91.66	92.03	0.4%	90.82	-0.9%
Force eigenmode 3 [kN]	91.66	92.03	0.4%	90.82	-0.9%
Force eigenmode 4 [kN]	91.66	92.03	0.4%	90.82	-0.9%
Eigenvalue Analyses, Applied Disp.					
CPU time [s]	3931.10	4256.90	8.3%	9355.90	138.0%
Disp. eigenmode 1 [mm]	2.74	2.75	0.0%	2.72	-0.8%
Disp. eigenmode 2 [mm]	2.74	2.75	0.0%	2.72	-0.8%
Disp. eigenmode 3 [mm]	2.74	2.75	0.0%	2.72	-0.8%
Disp. eigenmode 4 [mm]	2.74	2.75	0.0%	2.72	-0.8%
Linear Static Analyses, Applied Disp. of 3 mm					
CPU time [s]	29.4	41.5	41.2%	173.3	489.5%
Force [kN]	100.193	100.551	0.4%	100.091	-0.1%

Table 3.13: Eigenvalue and linear static analyses results for layup: $[0, 45, -45, 90]_s$, difference w.r.t. S4R results are shown in the shaded columns.

Element	S4R	SC8R		CSS8	
Elements T-t-T	1	1		1	
Eigenvalue Analyses, Applied Force					
CPU time [s]	1102.70	1300.00	17.9%	3117.90	182.8%
Force eigenmode 1 [kN]	173.78	173.85	0.0%	169.95	-2.2%
Force eigenmode 2 [kN]	173.78	173.85	0.0%	169.95	-2.2%
Force eigenmode 3 [kN]	173.81	173.90	0.1%	170.07	-2.2%
Force eigenmode 4 [kN]	173.81	173.90	0.1%	170.07	-2.2%
Eigenvalue Analyses, Applied Disp.					
CPU time [s]	1004.80	1334.50	32.8%	2780.80	176.8%
Disp. eigenmode 1 [mm]	0.88	0.88	0.1%	0.86	-2.1%
Disp. eigenmode 2 [mm]	0.88	0.88	0.1%	0.86	-2.1%
Disp. eigenmode 3 [mm]	0.88	0.88	0.1%	0.86	-2.1%
Disp. eigenmode 4 [mm]	0.88	0.88	0.1%	0.86	-2.1%
Linear Static Analyses, Applied Disp. of 1.5 mm					
CPU time [s]	30.1	48.8	62.1%	174.4	479.4%
Force [kN]	297.513	297.386	0.0%	297.214	-0.1%

Table 3.14: Eigenvalue and linear static analyses results for layup: $[36, 54 - 14, 31, -44, 83, 41, -34]$, difference w.r.t. S4R results are shown in the shaded columns.

Element Elements T-t-T	S4R 1	SC8R 1		CSS8 1	
Eigenvalue Analyses, Applied Force					
CPU time [s]	2632.20	1538.50	-41.6%	3096.00	17.6%
Force eigenmode 1 [kN]	167.36	180.09	7.6%	177.02	5.8%
Force eigenmode 2 [kN]	167.36	180.09	7.6%	177.02	5.8%
Force eigenmode 3 [kN]	167.39	180.29	7.7%	177.36	6.0%
Force eigenmode 4 [kN]	167.39	180.29	7.7%	177.36	6.0%
Eigenvalue Analyses, Applied Disp.					
CPU time [s]	2487.70	1350.40	-45.7%	3032.00	21.9%
Disp. eigenmode 1 [mm]	0.96	1.03	7.5%	1.02	5.8%
Disp. eigenmode 2 [mm]	0.96	1.03	7.4%	1.02	5.8%
Disp. eigenmode 3 [mm]	0.96	1.03	7.6%	1.02	6.0%
Disp. eigenmode 4 [mm]	0.96	1.03	7.6%	1.02	6.0%
Linear Static Analyses, Applied Disp. of 1.5 mm					
CPU time [s]	29.5	32.5	10.2%	165.1	459.7%
Force [kN]	261.309	261.471	0.1%	261.307	0.0%

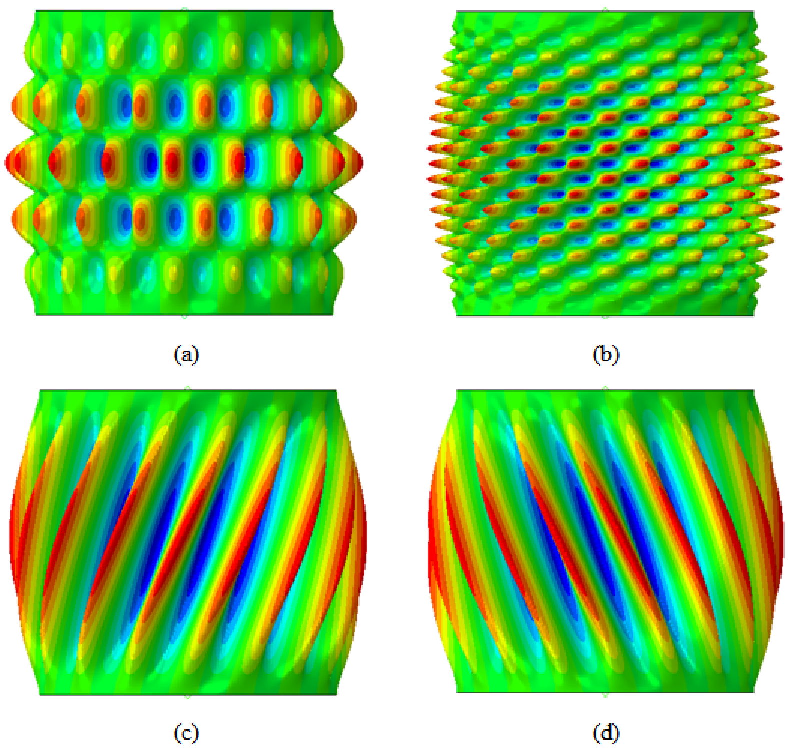

Figure 3.7: Modeshapes for the S4R element, showing radial displacement for 4 different layups: (a) $[0]_8$, (b) $[90]_8$, (c) $[0, 45, -45, 90]_s$, (d) $[36, 54 - 14, 31, -44, 83, 41, -34]$.

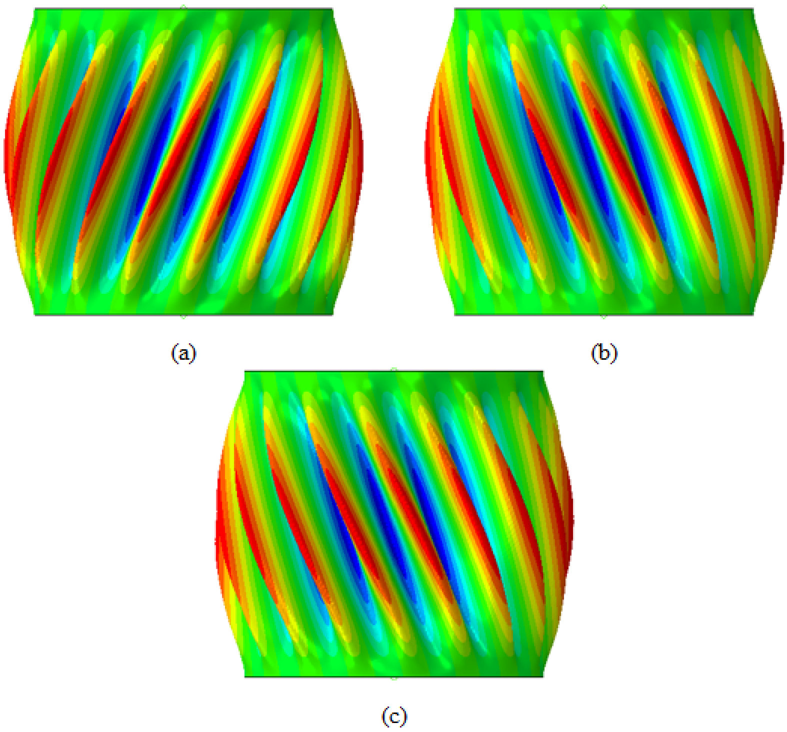

Figure 3.8: Modeshape comparison, showing radial displacement for the quasi-isotropic layup: $[0, 45, -45, 90]_s$, showing radial displacement for 3 configurations: (a) S4R, (b) SC8R, (c) CSS8 1 T-t-T.

3.3 Discussion and Outcome

The preliminary analysis of a cylindrical shell has lead to a set of results, for two types of materials and design combinations. For the mesh sensitivity investigation, a 10 mm mesh already showed great results, while there were differences seen when a mesh of 5 mm was used. A 5 mm mesh is deemed to be the better option for next chapters, not just because of the results seen in this chapter, but also due to the investigations into imperfections. The imperfections itself will be more accurately modelled with a finer mesh, and it is preferred to be consistent with the mesh size to be able to compare all the results. Three elements have shown great results, which are the S4R, SC8R and CSS8 element. The S4R and SC8R element are in favour when compared to the other elements based on the results in this chapter. They are computational efficient, show buckling loads close to the analytical solution and are convenient to model as well. In general the S4R showed to be less sensitive to mesh size in comparison to the other elements. The CSS8 element is very useful as well, but it should only be used when a 3D material model is needed or for other element comparisons, as it is computationally inefficient in comparison to the other two elements when modelling a shell.

3.4 Summary

The chapter showed a large set of results of linear FE analyses for a 800 mm x 800 mm cylindrical shell using both aluminium and composite materials. A mesh size comparison was executed, which showed that reasonable results could be achieved for a mesh size of 20 mm. A mesh size of 10 mm resulted in a similar modeshape as the 20 mm mesh and the mesh size of 5 mm showed a different modeshape compared to the two other mesh sizes. A element comparison was executed for both a mesh size of 10 mm and two shell thicknesses, which saw good results from the S4R, SC8R and CSS8 element. The buckling loads are close for all three elements, where the biggest difference between the elements is seen for the resulting modeshape. The C3D8R element showed inaccurate results, and was therefore discarded for following analyses. A second element comparison was executed for a mesh size of 5 mm using the thin shell, which showed that the results from all elements converged further towards each other.

Then a composite cylindrical shell was used for a element comparison using four different layups. The elements used for the composite cylindrical shell showed good agreement for the buckling load and displacements and corresponding modeshapes. The main difference w.r.t. the results of the aluminium cylindrical shell is that the composite cylindrical shell showed better agreement for the modeshapes, which is most likely caused by the modeshape being more pronounced for a composite material compared to a isotropic material. The FE analyses of the aluminium cylindrical shell showed buckling loads close to the analytical solution. The composite cylindrical shell showed similar buckling loads resulting from the FE analyses and analytical solution for three out of four layups. The layup that showed a difference in buckling loads, is a random generated layup with a considerable amount of coupling which is most likely the cause of this difference.

Chapter 4

Scaled Solid Laminate Cylindrical Shell

This chapter will go in depth on the scaled solid laminate cylindrical shell which was designed according to the scaling procedure as published in 2018 by Uriol Balbin et al. [4]. The focus is again on FE analyses, to investigate if this scaled cylindrical shells do provide representative behaviour of its full scale counterpart. The scaled cylindrical shell is a scaled version of the CTA 8.1 cylindrical shell, which was elaborated on in the literature review. The FE analyses will focus on an element comparison, containing the S4R, SC8R and CSS8 element, next to comparing different types of imperfections. The comparison including different types of imperfections at different amplitudes should provide insight on the imperfection sensitivity of this cylindrical shell. At first a simplified version of the scaled cylindrical shells was used, excluding the edges which containing pad-ups and potting for load introduction. This considerably simplifies the creation of FE models, which is convenient for the large portion of FE analyses to be executed. In the latter part of the chapter, a test article version of the scaled cylindrical shells was modelled.

4.1 Solid Laminate Cylindrical Shell

The solid laminate cylindrical shell is the first scaled configuration that was modelled. The scaling procedure uses a set of six equations, which are based on both the geometry of the cylindrical shell and the stiffness and compliance matrices of the composite laminate. The resulting nondimensional parameters as a result of the six equations, are firstly calculated for the full scale cylindrical shell. After which the scaling procedure determines the scaled cylindrical shell, by matching these nondimensional parameters with the full scale cylindrical shell. One of these equations include the nondimensional load, which was used to compare the FE results of the different scales in the last chapter. The choice for a solid laminate is due to manufacturing problems with scaled sandwich composite cylindrical shells, as the scaling process can result in a core thickness which is too thin to manufacture. It is therefore of interest, to investigate if the full scale and scaled cylindrical shell both need to be of the same construction type or not. It would be ideal if a scaled cylindrical shell constructed from a solid laminate, can show representative behaviour for a full scale sandwich cylindrical shell. This would increase the design space of scaled cylindrical shells immensely and could decrease cost of scaled test cylindrical shells. The imperfection sensitivity is one of the main interests of the scaled cylindrical shells. As the imperfection sensitivity can be one of the indications if the cylindrical shell was representative for the full scale cylindrical shell or not. The different scales of cylindrical shells might need different manufacturing methods, which will lead to different imperfection signatures. Even if the cylindrical shell without imperfection can show representative behaviour, it is more important that the behaviour is also representative when actual imperfections are included. This would more closely represent the general problem, as a structure without imperfection does not exist in practice.

The first portion of FE analyses, will use a slightly shortened version of the scaled solid laminate cylindrical shell. As the edges of the cylindrical shell contain padups and potting, these edge areas add considerable complexity to the model while not having a considerable influence on the element comparison or imperfection type comparison. Therefore, only the middle part of the cylindrical shell with one consistent layup was modelled firstly, for which the structural properties are shown in Table 4.1. The cylindrical shell was constructed of the IM7/8552 composite material, of which the properties of this material can be seen in Table 4.2. These properties are slightly different compared to the IM7/8552 used in the chapter about the 800 mm x 800 mm cylindrical shell. At this part of the thesis, new material properties were received for the batch of materials which would be used, which were implemented. This does not influence the conclusions from the previous chapter, as those conclusions are based on the comparisons and not the actual result values itself. The general modelling technique is equal to the explanation shown in subsection 3.1.1. This cylindrical shell will also be used for an imperfection sensitivity investigation and therefore both the analytical buckling load for a cylindrical shell with and without imperfections was calculated, see Table 4.3.

Table 4.1: Solid laminate scaled configuration.

Layup	$[23, 0, -23]_{4s}$
Diameter [mm]	800
Length [mm]	1120

Table 4.2: IM7/8552 Material Properties. Material strength from [56]. Strain values based on CLT calculations from material strength data.

E_{11} [MPa]	E_{22} [MPa]	ν [-]	G_{12} [MPa]	ρ [kg/m^3]	t_p [mm]
140928	9721	0.356	4688	1580	0.175
F_1^{tu}	F_1^{cu}	F_2^{tu}	F_2^{cu}	F_{12}	[MPa]
2212	1731	64	286	54	
ε_{11}^{t}	ε_{11}^{c}	ε_{22}^{t}	ε_{22}^{c}	ε_{12}	[microstrain]
15969	12280	6584	29400	11520	

Table 4.3: Analytical buckling loads and corresponding knockdown factor according to NASA SP-8007 [2].

Buckling Load [kN]	
Without Imperfection	2275.5
With Imperfection	1343.8
Knockdown Factor	0.6

4.2 Linear Analysis of the Solid Laminate Cylindrical Shell

This section focus on linear static and linear eigenvalue analyses of the solid laminate cylindrical shell. These analyses are executed to provide a set of buckling loads and stiffness before the step to non-linear analyses is made, but are kept at a minimum as the main focus are the non-linear analyses. Non-linear analysis was able to capture the full buckling behaviour, next to the possible non-linear behaviour before buckling. In the previous chapter on the 800 mm x 800 mm cylindrical shell, it was shown that the three elements considered are closely matched result wise for linear analyses and a mesh size of 5 mm. Therefore the whole set of linear analyses were executed by using only the S4R element combined with a mesh size of 5 mm, and the force based eigenvalue analyses ere executed for all of the three elements also for a mesh size of 5 mm. These eigenvalue analyses provide the modeshape to be used as an imperfection for the non-linear analyses section later on in the thesis. The linear static analysis will result in a load-displacement curve, which was used as a stiffness reference for the results of the non-linear analyses later on. The results of the linear analyses are shown in Table 4.4.

Table 4.4: Linear analyses results table for the scaled solid laminate cylindrical shell.

Force Eigenvalue Analyses			
Element	S4R	SC8R	CSS8
Buckling load [kN]	2289.1	2295.9	2292.7
Displacement Eigenvalue Analyses			
Element	S4R		
Displacement [mm]	2.3644		
Linear Static Analysis, Applied Disp.			
Element	S4R		
Load [kN]	2904.4		
Displacement [mm]	3		

It can be seen that the force eigenvalue analyses shows closely matched results for all 3 elements, and thus confirming results shown in the previous chapter. The linear analyses results of the S4R element, which is the base set for comparisons further on in the thesis, are shown in Figure 4.1. The graph shows that the results do match closely, the eigenvalue analyses results match with the linear static results and are just slightly above the analytical buckling load.

The modeshapes resulting from the eigenvalue analyses were used as an imperfection in next sections. For the all 3 elements, a antisymmetric modeshape was used, and only for the S4R element a diamond modeshape was used as an imperfection as well. The first four modeshapes of the S4R, SC8R and CSS8 element are shown in Figure 4.2,Figure 4.3 and Figure 4.4 respectively. The modeshapes show an axisymmetric shape in general, with slight differences. The first three modeshapes look visually very similar, but the third modeshape does show slight differences. The S4R and SC8R element have an outwards wave in the middle of the cylindrical shell longitudinally, while the CSS8 element has an inwards wave in the middle. It can be seen that the third modeshape of the CSS8 element does correspond partially with the fourth modeshape of the S4R and SC8R element, but they all show slight differences. The fourth modeshape of the CSS8 element is again similar to the first two modeshapes seen for all elements. The diamond modeshape is modeshape no. 83 for the S4R element, and is shown in Figure 4.5. Although this is not a classical diamond shape as seen in literature, it is the closest diamond shape achievable from the first 100 modeshapes. This is most likely caused by the layup having the 23 and -23 layers.

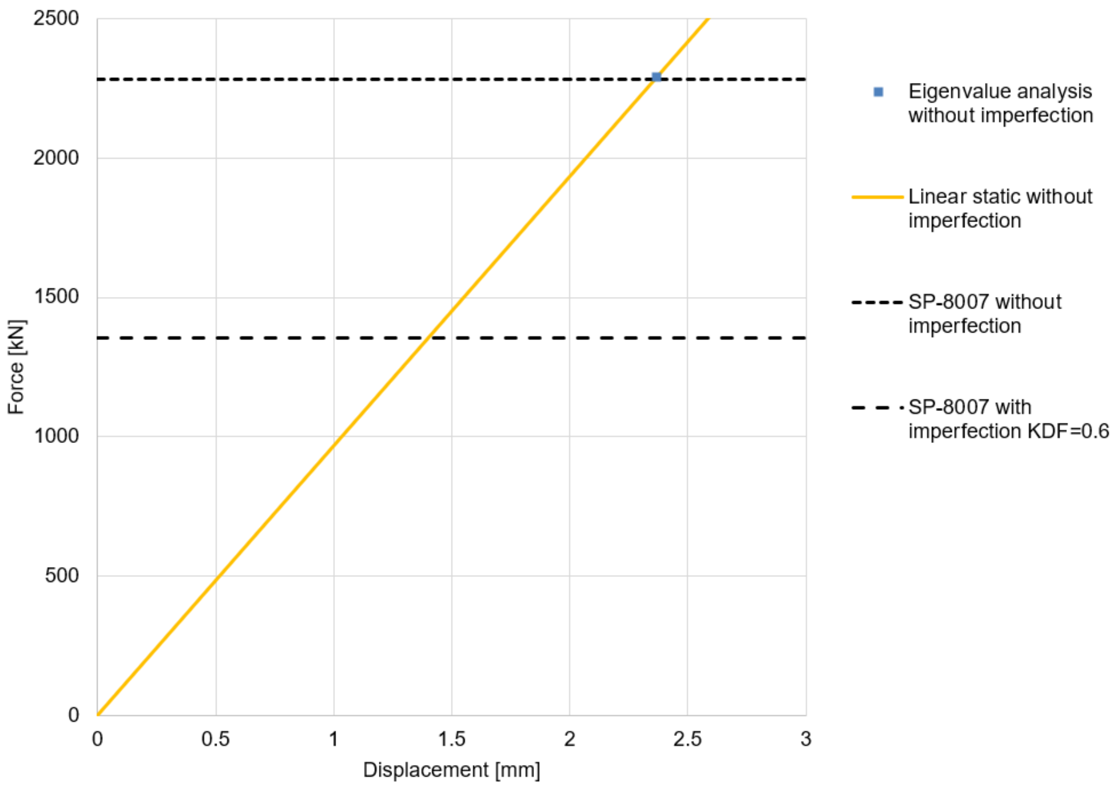

Figure 4.1: Linear analyses results graph for the solid laminate cylindrical shell.

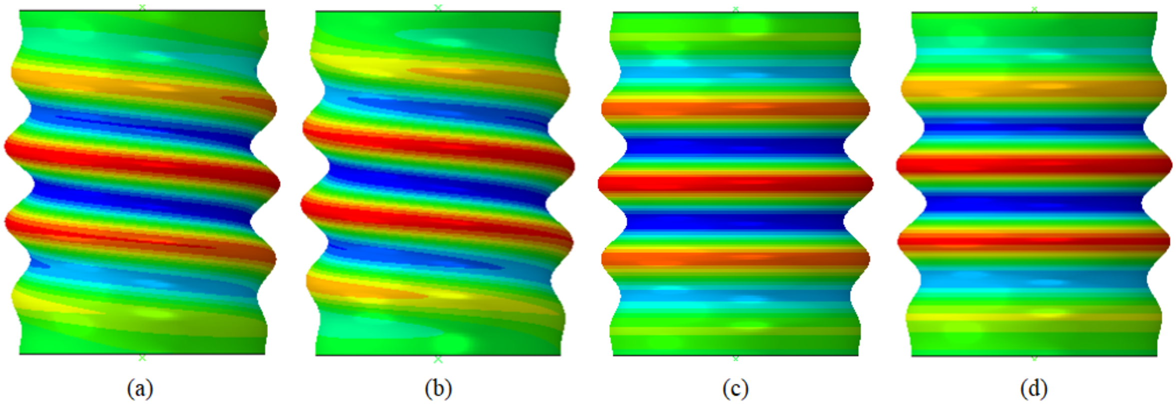

Figure 4.2: First four modeshapes of the scaled solid laminate cylindrical shell for the S4R element, showing radial displacement with modeshape numbering: (a) 1, (b) 2, (c) 3, (d) 4.

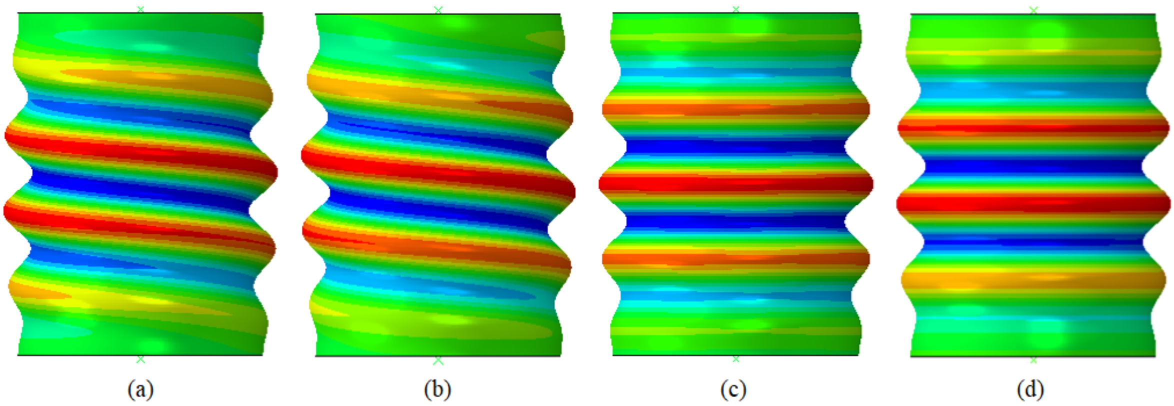

Figure 4.3: First four modeshapes of the scaled solid laminate cylindrical shell for the SC8R element, showing radial displacement with modeshape numbering: (a) 1, (b) 2, (c) 3, (d) 4.

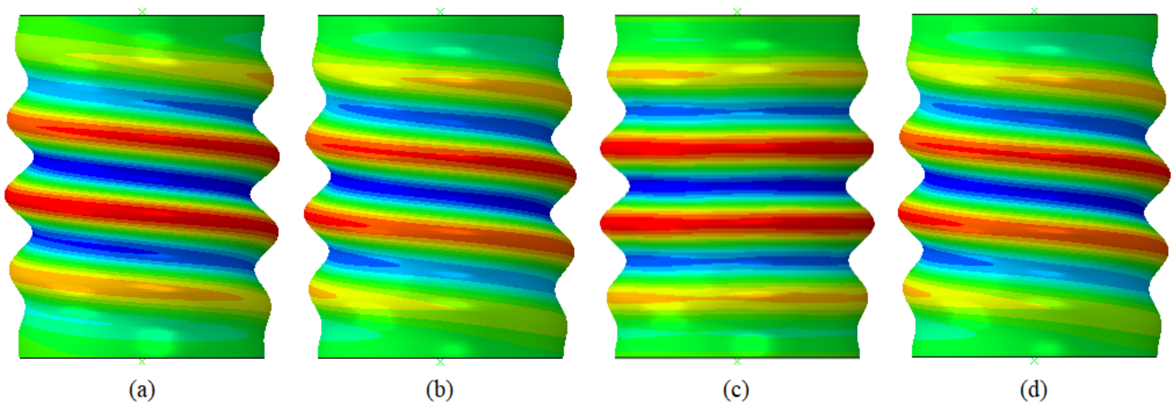

Figure 4.4: First four modeshapes of the scaled solid laminate cylindrical shell for the CSS8 element, showing radial displacement with modeshape numbering: (a) 1, (b) 2, (c) 3, (d) 4.

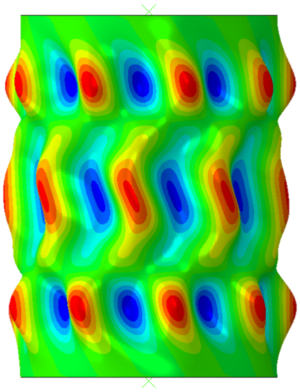

Figure 4.5: S4R modeshape no. 83 of the scaled solid laminate cylindrical shell, diamond shape, showing radial displacement.

4.3 Non-linear Analyses of the Solid Laminate Cylindrical Shell

The next step is to focus on the non-linear analyses of the solid laminate cylindrical shell. The type of analysis that was used is dynamic implicit. The choice for a dynamic type of analysis is due to the drop in stiffness and load carrying ability of the cylindrical structure when it buckles, which is intended to be captured as well. In general space structures are designed to not buckle for their design load, but the post-buckling field is interesting to capture to see when failure would happen. The choice for the implicit analysis is due to the computational efficiency compared to explicit analysis. As a large portion of analyses were executed, computational efficiency becomes a priority as well. The non-linear analyses were executed in several steps. First the displacement rate to be used through out this chapter has to be determined, for which a comparison using an axisymmetric imperfection was shown. This section is followed by a comparison for different types of imperfections for several amplitudes w.r.t. the thickness. The 3 types compared are the axisymmetric imperfection, diamond imperfection and a loading imperfection. Then, a comparison is executed for the 3 elements, using an axisymmetric imperfection for different amplitudes with respect to the thickness. This is followed by a section on the implementation of mandrel imperfections, which is compared to a diamond imperfection. The last section focusses on a test article model including the mandrel imperfections, padups and potting.

4.3.1 Sensitivity to Displacement Rate

The displacement rate of a dynamic analysis is determined through a combination of the applied displacement and the analysis time. The choice for a displacement rate is a trade off between computational time and analysis accuracy. Due to the quasi-static nature of the structural problem, it would be ideal to have a low displacement rate, but this would result in a low computational efficiency. It is thus the goal to have the displacement rate as high as possible, without the analysis showing dynamic influences. To test the effect of the displacement rate, 4 different displacement rates were chosen: 1, 2, 5 and 10 mm/s. These displacement rates were used in combination with an axisymmetric imperfection, as the main focus is on cylindrical shells with imperfections. The cylindrical shells without imperfection are seen as a reference to determine the drop in buckling load. Furthermore, a imperfect cylindrical shell is seen as more reliable, as the the imperfection triggers a certain modeshape under buckling, while a cylindrical shell without imperfection can show different modeshapes. This prevents the comparison showing the effect of different modeshapes, instead of showing the effect of the displacement rate itself. The effect of the displacement rate was judged according to the load-displacement curve each displacement rate results in, next to the CPU time for each analysis. The results of the analyses can be seen in Table 4.5 and Figure 4.6 for the CPU times and load-displacement graphs respectively.

Table 4.5: S4R dynamic implicit analysis CPU time for four different displacement rates.

Displacement rate [mm/s]	1	2	5	10
CPU time [s]	88126	61821	39741	30030

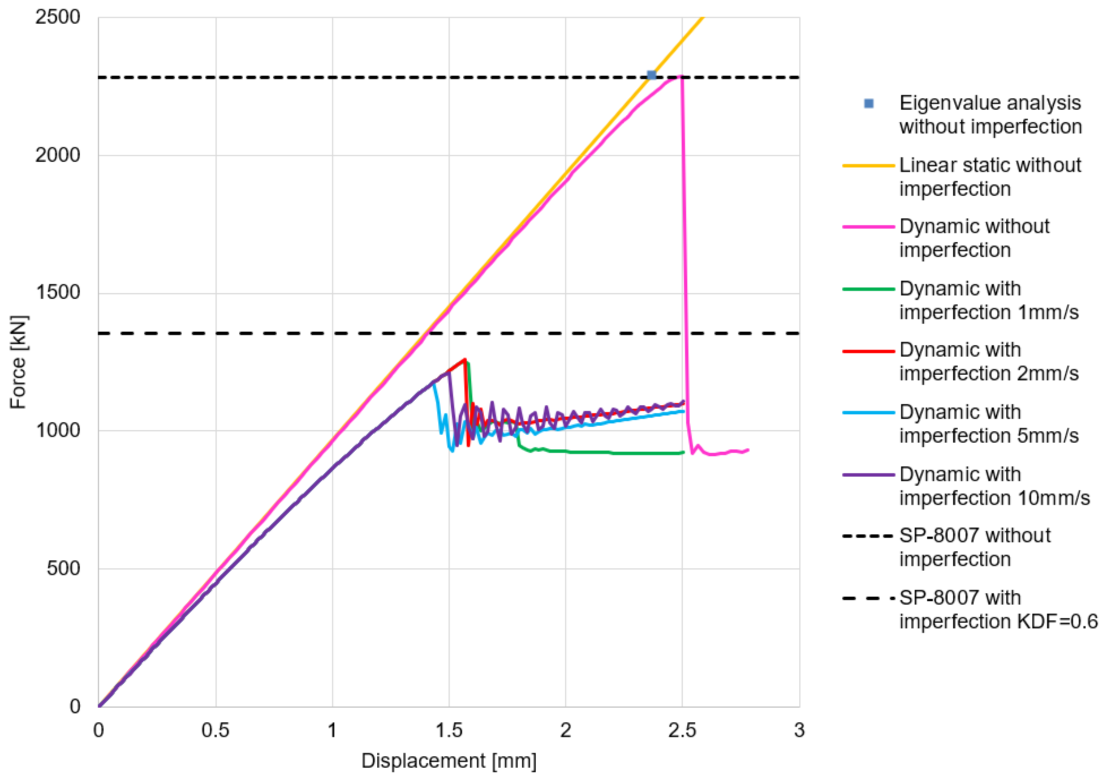

Figure 4.6: Load-displacement graph for the S4R solid laminate cylindrical shell comparison of 4 displacement rates.

CPU time increases considerably for lower displacement rates, as was to be expected. The load-displacement graph does show a bit of an unexpected result. The dependency does not necessarily converge into one direction, for a higher or lower displacement rate. The 1 and 2 mm/s results are very close, while the 5 mm/s analysis results in the lowest buckling load and the 10 mm/s analysis is in between. The 10 mm/s analysis also shows severe oscillations in the post-buckling field, most likely caused by dynamic effects. Due to the 2 mm/s analysis showing results very close to the 1 mm/s analysis with a considerably lower CPU time, it is chosen for following analyses. Lower displacement rates were not considered after seeing these results, as the two lowest displacement rates show similar results and look to be converged already. There is a difference in the post-buckling field between the 1 and 2 mm/s analyses, most likely due to a change in modeshape. However, this is far enough into the post-buckling field, that it is not of most importance. The analyses of the cylindrical shell without imperfection uses a displacement rate of 2 mm/s, which corresponds to the displacement rate chosen for following analyses.

4.3.2 Modeshape and Loading Imperfection

This section will focus on a comparison between three types of imperfection using the S4R element. For each type of imperfection four different amplitudes were used for the analyses. The first two imperfections are based on the modeshape resulting from the eigenvalue analyses shown previously in this chapter. Both an axisymmetric imperfection and a diamond imperfection was used. These modeshapes are a direct output of the eigenvalue analyses, and are then used as an input for the dynamic implicit analyses. The input is specified as the modeshape number and amplitude. The modeshape numbers are 3 and 83 for the axisymmetric, seen in Figure 4.2, and diamond modeshape, seen in Figure 4.5, respectively. The amplitude is a percentage, which defines the maximum out of plane displacement of the imperfection with respect to the thickness of the laminate, which is 4.21 mm.

The loading imperfection is based on that the loading platform of the test setup would be slightly rotated, and thus cause a loading imperfection. In the FE model, this would result in the reference point being rotated, with the amplitude defined as the degrees of rotation named alpha, see Figure 4.7. The loading imperfection analyses are executed by using two steps. The first step is to apply the rotation of the reference point and the second step is the application of the displacement. This type of analysis is chosen as this would correspond with the idea behind the loading imperfection. If the loading platforms of the experimental setup are not exactly parallel, it is assumed that the offset remains constant with respect to the magnitude of the final applied displacement. This would make the two step analyses a more accurate representation then applying both displacement and rotation simultaneously. The range of the imperfection amplitudes are chosen such that a wide range of buckling loads are obtained. As this results in load-displacement graphs from which the imperfection sensitivity can be observed clearly. The amplitudes for the modeshape imperfection are: 5%, 10%, 20% and 50%. The amplitudes for the loading imperfection are: 0.025° , 0.05° , 0.1° and 0.2° . This will result in a load-displacement graph for each imperfection, which will compare the four different amplitudes with the cylindrical shell without imperfection. This results in the load-displacement graphs shown in Figure 4.8, Figure 4.9 and Figure 4.10 with the corresponding buckling loads shown in Table 4.6.

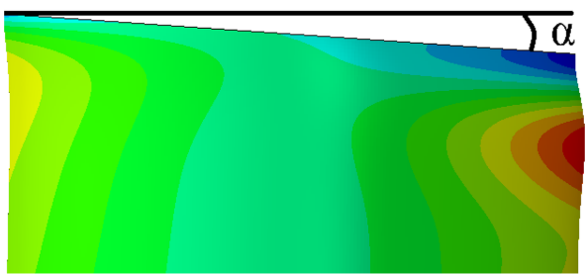

Figure 4.7: Loading imperfection illustration showing degree of rotation alpha.

Table 4.6: Buckling loads for three types of imperfections at five different amplitudes.

Axisymmetric Imperfection					
Amplitude	0%	5%	10%	20%	50%
Buckling Load [kN]	2289.1	1810.4	1523.0	1259.3	829.0
Diamond Imperfection					
Amplitude	0%	5%	10%	20%	50%
Buckling Load [kN]	2289.1	1859.2	1670.1	1406.2	1003.8
Loading Imperfection					
Rotation	0°	0.025°	0.05°	0.1°	0.2°
Buckling Load [kN]	2289.1	2026.6	1843.2	1450.4	667.8

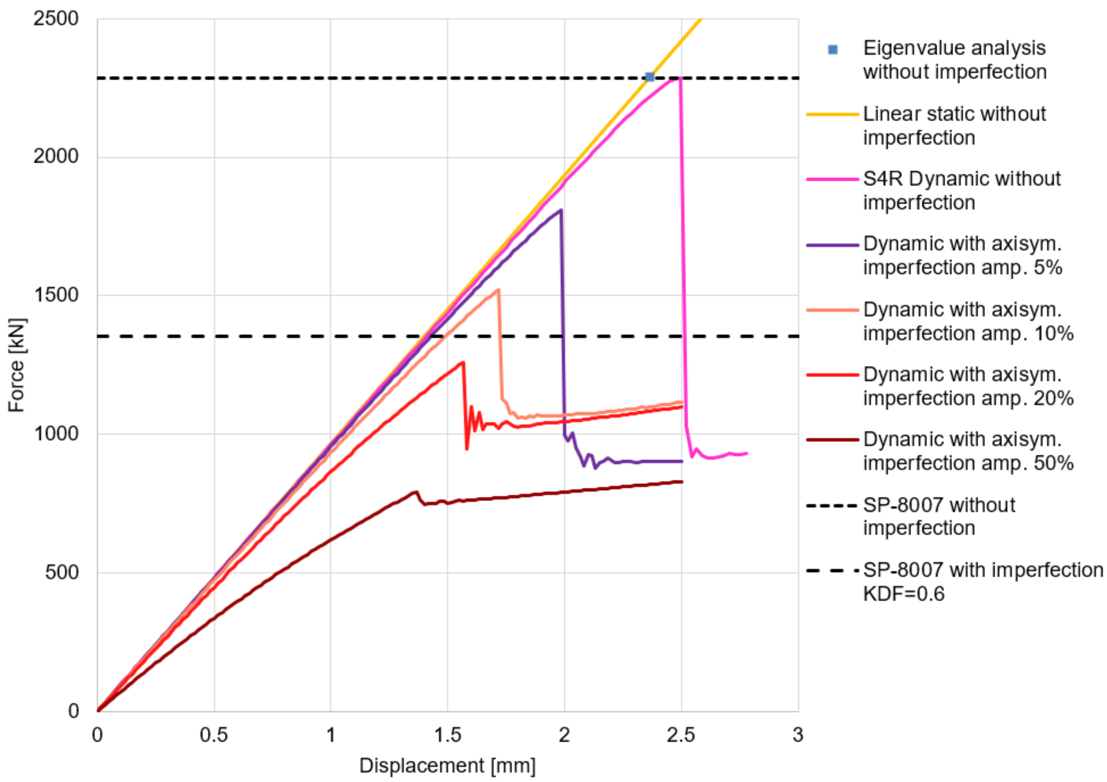

Figure 4.8: Load-displacement graph for the axisymmetric imperfection for four amplitudes.

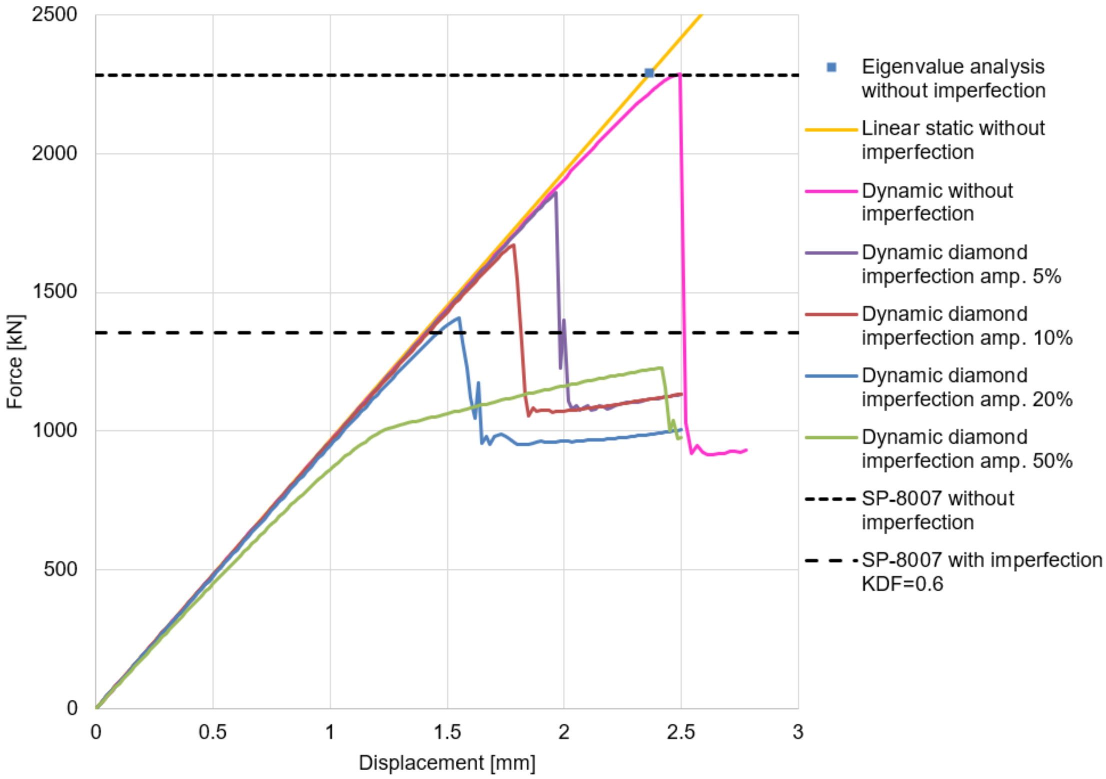

Figure 4.9: Load-displacement graph for the diamond imperfection for four amplitudes.

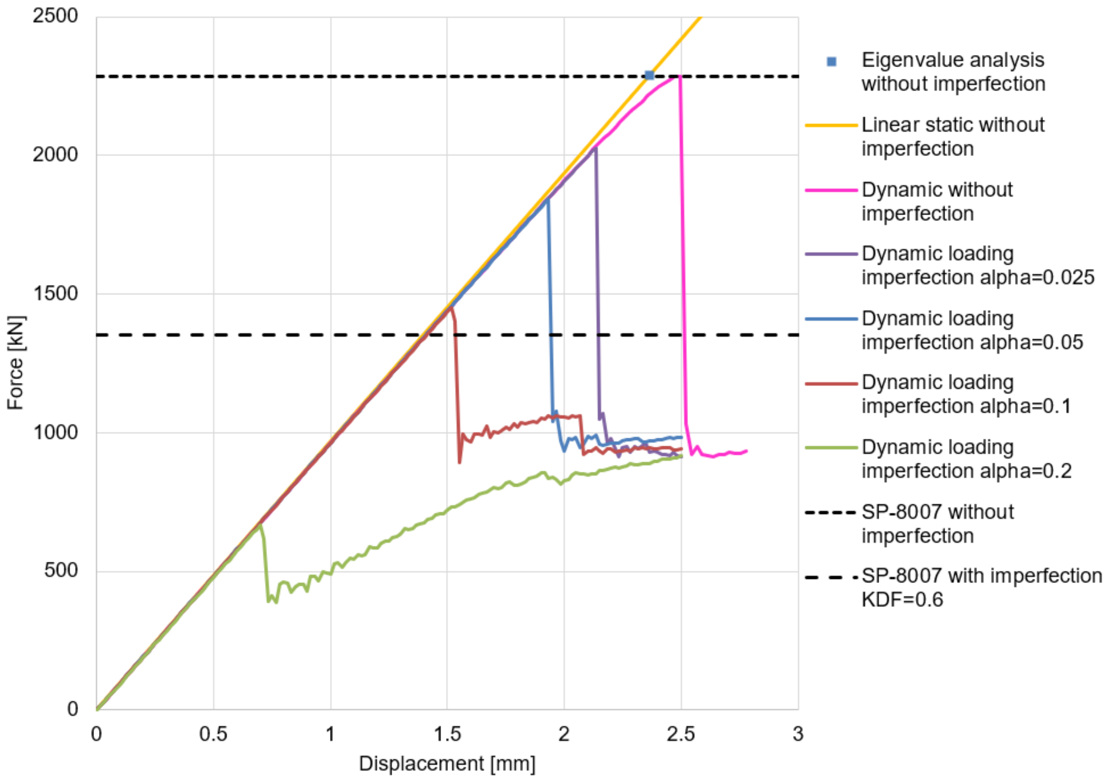

Figure 4.10: Load-displacement graph for the loading imperfection for four amplitudes.

When comparing the buckling loads of the modeshape imperfections in Table 4.6, it can be seen that for an amplitude of 5% the buckling loads are relatively close. The buckling loads do however diverge for higher imperfection amplitudes.

When the load-displacement graphs of the modeshape imperfections are compared, the most notable difference is the drop in stiffness for the axisymmetric imperfections. A amplitude of 20% for a laminate of 4.21 mm would result in an imperfection of 0.842 mm. For a radius of 400 mm, an imperfection of 0.842 mm can be considered small, but does however already result in a severe decrease in stiffness for the axisymmetric imperfection in comparison to the diamond imperfection. The buckling loads of the two modeshape imperfections are thus difference, but this is most likely caused by the difference in stiffness. As another comparison could be made by looking at the displacement at which buckling occurs for the two modeshape imperfections at 20% amplitude. The displacement at which they both buckle is very similar for this amplitude, but this behaviour is not consistent throughout the different imperfection amplitudes. As the 10% amplitude modeshape imperfections do not show agreement for the displacement at which buckling occurs, and the 5% amplitude does show agreement. The 50% imperfection amplitude cases were difficult to compare, as these cases do not show typical buckling behaviour.

When the post-buckling field is investigated, it can be seen that for the axisymmetric imperfection the 10% and 20% amplitude and the 5% and 50% amplitude converge respectively. For the diamond imperfection the 5% and 10% amplitude converge, while the 20% and 50% might converge after the drop in load of the 50% amplitude imperfection, but that's not captured clearly within the range of the graph. That the different amplitudes converge is most likely caused due to the analyses having the same modeshape in the post-buckling field, where the imperfection itself does not have the same influence it had in the pre-buckling field.

The comparison between the modeshape and loading imperfection is not straight forward, as it is a totally different type of imperfection. The effect of the magnitude of the imperfection is also quite different for the loading imperfection. There is no decrease in stiffness to be seen and even for the highest rotation the cylindrical shell still shows a distinctive point of buckling. All the four analyses seem to converge to the post-buckling behaviour of the cylindrical shell without imperfections, with the 0.05° analyses showing a bit of an offset in the post-buckling field.

In general, it can be concluded that the cylindrical shell is very sensitive to imperfections, as an imperfection of 10% w.r.t. to the thickness already leads to a buckling load reduction of 30%. To put it into perspective, that would be an imperfection of 0.4 mm with the thickness being 4.21 mm. On a radius of 400 mm that could mean a radial deviation of 0.1%, which can be considered precise in manufacturing terms. It is thus of utmost importance, that the manufacturing is very precise, otherwise large buckling load reductions will be unavoidable.

4.3.3 Element Comparison

The element comparison will consist of the 3 elements that have shown good results in the previous chapter, namely the S4R, SC8R and CSS8 elements. The comparison will make use of the axisymmetric imperfection, for the imperfection amplitudes of 10%, 20% and 50% next to the cylindrical shell without imperfections. The axisymmetric imperfection was chosen as it shows a larger variation in behaviour due to the different amplitudes, as it shows both a remarkable decrease in stiffness and buckling load. The analyses that were executed are thus similar to the analysis of the axisymmetric imperfection shown in the previous section, but now using the SC8R and CSS8 element. The results were shown in the form of two load-displacement graphs and a comparison of buckling loads in a table format. The buckling loads resulting from these analyses are reported in Table 4.7, and the load-displacement graphs are shown in Figure 4.11 and Figure 4.12.

Table 4.7: Comparison of buckling loads using the three elements for the scaled solid laminate cylindrical shell.

Axisymmetric Imperfection				
Amplitude	0%	10%	20%	50%
Buckling Load S4R [kN]	2289.1	1523.0	1259.3	829.0
Buckling Load SC8R [kN]	2284.4	1471.5	1165.6	776.9
Buckling Load CSS8 [kN]	2300.4	1461.3	1174.3	786.9

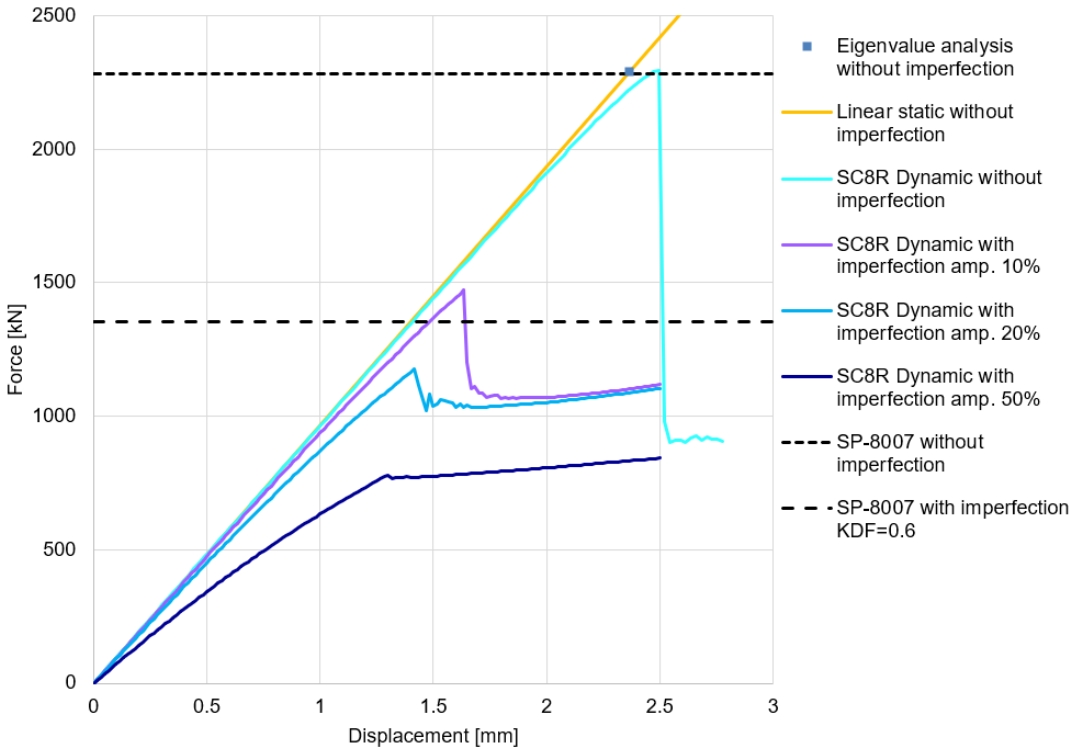

Figure 4.11: Load-displacement graph for the scaled solid laminate cylindrical shell and the SC8R element.

When the buckling loads of the three elements are compared for all amplitudes, it can be seen that the S4R and SC8R match for the cylindrical shell without imperfection. While for the cylindrical shells containing imperfections, the SC8R and CSS8 show very similar results. The difference in buckling load for the cylindrical shell without imperfection, could be explained by the CSS8 element showing a loading plateau, but it does not seem to increase the buckling load by a large margin. This loading plateau is most likely caused by it being a perfect structure forming a axisymmetric modeshape, where the analyses does not seem to be able to initiate buckling.

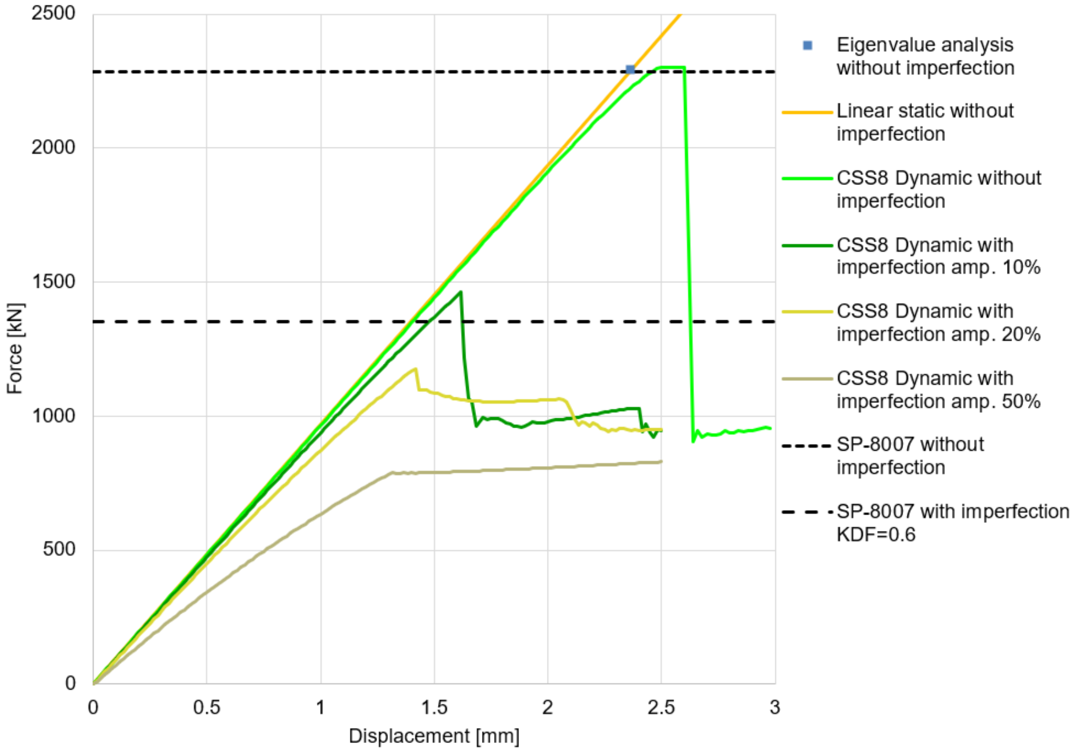

Figure 4.12: Load-displacement graph for the scaled solid laminate cylindrical shell and the CSS8 element.

When the load-displacement graphs of the SC8R and CSS8 are compared, the initial point of buckling is relatively close, but in the post-buckling field it can be seen that both the 10% and 20% amplitudes for the CSS8 element shows another drop off point of the load. This is most likely caused by the change of modeshape, and is not seen for the S4R and SC8R element. When looking back at the behaviour of the S4R element in Figure 4.8, it can be seen that there were oscillations in the post-buckling field for the 20% amplitude, where the CSS8 element does not show oscillations, and the SC8R element shows a minimal amount of oscillations. The SC8R and CSS8 show similar buckling loads when compared with the S4R. The S4R results in 5% higher buckling loads on average, and is deemed to be the outlier. Due to these differences, the SC8R and CSS8 elements would be in favour. It is however the computational efficiency of the SC8R element in comparison to the CSS8 element which determined that the SC8R element will be used for the next sections.

4.3.4 Mandrel Imperfections Solid Laminate Cylindrical Shell

The next step of the thesis was to include mandrel imperfections and compare them to previous results of the solid laminate cylindrical shell. The measurements were executed at NASA, on the mandrel which will be used for production of the solid laminate cylindrical shell. The first portion of this section will explain the work flow for the processes that were needed to incorporate the measurement data into a FE model in Abaqus. Previous imperfections were used at several amplitudes, to be able to see the imperfection sensitivity. To be able to do the same kind of comparison for this imperfection data as well, two kinds of imperfection amplitudes were used. The first amplitude consists of the interpolated imperfection at its original amplitude, and the second amplitude consists of an exaggeration of the interpolated imperfection, to match 20% w.r.t. to the thickness of the laminate. This 20% is the amplitude most commonly used in previous comparisons and should provide a insight into the sensitivity to the mandrel imperfection on different amplitudes. The following bullet points will show the general processing steps for the imperfection data:

- The measurement data was imported into Python, after which the data was filtered on incomplete coordinates which were removed and the edge regions were excluded.
- The measurement data consisted of x,y,z coordinates, which were transformed to a cylindrical coordinate system. Using a cylindrical coordinate system has several advantages for further steps, with the most important advantage being able to use 2D interpolation.
- Determine a regular grid which will be used for the 2D interpolation. This regular grid is based on the amount of elements in circumferential and axial as was used in previous analyses. This ensures that the mesh is consistent with previous analyses for accurate result comparisons later on.
- The processed measurement data was interpolated onto the regular grid. Inputs from the regular grid are the angular and z coordinate, with the output being the radius at each location.
- This step is only used for the 20% amplitude imperfection. A histogram plot was made for the radial coordinates, to determine the mid-plane of the imperfection data, which can be seen as the general radius of the mandrel. After the mid-plane was determined, the mid-plane radial distance was subtracted from the previous mentioned radial coordinates, which results in a set of imperfection amplitudes. The maximum imperfection amplitude was then determined to be able to calculate the scaling factor, after which the imperfection amplitudes were scaled to match the 20% amplitude. Summing up this 20% amplitude data with the mid-plane radial distance, results in a new set of radial coordinates for the 20% amplitude.
- The last step is to format the output data from 2D interpolation or scaling procedure, to be used as node coordinates for a Abaqus input file.

The measurement data was also 2D interpolated onto a regular grid, containing the same amount of coordinates of the original data. This was done to be able to show the imperfection in a coloured graph, which requires the datapoints to be on a regular grid in python. This results in the graph shown in Figure 4.13. The total variation over the whole mandrel is just 0.24 mm, which is considerably lower than the imperfections that were used in previous analyses.

For the solid laminate cylindrical shell as used in previous analyses, a length of 1120 mm is needed. The interpolation on the regular grid which is equal to the mesh size for the length of 1120 mm, results in the graph seen in Figure 4.14. Due to a smaller portion of the mandrel being used, the maximum variation is 0.18 mm, which is impressively low for a mandrel.

To be able to create the 20% amplitude imperfection, a histogram plot was made, which can be seen in Figure 4.15. From this histogram plot the mid-plane of 400.094 mm was determined, as it had the highest amount of occurrences. Determining the mid-plane by

amount of occurrences was deemed to be a more representative method to determine the mid-plane, instead of just determining the average radial coordinate. With the mid-plane being at 400.094 mm, the maximum imperfection is 0.12 mm which is 2.85 % w.r.t. to a laminate thickness of 4.21 mm. Scaling the imperfection to an amplitude of 20% w.r.t. to the laminate thickness, results in Figure 4.16.
The cylindrical shell resulting from the mandrel imperfection has a radius of 402.2 mm, which is slightly larger compared to the previously used cylindrical shell. To be able to investigate the stiffness reduction due to the mandrel imperfection, another linear static analysis was executed using a radius of 402.2 mm for a cylindrical shell without imperfections.

With the imperfections ready for FE analyses, the last step is to be able to have an imperfection similar to previous analyses, which can be directly compared to the mandrel imperfection. From previous analyses it was seen that the axisymmetric imperfection showed a high reduction in stiffness, which was not expected to happen for the mandrel imperfection. The diamond imperfection was therefore seen as more compatible, but it was not yet determined for the SC8R element. This required another eigenvalue analysis to be executed for the SC8R containing more eigenmodes, to be able to create the diamond imperfection. The diamond shape that was chosen was exactly the same visually to the S4R diamond shape as seen in Figure 4.5, and also had modeshape no. 83. This diamond modeshape was then used for both 2.85% and 20% w.r.t. to the thickness in the previously used SC8R models, as these are then a direct comparison with the mandrel imperfection. These two imperfection types, in combination with two imperfection amplitudes each, were used in a dynamic analysis, which resulted in the load-displacement graph as shown in Figure 4.17 with the corresponding buckling loads reported in Table 4.8.

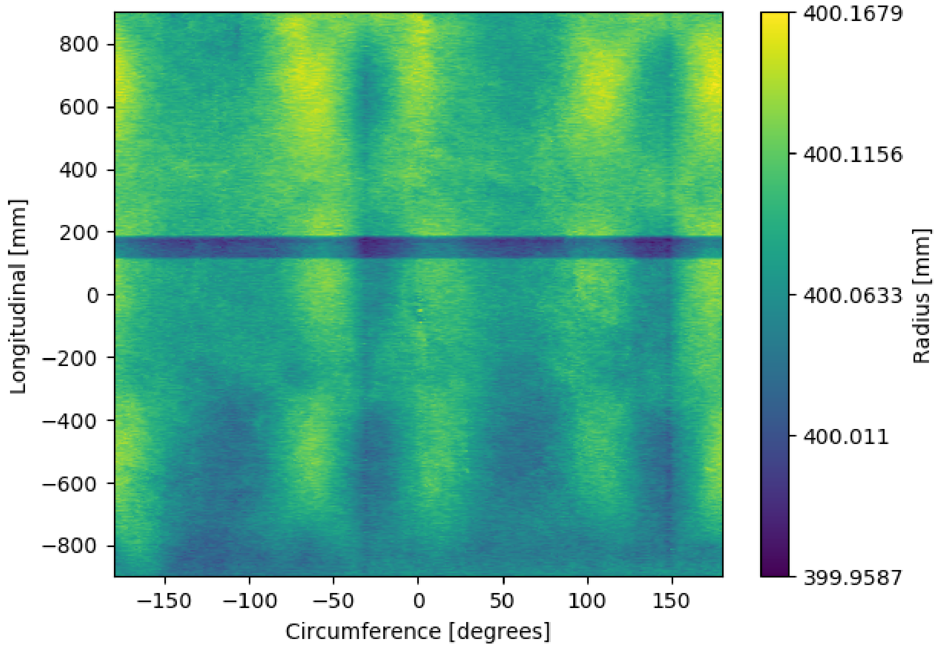

Figure 4.13: 2D representation of the mandrel measurement data.

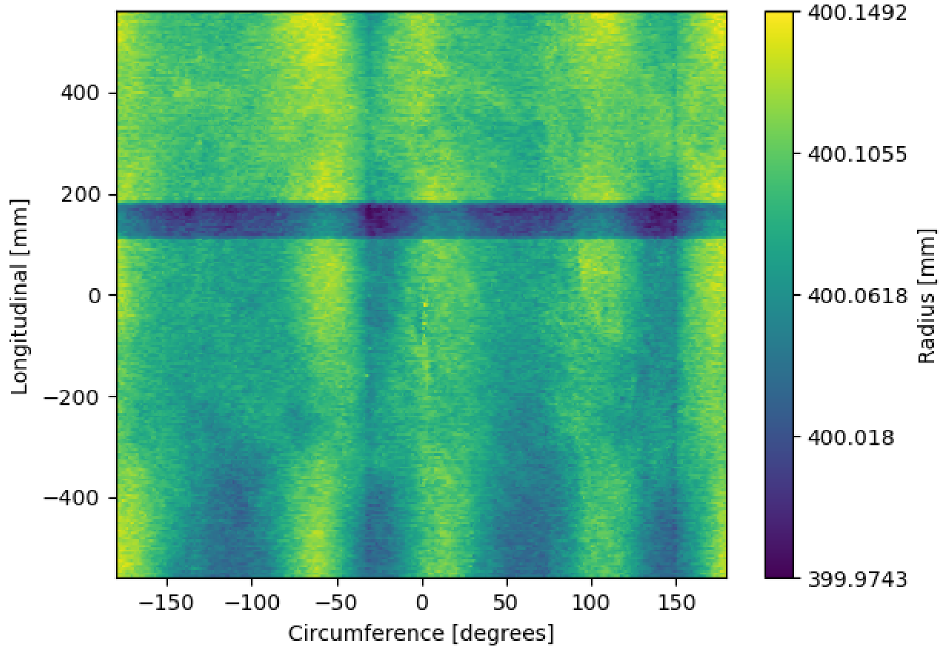

Figure 4.14: 2D representation of the radial coordinates 2.85% mandrel imperfection and 1120 mm length cylindrical shell.

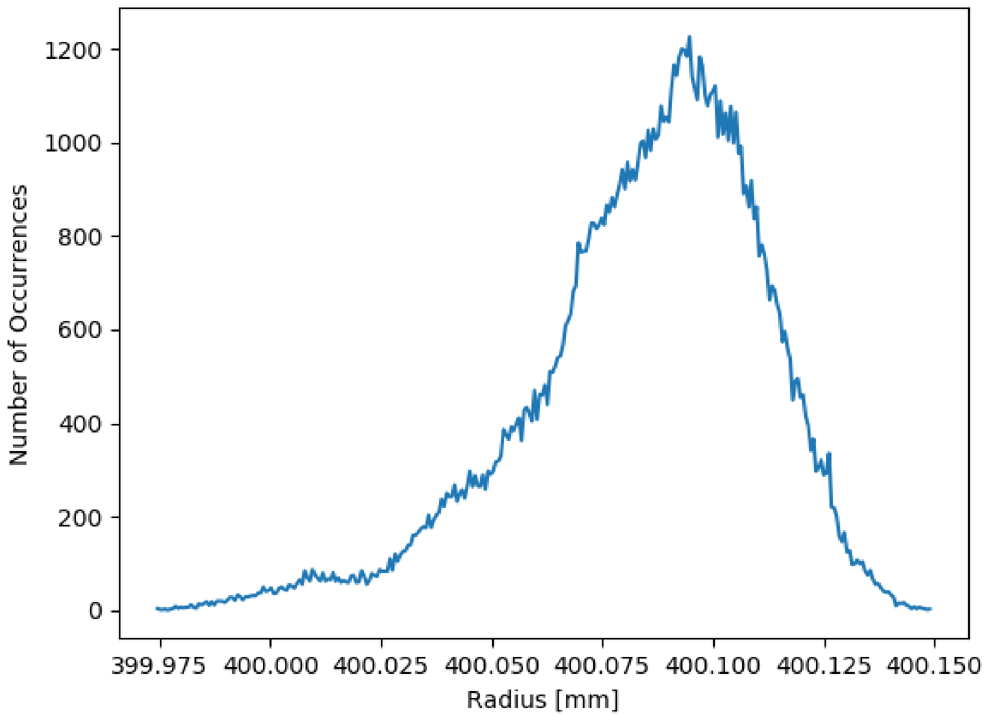

Figure 4.15: Histogram plot for the mandrel imperfection and 1120 mm length cylindrical shell.

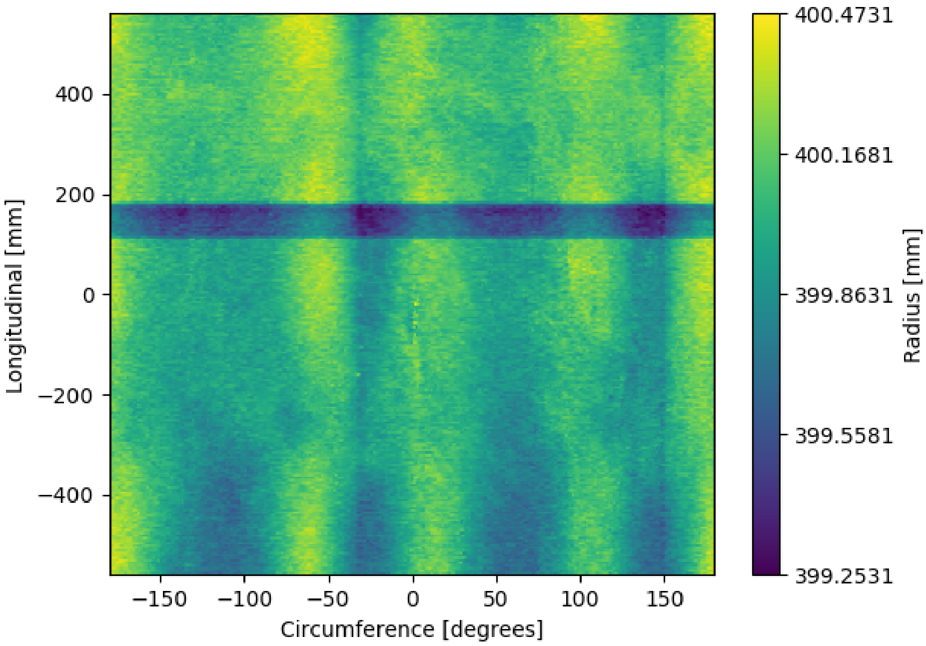

Figure 4.16: 2D representation of the radial coordinates of the 20% mandrel imperfection and 1120 mm length cylindrical shell.

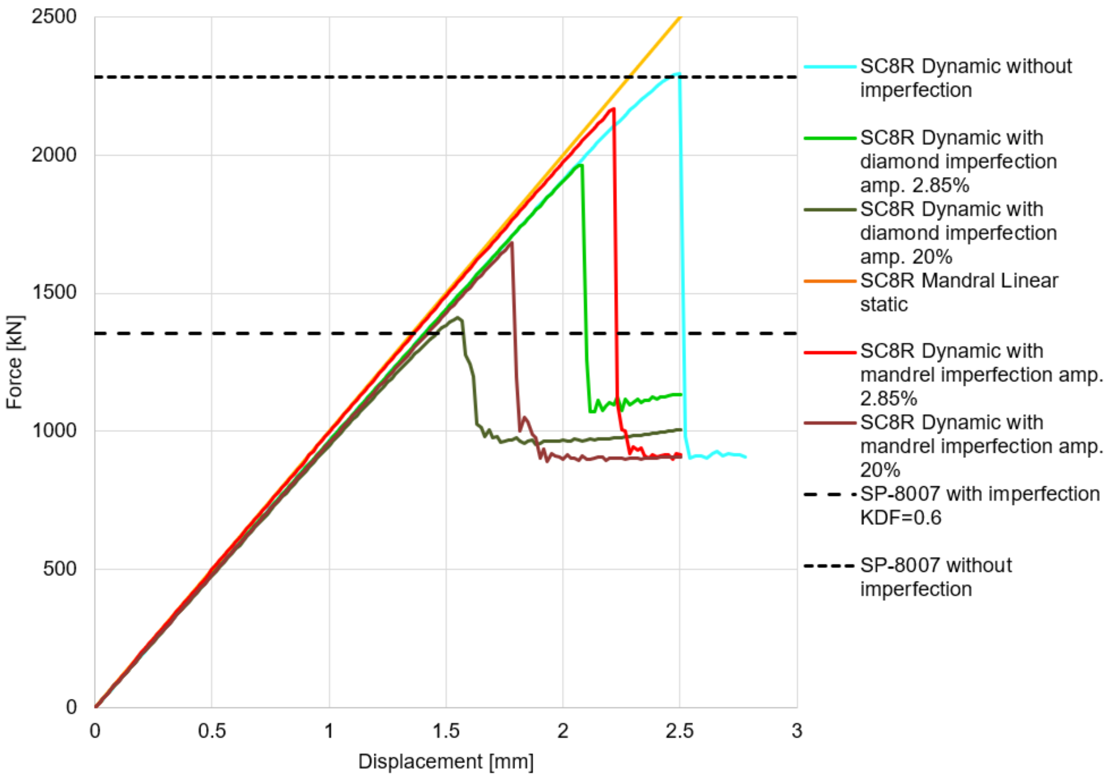

Figure 4.17: Load-displacement graph containing the mandrel and diamond imperfection comparison for the 1120 mm length cylindrical shell.

Table 4.8: Comparison of buckling loads between the diamond modeshape and mandrel imperfection for the 1120 mm length cylindrical shell.

Imperfection amplitude	2.85%	20%
Mandrel imperfection buckling load [kN]	2166.5	1684.3
Diamond imperfection buckling load [kN]	1962.5	1411.6

The first observation of the whole comparison including the mandrel and diamond imperfections, is that the models based on the mandrel have a slightly higher stiffness, which is caused by the slightly larger diameter. This raised some concerns as the increased radius might have implications for the experimental tests. Therefore a study was executed on the effect of increased radius and thickness of the laminate, to ensure the experimental test equipment can handle the cylindrical shell if it is slightly different than the actual design. This study will be shown in the next paragraph, as first the rest of the comparison will be analysed.

With the attention back to the load-displacement graph, it can be seen that the imperfection sensitivity to the mandrel imperfection is considerably lower compared to the diamond imperfection. The difference in buckling load between the two imperfection types is 10% and 19% for the 2.85% and 20% imperfection amplitude respectively. For the same imperfection amplitude the buckling loads are higher, especially for the 20% amplitude. When both imperfection amplitudes of the mandrel imperfection are compared, it can be seen that they converge towards each other in the post-buckling field. These models converge towards the post-buckling behaviour of the cylindrical shell without imperfection. The mandrel imperfection has less influence on the post-buckling behaviour, most likely caused by the imperfection not being equal to a modeshape as was the case with previous comparisons. The loading imperfection showed similar behaviour, as it also converged towards the cylindrical shell without imperfection in the post-buckling field. The post-buckling behaviour difference underlines that the influence of mandrel imperfections can be quite different in comparison to modeshape imperfections. The modeshape imperfections seem to induce behaviour, which might not be representative of reality as mandrel imperfections rarely have a modeshape-like shape.

As mentioned before, cylindrical shells for the use in launch vehicles are design to not buckle or have material failure for their design load. To check the state of the material at the last increment before buckling, as this would be the maximum load before buckling, the strains were also determined by the 5 analyses shown in Figure 4.17. The strains of the first 6 plies, are reported in Table 4.9. The first six plies are only shown, as these are the most critical based on the strain values. When comparing the strain values for each of the five cases, they all show that the second ply is the most critical. This ply shows the highest strains in the 2nd material direction, which is the matrix dominated direction. The shear strain of the first plies is high aswell, but not be considered critical in comparison to the second ply. The strain of the second ply in the 2nd material direction is in tension, to which the matrix is weakest. The reason for this ply becoming critical. is that it is a zero ply. Which means the second material direction is in line with the circumferential direction of the cylindrical shell and therefore show the highest amount of tension. The strain values are high, but not to the point of material failure. This is an important conclusion, as the cylindrical shell should not show material failure before buckling to be able to be representative of the full scale cylindrical shell.

From the five cases that are compared, the most critical strains are seen for the cylindrical shell without imperfection. This can be explained by the fact that this cylindrical shell was under a higher load which lead to higher strains for this case. When comparing the strains of the two cylindrical shells with a 2.85% amplitude imperfection, the mandrel imperfections shows higher strain values in general, but the cases are comparable. When the strains of the two cylindrical shells with a 20% imperfection are compared, larger differences are seen. The strain differences between each ply of the 20% diamond imperfection are vastly different compared to the mandrel imperfection, as the diamond imperfection shows very similar strains for each ply. This is most likely caused by the diamond shape showing a slightly twisted shape, as seen in Figure 4.5. The different behaviour of the diamond imperfection with 20% amplitude also shows that an imperfection can show very different behaviour for different amplitudes. While the mandrel imperfection did show relatively similar behaviour for the two imperfection amplitudes.

The strain values of the second ply are shown as contour plots in Figure 4.18. From these plots it can be seen how much effect the applied imperfection has on the shape just before buckling. The only two cases showing slightly similar behaviour are the cylindrical shell without imperfection and the cylindrical shell with the 2.85% mandrel imperfection. This could already be seen from the load-displacement graph that the mandrel imperfection was the type of imperfection the cylindrical shell was least sensitive to. The differences between the 2 amplitudes for each imperfection are notable. The difference for the diamond imperfection per amplitude looks straight forward, what is seen for the 2.85% amplitude is more extreme for the 20% amplitude. The difference between the two mandrel imperfections shows more differences in comparison. The imperfection signature as shown in Figure 4.14 shows a clearly defined band across the mandrel. This imperfection band is slightly visible in the strain results for the 2.85% amplitude, but for the 20% it causes a deeper inwards half wave Due to the exaggeration of the imperfection, this band causes two slightly sharp edges combined with a lower radius of that region of the cylindrical shell.

Table 4.9: Maximum strains ($\mu\varepsilon$) of the inner first six plies of the 1120mm length scaled solid laminate cylindrical shell.

Without imperfection	ε_{11}	ε_{22}	ε_{12}
Ply 1	-2266	3434	5895
Ply 2	-3417	4684	9
Ply 3	-2101	3464	-5755
Ply 4	-2019	3478	-5686
Ply 5	-3126	4683	7
Ply 6	-1855	3507	5574
Mandrel imperfection 2.85%	ε_{11}	ε_{22}	ε_{12}
Ply 1	-1892	2835	4749
Ply 2	-2778	3783	-665
Ply 3	-1784	2839	-4652
Ply 4	-1730	2840	-4609
Ply 5	-2589	3765	-558
Ply 6	-1621	2835	4531
Mandrel imperfection 20%	ε_{11}	ε_{22}	ε_{12}
Ply 1	-1661	2267	3694
Ply 2	-2276	2921	-653
Ply 3	-1555	2213	-3754
Ply 4	-1505	2209	-3705
Ply 5	-2090	2904	-553
Ply 6	-1420	2244	3513
Diamond imperfection 2.85%	ε_{11}	ε_{22}	ε_{12}
Ply 1	-1858	2586	4550
Ply 2	-2561	3356	-776
Ply 3	-1786	2551	-4397
Ply 4	-1729	2543	-4336
Ply 5	-2382	3307	-644
Ply 6	-1607	2512	4242
Diamond imperfection 20%	ε_{11}	ε_{22}	ε_{12}
Ply 1	-2131	2957	-2297
Ply 2	-2060	2861	-2158
Ply 3	-1988	2772	-2019
Ply 4	-1917	2689	-1880
Ply 5	-1847	2613	-1751
Ply 6	-1776	2541	-1630

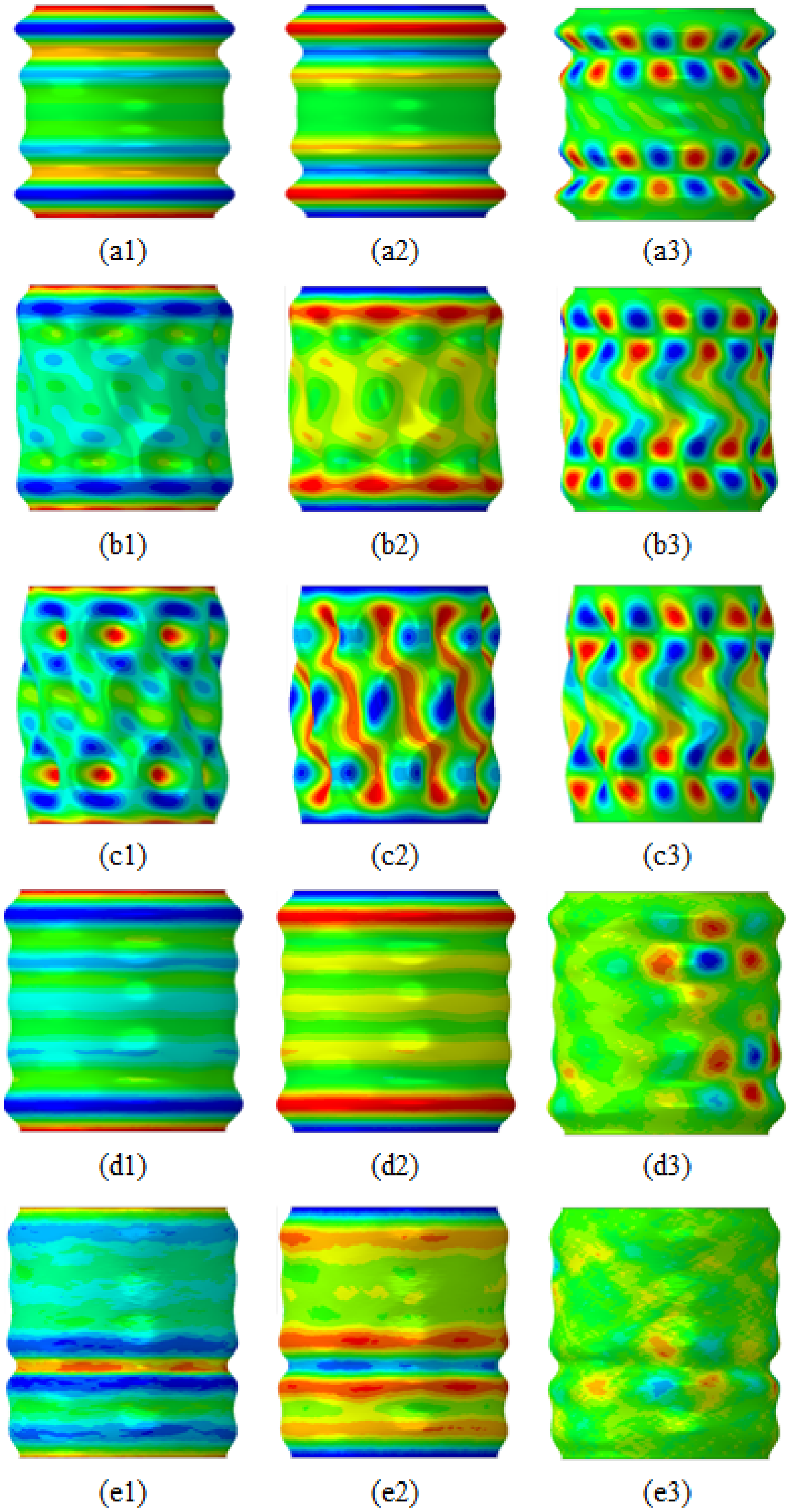

Figure 4.18: Strain contour plots of the 1120 mm scaled solid laminate cylindrical shell with a deformation scale of 50. Each row is one type of imperfection: a = without imperfection ; b = diamond imperfection 2.85%; c = diamond imperfection 20%; d = mandrel imperfection 2.85% ; e = mandrel imperfection 20%. The number notation: 1,2 and 3 are ε_{11},ε_{22},ε_{12} respectively.

4.3.5 Sensitivity to Laminate Thickness and Radius

Due to a possible increase of the radius of the cylindrical shell as a result of the mandrel being slightly larger than expected, a investigation was executed in the effect of thickness and radial variations. The main focus is to see how much the buckling load is affected by the increase of the radius and thickness. As the buckling load should not exceed the maximum load of the experimental test setup which is intended to be used. The choice was made to use a 10% larger radius, 10% thicker laminate and 20% thicker laminate for the investigation, combined with a cylindrical shell without imperfection and an axisymmetric imperfection with 20% amplitude w.r.t. to the thickness. The axisymmetric imperfection is chosen instead of a diamond imperfection, due to the increase of computational time of the eigenvalue analysis when a diamond modeshape needs to be captured. For each of the 3 cases an eigenvalue analysis has to be executed. For an axisymmetric imperfection only 4 eigenvalues are needed, where the diamond modeshape has been shown to need in the region of 100 eigenvalues for it to be captured. This would increase the total computational time, without having a huge impact. The thickness and radius variations result in a total of 6 analyses to be executed. The resulting buckling loads of these analyses are shown in Table 4.10, and the load-displacement graphs are shown in Figure 4.19 and Figure 4.20.

From these results it can be concluded that the larger diameter should not be an issue for the experimental test to reach the necessary load, it is most likely more of a concern if the larger diameter cylindrical shell would fit the testing equipment or not. There is an increase in stiffness but that should not be an issue for the testing equipment. The thicker laminate does however greatly influence the necessary load, as a 10% increase in thickness already results in an increase of the buckling load of 19%, with the 20% increase in thickness causing an increase of 42% for the buckling load. It should be said however, that these are large steps in thickness, and the variation in thickness should not even reach the 10% increase. The range of 10% and 20% increase in thickness, was also chosen to be able to show a clear change in buckling load. There is a clear trend in the increase in buckling load, where the points of buckling are almost in line for the cylindrical shell without imperfection. The testing equipment to be used has a maximum load capability of 600 kips, which would convert to 2669 kN. Judging from the load-displacement graph for the thickness variations, this would be the buckling load for a cylindrical shell which has in increase of 7-8% in laminate thickness. The thickness is not expected to vary by that high of an percentage, so the experimental testing should not have an issue due to the variations tested in this section.

Table 4.10: Buckling loads for thickness and radial variations.

	Original	10% thicker	20% thicker	10% larger diameter
Without imperfection	2284.4	2718.2	3232.4	2238
With imperfection	1176.8	1381.5	1681.2	1192.3

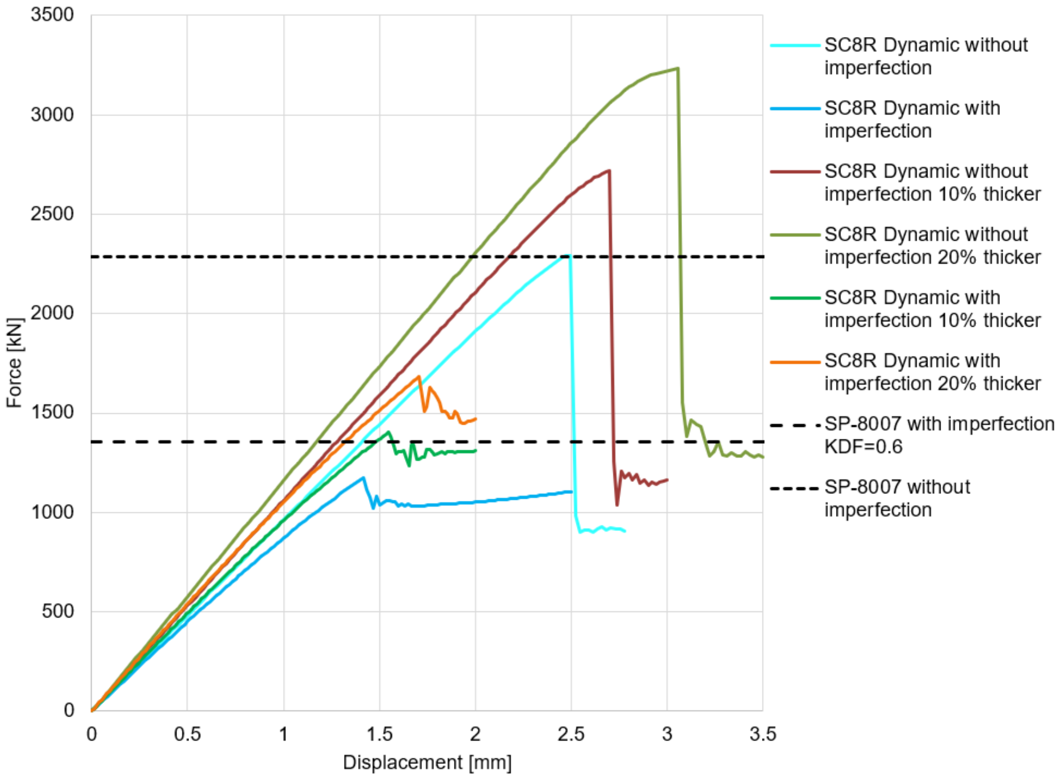

Figure 4.19: Load-displacement graph for the variation in laminate thickness.

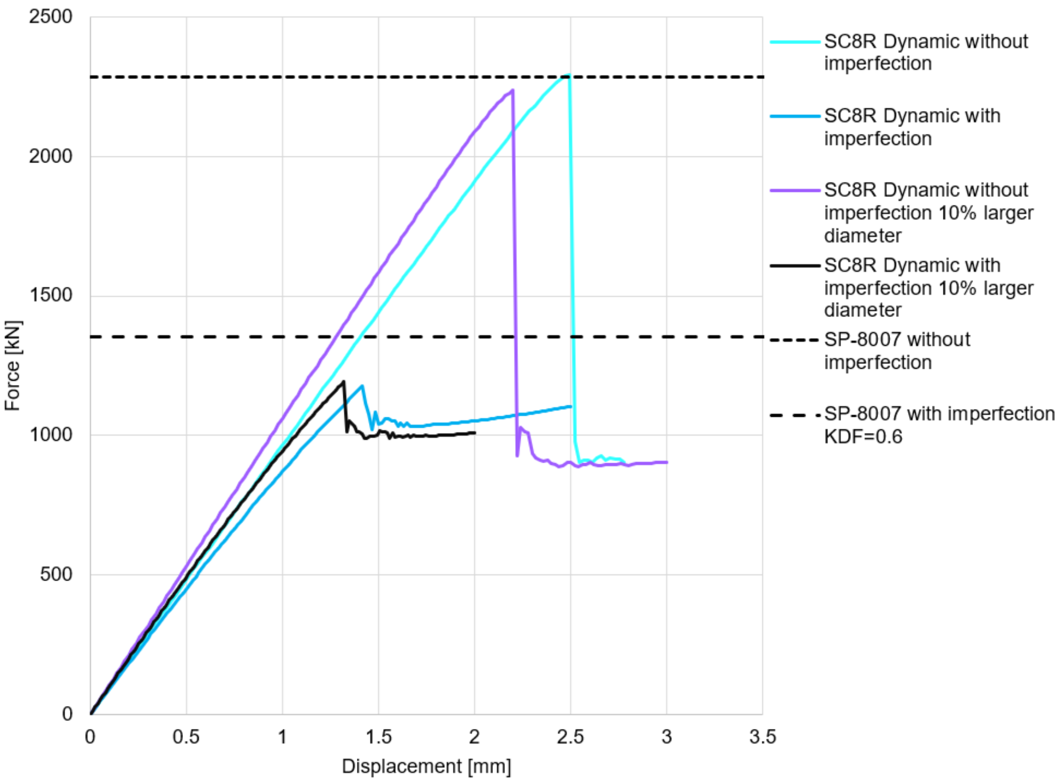

Figure 4.20: Load-displacement graph for the variation in diameter.

4.3.6 Solid Laminate Test Article

The last step for the non-linear analyses of the solid laminate cylindrical shell is to use a version of the cylindrical shell which will represent the actual test article. This cylindrical shell will include the pad-up regions and the potting applied to the edge of the cylindrical shell. The pad-ups and potting are added to the test article, to aid in the load introduction during experimental testing. To prevent material failure at the edges where the load is introduced. Due to the cylindrical shell being increased in length to include the pad-up regions, a new imperfection signature has to be determined. This was done by the same steps as used previously, but now for a cylindrical shell length of 1220 mm. This results in an imperfection signature as shown in Figure 4.21 for the original amplitude imperfection and shown in Figure 4.22 for the 20% amplitude imperfection. The implementation of the imperfections itself is done in a similar manner as described in subsection 4.3.4. However, the mesh does not have constant thickness for the whole cylindrical shell, due to the pad-ups. This required the mesh, generated with the imperfection included, to be slightly thickened in the edge regions. This thickening is done in 3 steps, as this would be in agreement with the dropping of pad-up plies. The last step is to add the potting material, which is added both on the in- and outside of the cylindrical shell, with a thickness of 25 mm and height of 50 mm, for which the material properties shown in Table 4.11 are used. This is a chopped fibre epoxy composite material. The mesh of the potting consists of C3D8R classical solid elements, with a mesh size of 5 mm so that it coincides with the mesh of the composite laminate. An illustration of the whole mesh construction of the edge region is shown in Figure 4.23 on the left, where the different colours show the regions containing different material properties. On the right in Figure 4.23 the complete test article is shown. For the regions containing different lay-ups, the layup details are shown in Table 4.12. The outer three regions thus contain padup plies which are shown in red in the layup table, where one padup ply is dropped on each region transition. A test article model was build for three different cases, the 2.85% amplitude imperfection, the 20% amplitude imperfection and one without imperfection. These three cases are then used in a dynamic implicit analyses, and were compared with the 1120 mm length cylindrical shell without imperfection. The results of the analyses are shown in the load-displacement graph in Figure 4.24, with the corresponding buckling loads shown in Table 4.13.

Table 4.11: Potting Material Properties.

E [MPa]	ν [-]	ρ [kg/m^3]
4500	0.3	1200

Table 4.12: Lay-up regions of the solid laminate test article, with the pad-up plies shown in red.

Blue	$[(23/0/-23)_{s2}/23/0/-23/45/-23/0/23/-45/23/0/-23/90/-23/0/23]$
Red	$[(23/0/-23)_{s2}/23/0/-23/-23/0/23/-45/23/0/-23/90/-23/0/23]$
Cream	$[(23/0/-23)_{s2}/23/0/-23/-23/0/23/23/0/-23/90/-23/0/23]$
Green	$[(23/0/-23)_{s2}/23/0/-23/-23/0/23/23/0/-23/-23/0/23]$

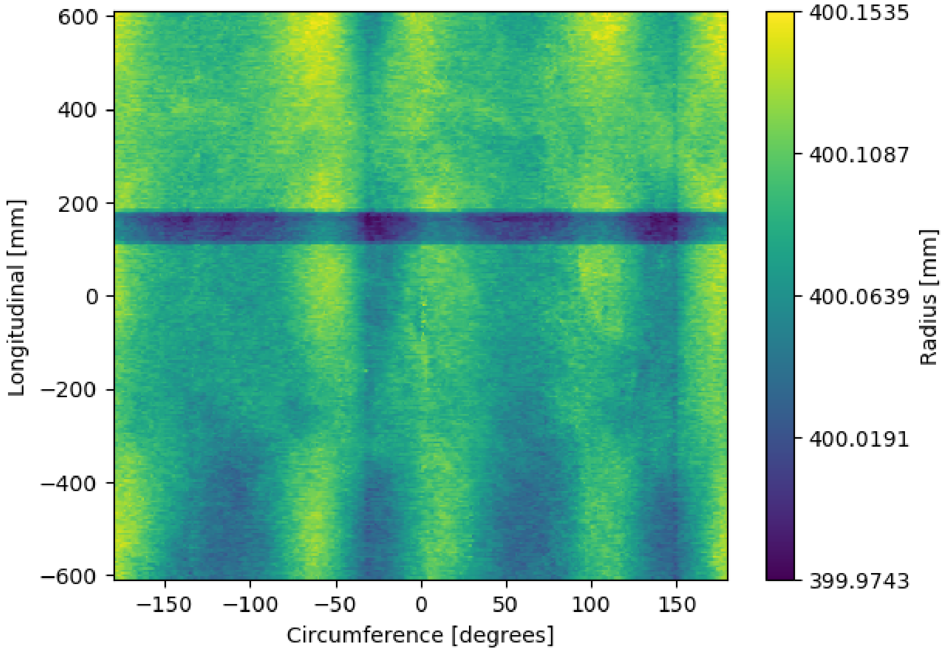

Figure 4.21: 2D representation of the radial coordinates of the 2.85% mandrel imperfection and 1220 mm solid laminate test article.

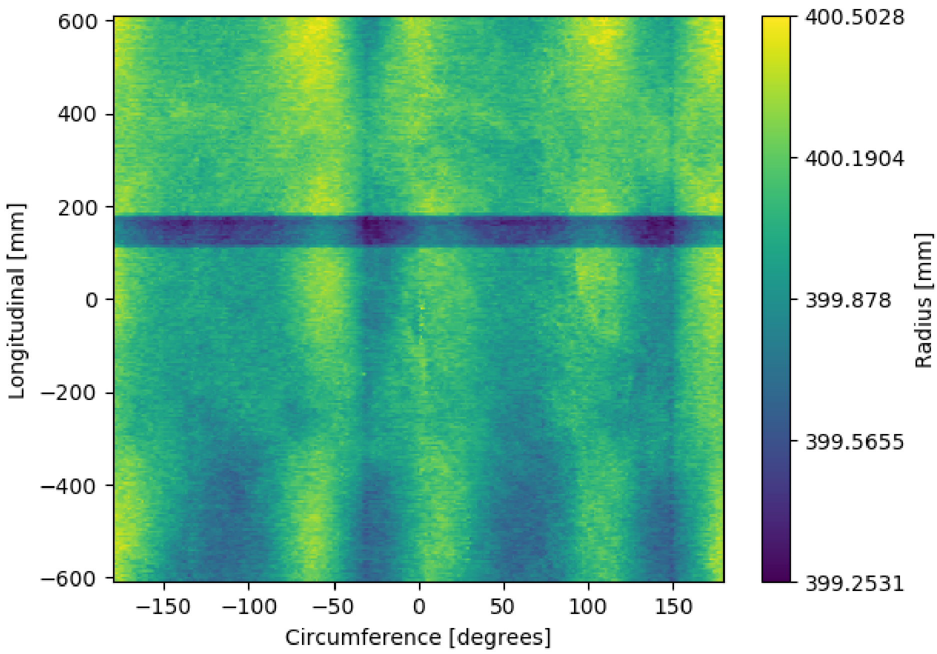

Figure 4.22: 2D representation of the radial coordinates of the 20% mandrel imperfection and 1220 mm solid laminate test article.

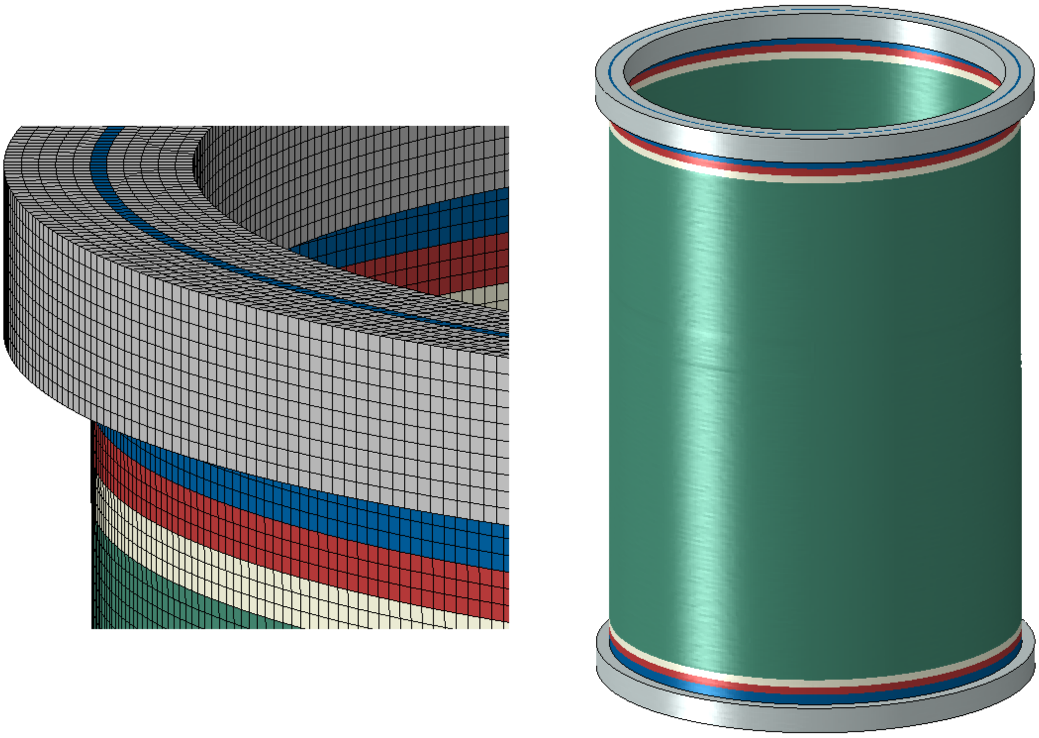

Figure 4.23: (left) Mesh and section construction of the edge, including potting and pad-ups, (right) test article FE model of the solid laminate cylindrical shell.

The resulting behaviour of the test article models are very similar to the models containing the mandrel imperfection but without the edge zones, when only the load-displacement curves are examined. The main difference compared to the previous models is that the cylindrical shell has become less stiff, due to the increased length. The mandrel cylindrical shell without imperfection shows almost the exact same buckling load as the cylindrical shell without imperfection and edge zones. Another difference is that the mandrel cylindrical shell without imperfection shows a small loading plateau, which is a numerical problem that also occurred in a portion of previous analyses. The imperfection with an amplitude of 2.85% shows a drop in buckling load of 5%, and the amplitude of 20% shows a drop in buckling load of 27%. The imperfection sensitivity is similar, if not exactly the same as for the previous cylindrical shell containing the mandrel imperfection. This was to be expected but it had to be confirmed, and it does show that the influence of the pad-ups and potting is minimal on the load-displacement behaviour and the imperfection sensitivity.

Table 4.13: Buckling loads of the solid laminate test article.

Analysis	Buckling load [kN]
FE dynamic without imperfection	2288.8
FE dynamic with mandrel imperfection amp. 2.85%	2172.0
FE dynamic with mandrel imperfection amp. 20%	1669.7

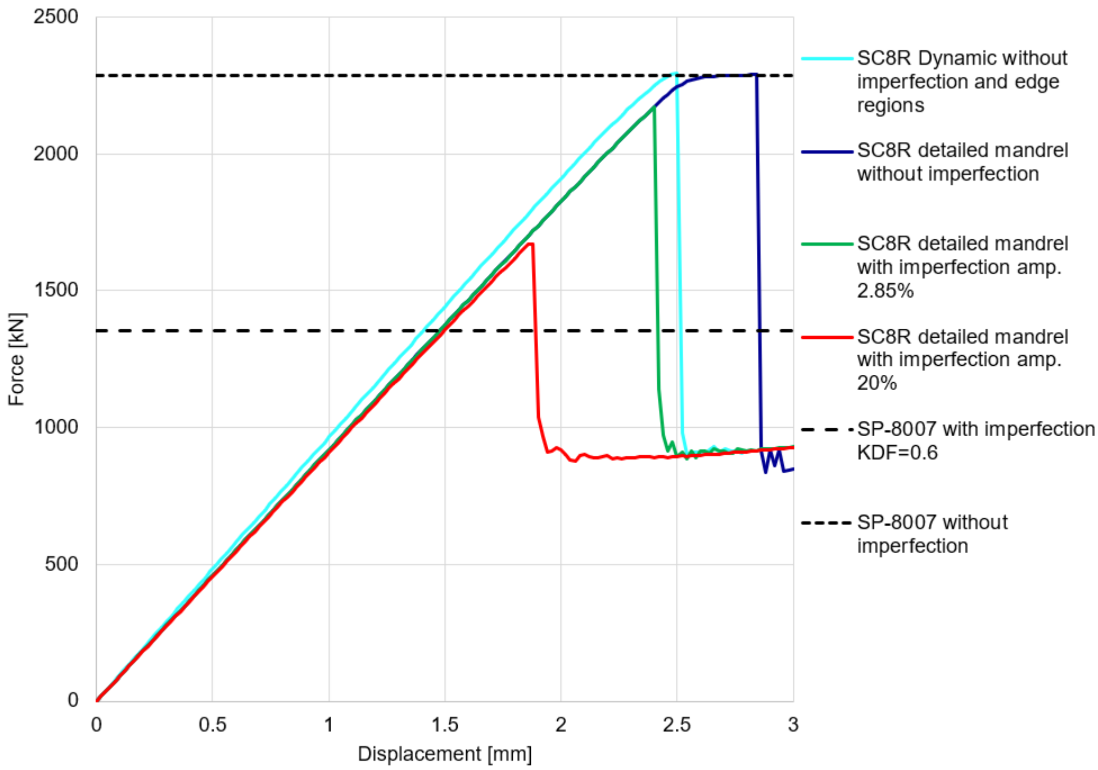

Figure 4.24: Load-displacement graph for the three solid laminate test article models.

The next step is to check the strains of the three cases for the last step before buckling, the strain values for the first six plies are reported in Table 4.14. When comparing the strains of the first six plies between the test article and 1120 mm model, it can be seen that the cylindrical shell without imperfection shows lower strains for the test article model, while the strains for the cylindrical shell with imperfections are higher for the test article model. The strain values are thus still high in general, but not an indication of material failure before buckling. For the three cases, the second ply is still deemed to the most critical. The explanation for it being critical is due to it being a zero ply, which is under tension in the second material direction. A more elaborated explanation was given in the precious section, which is also valid for this test article. Due to the second ply being critical, the contour plots will again be shown for the strain in the second ply, see Figure 4.25.
From the contour plot of the cylindrical shell without imperfection, it can be seen that the pre-buckling shape of the has changed to an axisymmetric shape, which was not seen for the cylindrical shell without the edge zones. This does confirm that the load plateau can be caused due to a axisymmetric pre-buckling shape. The pre-buckling shape of the cylindrical shells including imperfection might look more different than they are, as these test article include the extra edge sections. There are some changes to the middle section of the cylindrical shells with imperfection but these are minimal.

When comparing the two cylindrical shells which include imperfections, the most noticeable difference is the location of the maximum strain. As the lower amplitude imperfection shows the maximum strains at the bottom, while the higher amplitude imperfection shows the maximum strains at the top. At the top of the cylindrical shell which include the imperfection, an imperfection band is located as mentioned before. This would mean that the maximum strain of the cylindrical shell with 2.85% mandrel imperfection is not located at the imperfection band, while this is the case for the 20% imperfection amplitude. It seems the imperfection band prevents the extra circumferential half waves from forming at the top of the cylindrical shell, which did form at the bottom of the cylindrical shell. As it can be clearly seen from the contour plot showing the strain in the first material direction, that there are dimples formed at the bottom. Due to this phenomena being unexpected, these results were checked in detail. When the strain contour plot is looked at in detail, by zooming in considerably, the imperfection band can be visually located at the top of the cylindrical shell. This does thus confirm that these results are correct.

For the test article models, the failure criteria output available in Abaqus was used, which consists of the following failure criteria: Max Stress, Max Strain, Tsai-Wu, Tsai-Hill and Hashin damage. Due to the abrupt drop in load carrying ability of a cylindrical shell after buckling, these failure criteria all showed failure at similar locations of the load drop for each cylindrical shell, which can be seen in the load-displacement graph in Figure 4.26. It is of great importance that this cylindrical shell does not show any failure before buckling, which is confirmed by the failure criteria used. All of the failure criteria showing failure at the same increment can be considered unusual, but this can be explained by the high increase of stresses and strains after buckling. A more exact moment of failure during the load drop or after could be determined if needed, but would require a much smaller increment size or more output requests during buckling.

The contour plots for the radial displacement and Tsai-Wu criteria at the increment of failure are shown in Figure 4.27. It can be seen that the failure location is not always at the location of the highest radial displacement, but instead more often on the location with the highest amount of bending. It is important to note that failure does not happen at the edge, where the load is introduced, but in the middle section. The buckling shape of the cylindrical shell without imperfection shows less half waves compared to the 2.85% amplitude imperfection shape, while the 20% imperfection shape shows more similarity with the cylindrical shell without imperfection. This could be explained by the load at which failure occurs, where the cylindrical shell with 2.85% imperfection shows failure at a higher load compared to the other two cases, but this is most likely dependant on the location of the first increment or output request after buckling. In the load-displacement graph it can be seen that the graphs converge in the post-buckling field, which also indicate that the cylindrical shells will converge to similar modeshapes in the post-buckling field as well. This convergence in the post-buckling field was not always seen for other imperfection types.

Table 4.14: Strains of the inner first six plies of the solid laminate test article.

Without imperfection	ε_{11}	ε_{22}	ε_{12}
Ply 1	-2041	3293	5529
Ply 2	-3141	4467	-125
Ply 3	-1918	3319	-5416
Ply 4	-1855	3330	-5362
Ply 5	-2917	4467	-126
Ply 6	-1725	3350	5260
Mandrel imperfection 2.85%	ε_{11}	ε_{22}	ε_{12}
Ply 1	-2009	2864	5064
Ply 2	-2880	3862	-588
Ply 3	-1898	2900	-4879
Ply 4	-1840	2900	-4823
Ply 5	-2680	3841	-489
Ply 6	-1722	2870	4753
Mandrel imperfection 20%	ε_{11}	ε_{22}	ε_{12}
Ply 1	-1818	2173	3899
Ply 2	-2306	2893	-782
Ply 3	-1690	2166	-3789
Ply 4	-1631	2155	-3734
Ply 5	-2117	2837	-657
Ply 6	-1519	2133	3859

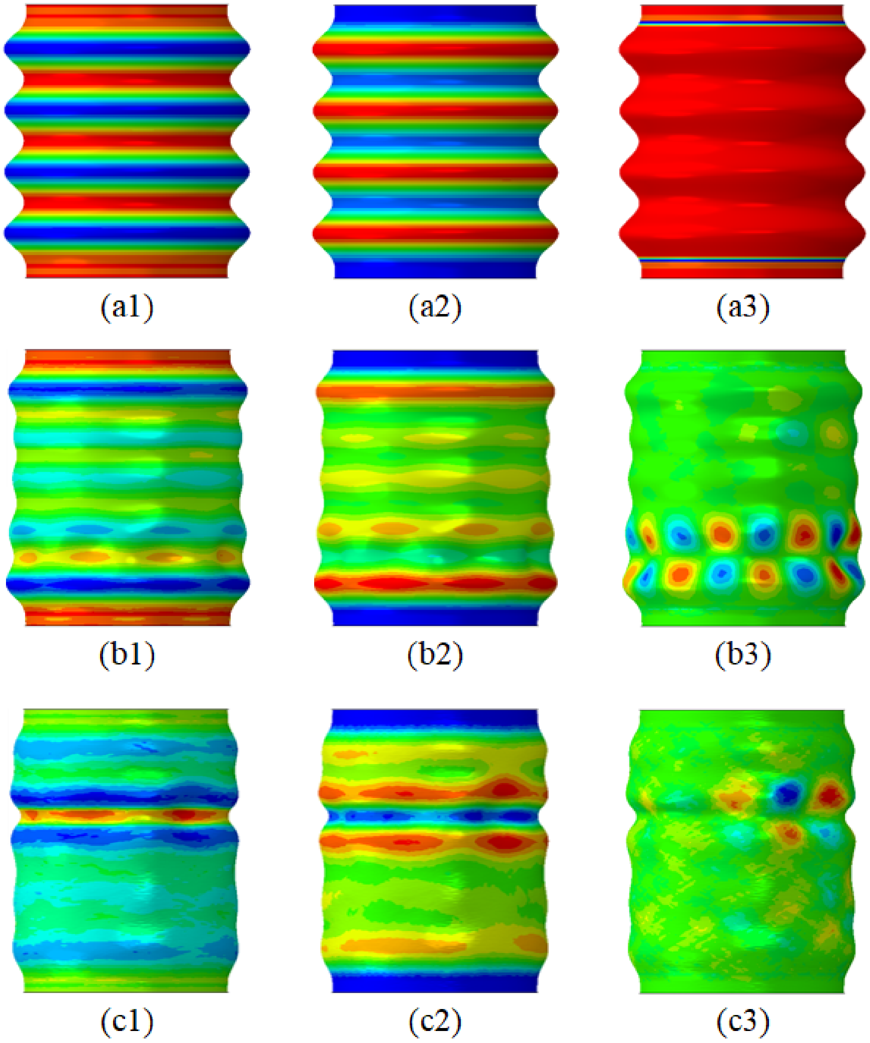

Figure 4.25: Contour plots for the strain of the second ply of the solid laminate test article with a deformation scale of 50. Each row is one type of imperfection: a = without imperfection ; b = mandrel imperfection 2.85% ; c = mandrel imperfection 20%. The number notation: 1,2 and 3 are ε_{11},ε_{22} and ε_{12} respectively.

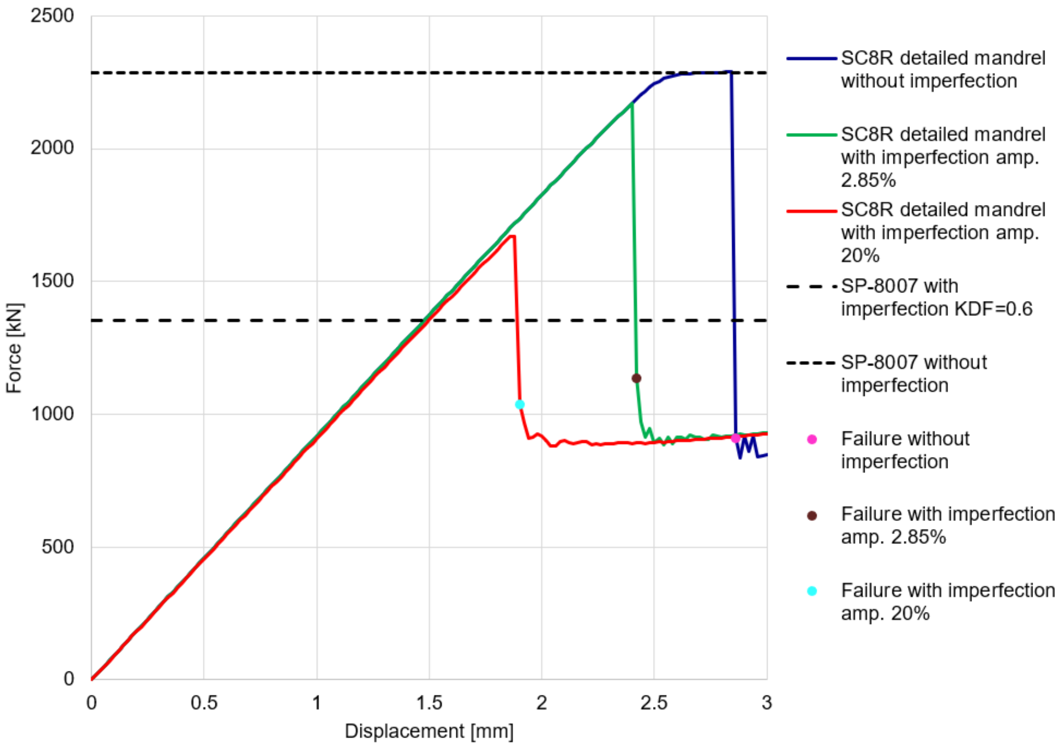

Figure 4.26: Failure criteria for the solid laminate test article.

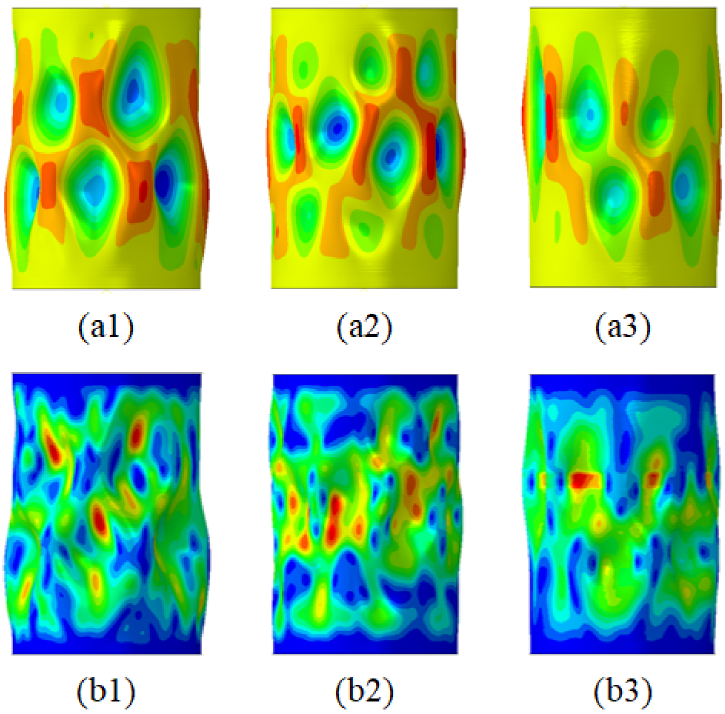

Figure 4.27: Post-buckling contour plots of the solid laminate test article model with a deformation scale of 4 for (a) radial displacement and (b) Tsai-Wu criteria. The notation 1,2 and 3 are for the cylindrical shell without imperfection, with 2.85% imperfection and 20% imperfection respectively.

4.3.7 Sensitivity to Numerical Damping

Due to the loading plateau that occurred for several of the FE results shown in this chapter, an investigation was executed to investigate the influence of the damping value for a dynamic implicit analyses. This loading plateau showed for cylindrical shells without imperfection, where this phenomena occurs due to it having no imperfections. It is most likely the case that the loading plateau takes as long as there is not a numerical error large enough to initiate buckling. The damping value alpha that was varied, is a parameter of the Hilber-Hughes-Taylor integrator which is the default integrator for a dynamic implicit analysis in Abaqus [57]. The damping is defined by one value, as the other two variables, named beta and gamma, are calculated by a set of equations which ensure desirable characteristics of the default integrator used for the dynamic implicit analysis. The alphas to be used consist of two pre-sets in Abaqus: Transient Fidelity alpha = -0.05, Moderate Dissipation alpha = -0.41421; and three custom values: 0, -0.01 and -0.025. For this investigation, the solid laminate test article without imperfection was used. This results in the load-displacement graph shown in Figure 4.28.

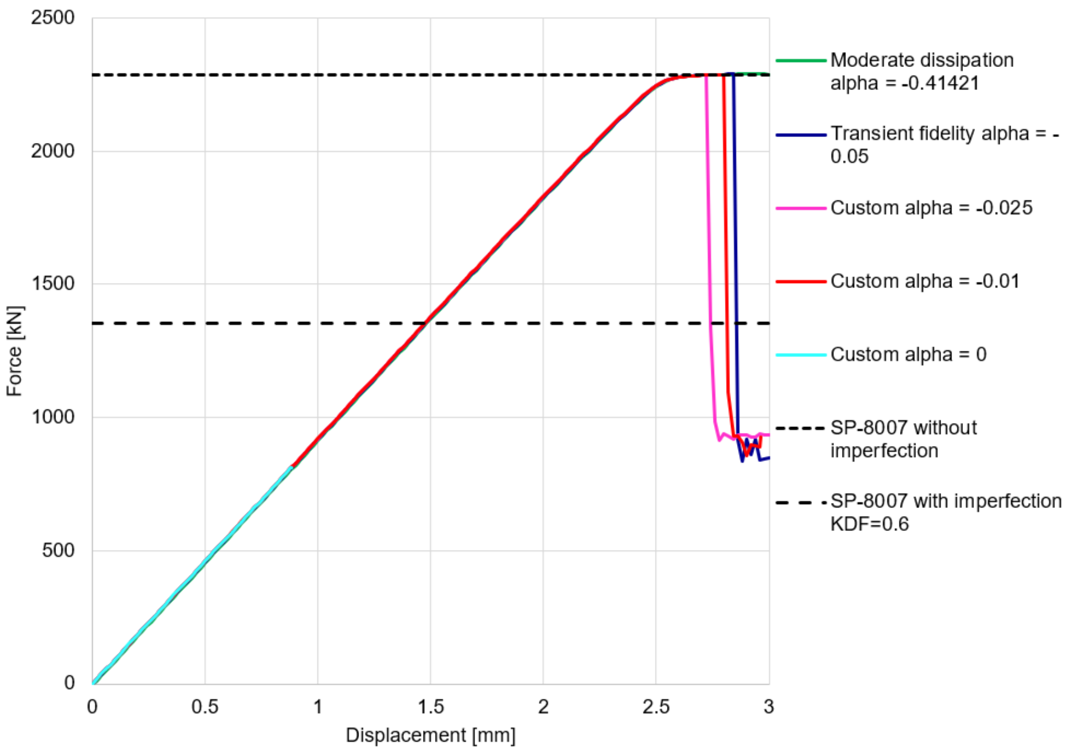

Figure 4.28: Load-displacement graph for the numerical damping comparison.

The result of the moderate dissipation preset was to be expected, as an increase in damping is most likely to minimize numerical errors and over-damp the analysis. The value of -0.025 for alpha does minimize the loading plateau, and is a improvement of previous results. A lower value of alpha however, a value of -0.01, increases the loading plateau again. When a value of 0 is used, thus without damping, the analysis does not converge and is stopped by Abaqus itself due to too many attempts for an increment. It can be expected from an analysis to not converge when there is no damping used, but actually showing it does not converge does add value to the investigation.

From the first three damping values and the lowest damping value, it would seem that there is convergence behaviour of the loading plateau until the analysis itself does not converge any more. It is however the result of the analysis for an alpha of -0.01 that shows a slight inconsistency of the behaviour as a function for the damping value. What the exact reason of this result is would require more research. From the test it can be concluded that improved results can be achieved, but it will require some fine tuning for each analysis for which it is questionable if it is actually worth it or not. The loading plateau only happens for cylindrical shells without imperfection, judged from the results in this thesis, where the buckling load itself does not increase due to the plateau. The buckling load is thus still obtained from these analyses. While the cylindrical shells without imperfection are important as they serve as a reference case to cylindrical shells with imperfections, spending more time on the fine tuning for models which include imperfections might add more to the value of the research.

4.4 Discussion and Outcome

The scaled solid laminate cylindrical shell has been analysed in detail, which has lead to a set of results which were used for a comparison w.r.t. the full scale cylindrical shell later on. From the element comparison it can be concluded that all elements showed good results, it is however the consistency and the computational efficiency which leads to the SC8R element being in favour of modelling the next scaled cylindrical shell. The imperfections that were compared, showed that the axisymmetric imperfection causes behaviour of the cylindrical shell which does not come close to a cylindrical shell including mandrel imperfections. The diamond modeshape imperfection would be a better option in most cases, as it does not show the drop in stiffness as was seen for the axisymmetric imperfection. The loading imperfection that was investigated showed its main effect on the buckling load, while the stiffness remained unchanged. Even the maximum amplitude used for the loading imperfection showed that it did not affect the stiffness of the cylindrical shell, which was surprising in comparison with the other imperfection types. The mandrel imperfections are ideal to use in an analyses, and would most likely lead to results closest to experimental test results. These mandrel imperfections are however not always available, making the diamond modeshape a valid option. Using several imperfection amplitudes does result in a more elaborate comparison of the imperfection types, as this provides a more clear behaviour pattern of each imperfection type as function of the imperfection amplitude. One of the examples where it did show an unexpected result, is the 20% amplitude diamond shape. This case saw a considerable change in the strain pattern which was not seen before.

From the analyses that were executed, the solid laminate cylindrical shell seems a valid option to be tested. It does not show material failure before buckling, but it does show a high imperfection sensitivity in some cases. The KDF resulting from using the mandrel imperfection can be considered high, but it should be said that the imperfection consists of the mandrel imperfection only and the real manufactured cylindrical shell might thus show more imperfections. The manufactured cylindrical shell will contain more imperfections due to the manufacturing, which can increase the imperfection amplitude next to changing the imperfection signature. A sensitivity analysis w.r.t. laminate thickness and cylindrical shell radius was executed, from which was seen that an increase in radius would not cause problem with experimental testing. It is however shown that an increase in laminate thickness can become problematic, when the laminate thickness becomes 7-8% thicker than it was designed to be. The likely hood of such a increase in thickness is low, and it should thus not become a problem for experimental testing. How representative the scaled solid laminate cylindrical shell is of the full scale cylindrical shell can only be determined during a comparison with the full scale cylindrical shell.

4.5 Summary

The scaled solid laminate cylindrical shell was used for both linear and non-linear analyses. The first set of linear analyses was executed for the S4R, SC8R and CSS8 element showing good agreement. Modeshapes for all three elements were shown, which showed small differences between the elements. The next step was to use non-linear analysis, for which dynamic implicit analysis is used. The first set of analyses compared the displacement rate, to find an optimum between computational efficiency and the accuracy of the buckling behaviour. Then two types of imperfections were compared: modeshape imperfections using both a axisymmetric and a diamond imperfection and a loading imperfection. For these analyses the S4R element was used. The results showed that the cylindrical shell is imperfection sensitive, where the sensitivity to the axisymmetric imperfection is higher than to the diamond imperfection. This is most likely caused by the drop in stiffness when the axisymmetric imperfection is applied, as the drop of stiffness is considerably higher compared to when the diamond imperfection is applied. The loading imperfection also shows considerable drops in buckling loads, but it is difficult to quantify the amplitude of the loading imperfection for a comparison with the modeshape comparison. The loading imperfection does hardly cause any drop in stiffness and only lowers the buckling load.

In the following step the three elements are again compared, now for a non-linear analyses using both cylindrical shells with and without imperfection. The SC8R and CSS8 elements show agreement for the buckling loads for the cylindrical shells with imperfection, where the S4R element showed small differences. For the cylindrical shell without imperfection, all three elements showed good agreement but the CSS8 element showed a short loading plateau. Due to these results it was chosen to continue with the SC8R element for further analyses of the solid laminate cylindrical shell.

In the following step, mandrel imperfections were included into the FE model. These mandrel imperfections are based on measurements executed at NASA on the mandrel which will be used for production of this cylindrical shell. The processing steps for the measurement data were elaborated on and the imperfection signatures were shown. The analyses which included the mandrel imperfection showed that the cylindrical shell is much less sensitive to the mandrel imperfection in comparison to modeshape comparisons. Maximum strain values were shown, to be able to determine that no material failure would occur before buckling.

The effect of laminate thickness and cylindrical shell radius were investigated. To ensure that the testing equipment would be capable of the experimental test, if the cylindrical shell would have a larger radius of thicker laminate then was intended. The results showed that the radius would not be a problem, but if the laminate thickness of the cylindrical shell increases more than 8% it could become a problem. This high increase of thickness is however unlikely to happen.

The last step of the chapter is to analyse a test article model of the solid laminate cylindrical shell. This cylindrical shell includes the pad-ups and potting material at the edge.

This cylindrical shell is slightly less stiff compared to the previous cylindrical shell using the mandrel imperfection, due to the increase in length. Maximum strain values are shown, both in table format and contour plot. Failure criteria are used to determine when failure happens, which is right after buckling as was intended. The cylindrical shell without imperfection shows a slight loading plateau, and therefore an investigation was executed to determine the effect of numerical damping on the analyses. A decrease of the loading plateau can be achieved, but this will require a fine tuning process to find the optimum damping value. When the damping value is too low, the analysis can stop to converge, which was shown for the extreme case of no damping.

The outcome of the chapter is that the best combination to model a cylindrical shell with imperfections, is to use the SC8R element combined with mandrel imperfections. When mandrel imperfections are not available, a diamond modeshape is a valid option. The scaled solid laminate cylindrical shell seems a valid option to be experimentally tested, but a final comparison with the full scale cylindrical shell will provide more clarity.

Chapter 5

Scaled Sandwich Cylindrical Shell

This chapter will go in depth on the modelling of a cylindrical shell constructed from a sandwich panel. This cylindrical shell is the second scaled configuration to be tested, which was designed according to the scaling procedure as published in 2018 by Uriol Balbin et al. [4]. The amount of analyses in this chapter are limited in comparison the chapter on the solid laminate cylindrical shell. As the knowledge on FE properties such as: mesh size, element type and displacement rate from the previous chapter is applicable for this cylindrical shell as well. The chapter will still incorporate an element comparison, but for a lower amount of models compared to the previous chapter. Due to the cylindrical shell being a sandwich panel, it is of interest for further research to use separate elements through the thickness for the facesheet and core respectively. In the preliminary phase of the thesis, a tensile specimen was used to test different elements configurations for the construction of a sandwich panel, which will also be shown. The benefit of multiple elements through the thickness can be in the form of improved bending behaviour, and also the ability to analyse facesheet separation when these models will continue to be used after the thesis.

5.1 Tensile Specimen

The tensile specimen is used for preliminary analysis of different element configurations to model a sandwich panel. Due to the sandwich consisting of different materials, it can be of interest to model the materials with different elements, or each layer of a different material as a separate element. Two configurations of the tensile specimen were analysed, for which the structural properties are reported in Figure 5.1. The difference between these two configurations, is the thickness of the core, which is 1 mm and 3 mm. The tensile specimen will make use of the IM7/8552 material, for which the properties can be seen in Table 3.9. This IM7/8552 material is from a different batch as the IM7/8552 material to be used for the sandwich cylindrical shell later on. The core material is a foam material, for which the material properties are reported in Figure 5.1. This core material is the same foam material that was used for the sandwich cylindrical shell. Two different mesh sizes were used for the modelling of the tensile specimen. For the core thickness of 1 mm, a mesh size of 1 mm and 5 mm were used, while the core thickness of 3 mm will only use a mesh size of 1 mm. Three types of element configurations were used. A single element through the thickness, for which the S4R, SC8R and CSS8 element were used, and three elements through the thickness for which a S4R and C3D8R combination, seen in Figure 5.2, and a SC8R and CSS8 combination, seen in Figure 5.3, were used. The FE model consists of the tensile specimen, which is clamped on one end and clamped except for a longitudinal translation on the other end. An illustration of the FE model is seen in Figure 5.1. The type of analyses is a linear static, for which a displacement of 3.2 mm is used. The comparison will consist of a resulting force comparison, from which the stiffness differences can be observed, and a CPU time comparison. The results of the linear static analyses of the first configuration, using a 1 mm core, can be seen in Table 5.3 and Table 5.4 for a mesh size of 5 mm and 1 mm respectively.

Table 5.1: Tensile specimen configurations.

Configuration	1	2
Facesheet Layup	$[0, 90]_s$	$[0, 90]_s$
Core Thickness [mm]	1	3
Width [mm]	60	60
Length [mm]	200	200

Table 5.2: Rohacell 300 WF material properties.

E [MPa]	ν	ρ [kg/m^3]
578	0.3	300

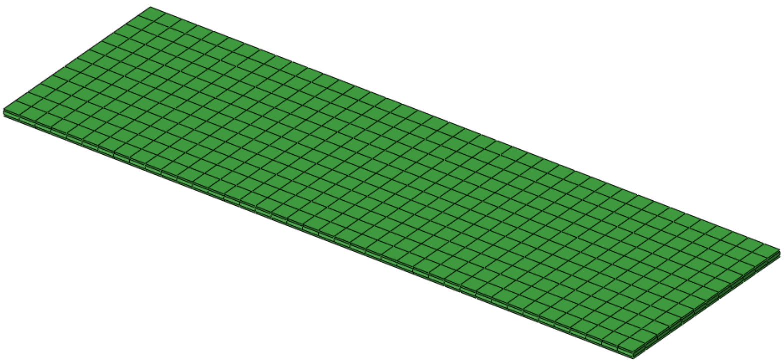

Figure 5.1: Tensile specimen FE model.

Figure 5.2: S4R facesheets with C3D8R core element configuration.

Figure 5.3: SC8R facesheets with CSS8 core element configuration.

Table 5.3: Tensile specimen results for a 5 mm mesh size and core thickness of 1 mm.

Elements	Force [kN]	Disp. [mm]	CPU time [s]
S4R	84.12	3.2	0.3
SC8R	84.16	3.2	0.4
CSS8	84.17	3.2	1.8
S4R+C3D8R+S4R	84.44	3.2	0.6
SC8R+CSS8+SC8R	84.39	3.2	0.9

Table 5.4: Tensile specimen results for a 1 mm mesh size and core thickness of 1 mm.

Elements	Force [kN]	Disp. [mm]	CPU time [s]
S4R	84.12	3.2	6.1
SC8R	84.13	3.2	6.8
CSS8	84.15	3.2	43.4
S4R+C3D8R+S4R	84.12	3.2	17.1
SC8R+CSS8+SC8R	84.18	3.2	25.3

Table 5.5: Tensile specimen results for a 1 mm mesh size and core thickness of 3 mm.

Elements	Force [kN]	Disp. [mm]	CPU time [s]
S4R	85.32	3.2	6.1
SC8R	85.33	3.2	7
CSS8	85.35	3.2	43.5
S4R+C3D8R+S4R	85.32	3.2	17.3
SC8R+CSS8+SC8R	85.38	3.2	25.2

For the coarse mesh, the resulting forces are close and all elements show results which can be considered accurate enough. When the mesh is refined, it can be seen that the resulting forces from the elements, besides the S4R element, converge towards the force obtained from using the S4R element. This kind of behaviour was also seen from previous element comparisons. The S4R is less sensitive to mesh size, and the remaining elements converge to similar results for finer meshes. When the CPU times are compared, the CSS8 showed the highest CPU time, which was to be expected from knowledge gain in previous element comparisons. The unexpected result from the CPU time comparison is that the combination of SC8R and CSS8 elements costs less CPU time compared to the CSS8 element alone. This can be explained however, as their is a considerable amount of integration points difference between the CSS8 element configurations for each analysis. When the CSS8 element is only used for the core, it has much less integration points than when it is used for both the facesheets and the core. The impact on the CPU time due to the added SC8R elements for the facesheets is minimal, as it is already computational efficient in comparison. The results of the second configuration, using a 3 mm core and a mesh size of 1 mm, can be seen in Table 5.5. These results are almost an exact copy of the previous analyses, there is just a small difference in load due to the added core thickness. This is to be expected due to the core being much less stiff compared to the facesheets and not having a large influence in tensile loading, while larger differences were seen under bending or compressional loads. From these results it can thus be said that all element configurations are viable options for the element comparison using a sandwich cylindrical shell.

5.2 Modelling of the Sandwich Cylindrical Shell

The sandwich cylindrical shell uses the same diameter of 800 mm as used previously for the cylindrical shell. The sandwich cylindrical shell is however considerably shorter in comparison to the other scaled configuration, with a length of 730 mm. All the structural properties of the sandwich cylindrical shell are reported in Table 5.6. The analytical buckling load is calculated by using two different methods. The reference case is the SP-8007 solution. The second solution is the method as published by Reese and Bert [58]. This solution is used as the SP-8007 method is not specifically developed for a sandwich composite, while the method by Reese and Bert is. The analytical buckling loads are reported in Table 5.7. The sandwich cylindrical shell uses the same composite material for the facesheets as the solid laminate cylindrical shell used, from which the material properties are shown in Table 4.2. The core will consist of a foam material, for which the properties are shown in Table 5.2. While the CTA 8.1 cylindrical shell uses a aluminium honeycomb core, the scaled cylindrical shell does not use the same core material. This is due to the core of the scaled configuration being considerably thinner compared to the full scale cylindrical shell, which causes issues with manufacturability of a honeycomb core. The manufacturability of a sandwich using a foam core can also become problematic when the core becomes too thin, but it is a much more viable option for thin cores in comparison to a honeycomb core.

The FE model is again constructed similar to previous cylindrical shells, with a reference points on each side, with the model shown in Figure 5.4. The first analysis that was executed with the sandwich cylindrical shell was a linear static general using the SC8R element for the cylindrical shell without imperfection. This provides a comparison to see potential stiffness drops. Three types of cylindrical shells were modelled for the dynamic implicit analyses: a cylindrical shell without imperfection, one cylindrical shell with the mandrel imperfection and one cylindrical shell with the exaggerated mandrel imperfection. The method of incorporating the mandrel imperfection is the same as for the solid laminate cylindrical shell. The main difference lies in the shorter cylindrical shell, as the sandwich cylindrical shell is 730 mm long. This requires a new imperfection mesh to be processed, which results in the imperfection signature shown in Figure 5.5. The actual amplitude of the mandrel imperfection is 4.1% w.r.t. to the thickness of the sandwich panel. The imperfection signature for the exaggerated imperfection can be seen in Figure 5.6, which is again scaled to 20% w.r.t to the thickness. Due to the different thicknesses of the two scaled cylindrical shells, the 20% amplitude mandrel imperfection has a different magnitude for the two scaled cylindrical shells. The analyses using the single SC8R through the thickness will include the failure criteria as available in Abaqus: Max-Stress, Max-Strain, Tsai-Hill, Tsai-Wu and Hashin damage. Only failure of the composite plies are checked, there is no failure included for the core material. The results of the analyses using the SC8R element are shown in Figure 5.7.

Table 5.6: Scaled sandwich cylindrical shell configuration.

Facesheet Layup	$[56, 0, -56]$
Core Thickness [mm]	1.9
Diameter [mm]	800
Length [mm]	730

Table 5.7: Analytical buckling loads and corresponding knockdown factor according to NASA SP-8007 [2] and Reese and Bert [58].

Buckling Load [kN]	
SP-8007 Without Imperfection	874.14
SP-8007 With Imperfection	517.7
Reese and Bert Without Imperfection	794.4
Knockdown Factor	0.6

Table 5.8: Buckling loads of the scaled sandwich cylindrical shell.

Analysis	Buckling load [kN]
FE dynamic without imperfection	767.1
FE dynamic with mandrel imperfection amp. 4.1%	727.8
FE dynamic with mandrel imperfection amp. 20%	582.6

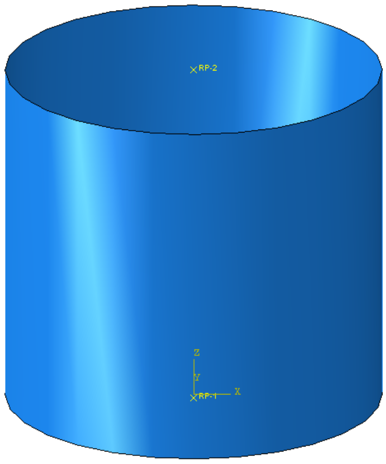

Figure 5.4: FE model of the scaled sandwich cylindrical shell.

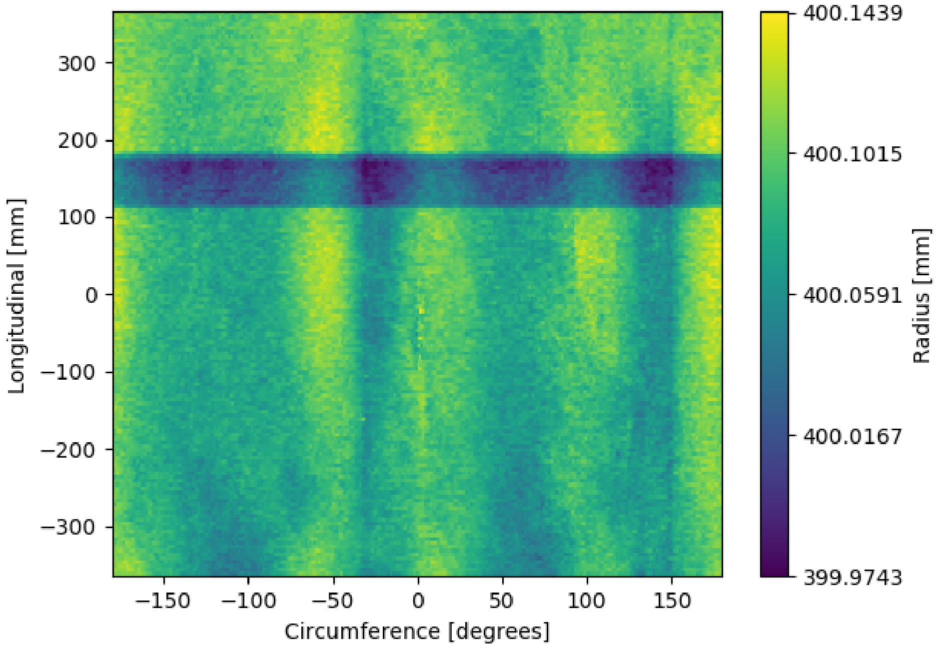

Figure 5.5: 2D representation of the radial coordinates of the 4.1% mandrel imperfection for the scaled sandwich cylindrical shell.

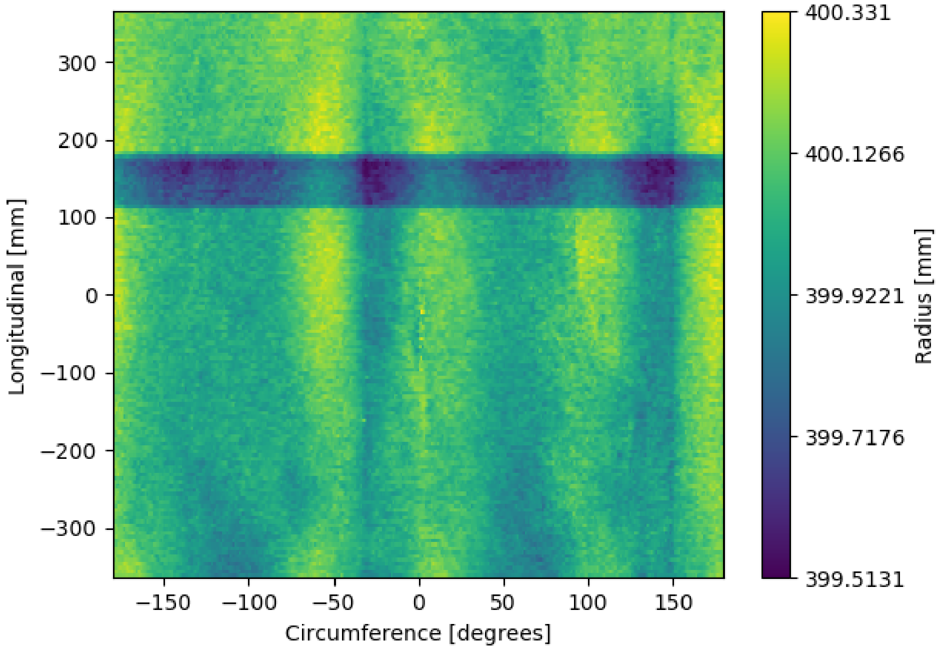

Figure 5.6: 2D representation of the radial coordinates of the 20% mandrel imperfection for the scaled sandwich cylindrical shell.

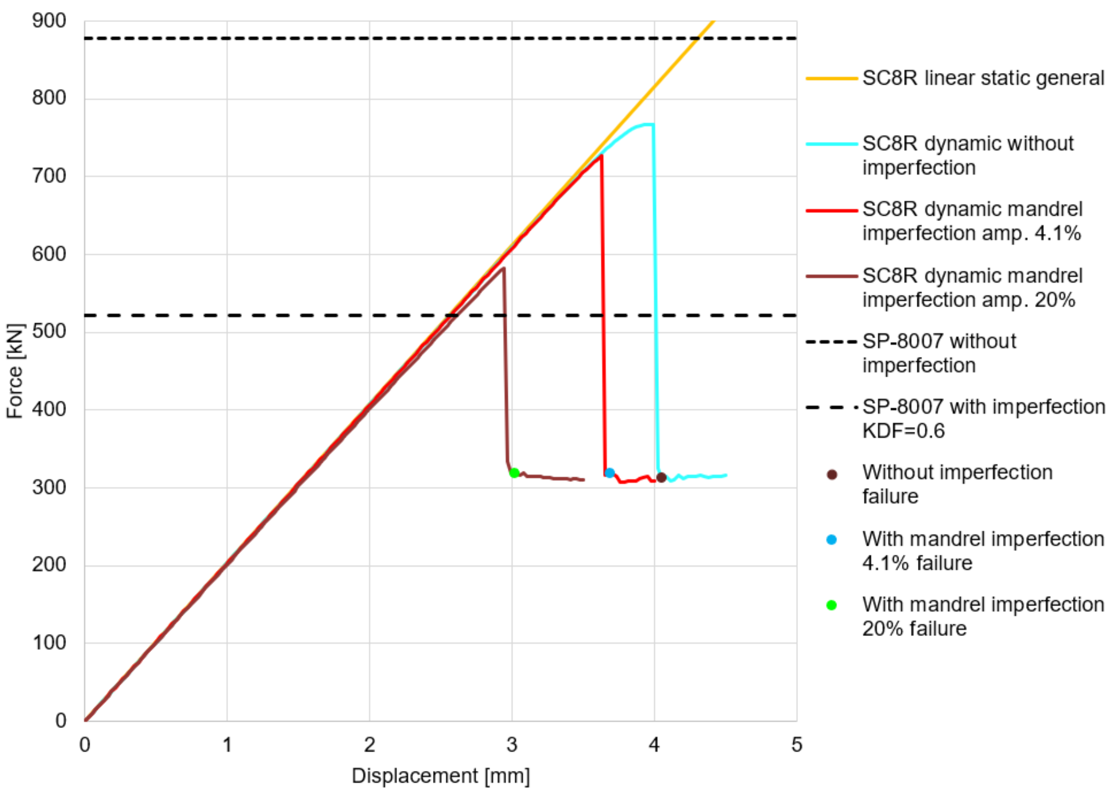

Figure 5.7: Load-displacement graphs of the scaled sandwich cylindrical shell using the SC8R element.

When taking a first look at the presented load-displacement graph, the most noticeable difference is that the buckling load resulting from the cylindrical shell without imperfection is 13 % lower compared to the SP-8007 analytical buckling load. The solution by Reese and Bert shows a smaller difference of 3.5%. This could be expected, as the solution by Reese and Bert is specifically for a sandwich panel, while the solution from SP-8007 is intended for a solid laminate. Comparing the results of the different imperfection amplitudes in Figure 5.7, it can again be seen that the cylindrical shells do not seem to have a high imperfection sensitivity to the mandrel imperfection. The 4.1% mandrel imperfection shows a 5% drop in buckling load in comparison to the cylindrical shell without imperfection, while the 20% mandrel imperfection shows a 24% drop in buckling load. The 20% mandrel imperfection is an exaggeration, and still shows a higher knockdown factor compared to the analytical results from SP-8007. As SP-8007 results in a KDF of 0.6, while the mandrel imperfection shows a KDF of 0.95 and 0.76 for the 4.1% and 20% mandrel imperfection respectively. The drop in stiffness due to the imperfection is also minimal, with only the exaggerated imperfection showing a slight drop in stiffness just before buckling, while the 4.1% imperfection showing practically no drop in stiffness.

The failure criteria that were included showed failure after buckling. This is coherent with the design of launch vehicle cylindrical shells, which are designed to not fail before buckling. Furthermore, it also means the experimental test will show buckling as intended, and not premature material failure. The failure criteria all showed failure at the same increment for each analysis, which is similar to the failure behaviour seen for the solid laminate cylindrical shell. The failure criteria all show failure at the same increment, due to the major portion of the drop in load occurring between two output requests. This problem could be prevented by decreasing the increment size and requesting more frequent outputs, but this would increase the computational time and output database size considerably. To compare the locations of failure with the locations of maximum radial displacement,the contour plots for the radial displacement and Tsai-Wu failure criteria are shown in Figure 5.8.

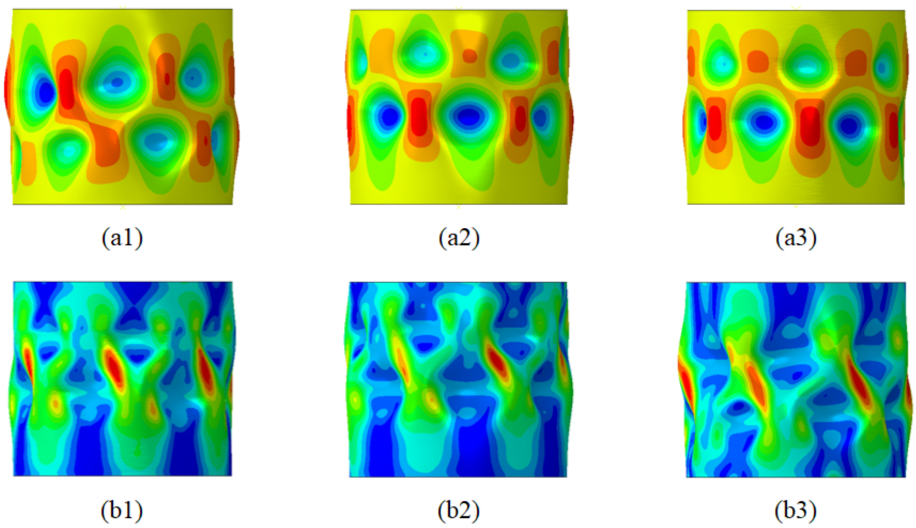

Figure 5.8: Post-buckling contour plots of the scaled sandwich cylindrical shell, with a scaling factor of 3, of the (a) radial displacement and (b) Tsai-Wu criteria, with the 1, 2 and 3 notation showing the cylindrical shell without imperfection, with 4.1% mandrel imperfection and 20% mandrel imperfection respectively.

The location of the failure with respect to the location of maximum radial displacement is similar to the location seen for the scaled solid laminate cylindrical shell. The locations showing high criteria values are at the location of highest bending and also located in the middle section of the cylindrical shell. The modeshapes of all three cylindrical shells show great agreement, which is most likely due to the buckling modeshape being fully or close to fully developed. As it can be seen that the failure increment is located after the steep drop in load. The last step for this cylindrical shell is to check the strains at the last increment before buckling, to ensure the cylindrical shell is not close to material failure before buckling. The strain values of the three plies of the inner facesheet are shown in Table 5.9.

Table 5.9: Maximum strains ($\mu\varepsilon$) of the inner facesheet of the scaled sandwich cylindrical shell.

Without imperfection	ε_{11}	ε_{22}	ε_{12}
Ply 1	-709	-4131	10970
Ply 2	-7566	4038	-36
Ply 3	-842	-3754	-10530
Mandrel imperfection 4.1%	ε_{11}	ε_{22}	ε_{12}
Ply 1	-765	-3513	8822
Ply 2	-6290	3115	226
Ply 3	-859	-3289	-8574
Mandrel imperfection 20%	ε_{11}	ε_{22}	ε_{12}
Ply 1	-933	-3675	7977
Ply 2	-5415	2833	1243
Ply 3	-974	-3263	-7625

When looking at the strain values of the three cylindrical shells, it can be seen that the shear strain of the first ply causes it to be critical for all the three cylindrical shells. The largest difference in strain between the three cases, is between the cylindrical shell without imperfection and the cylindrical shell with the 4.1% mandrel imperfection. The shear strain seen in the first ply, especially for the cylindrical shell without imperfection, is very close to the critical value and is thus a concern. It should be said however, that the cylindrical shell with the 4.1% mandrel imperfection does already show a considerable drop in the strain values, which is a more realistic case in comparison the to the cylindrical shell without imperfection.

To determine the location of the strain values, the strain values of the first ply are shown in a contour plot for the three cylindrical shells in Figure 5.9. The maximum strain values for the cylindrical shell without imperfection and the cylindrical shell with the 4.1% mandrel imperfection are located at the first half wave. A solution to lower the strain values at this location would be to add ply drops and potting, as was done with the solid laminate cylindrical shell. The effect of the ply drops will higher for the sandwich cylindrical shell, as it has only 3 plies per facesheet, 6 in total, in comparison the solid laminate cylindrical shell having 24 plies. It should thus be investigated if the extra plies are a problem for the scaling procedure and if the behaviour is still representative for the full scale structure. The location of the maximum strain values of the cylindrical shell with the 20% mandrel imperfection is in the region of the imperfection band, which was also seen in Figure 5.6. It can also be seen that this cylindrical shell does not show a similar half wave at the edges, which caused the high strain values for the other two cylindrical shell. The imperfection band can also be seen in the contour plots of the cylindrical shell with 4.1% mandrel imperfection, both by the shape and the colours. It does however not cause the highest strain values for this case. The reasoning for this imperfection band causing high strain values for the cylindrical shell with 20% imperfection, is that the exaggeration of the imperfection causes the edges of the imperfection to become relatively sharp next to the region having a lower radius for the whole imperfection band.

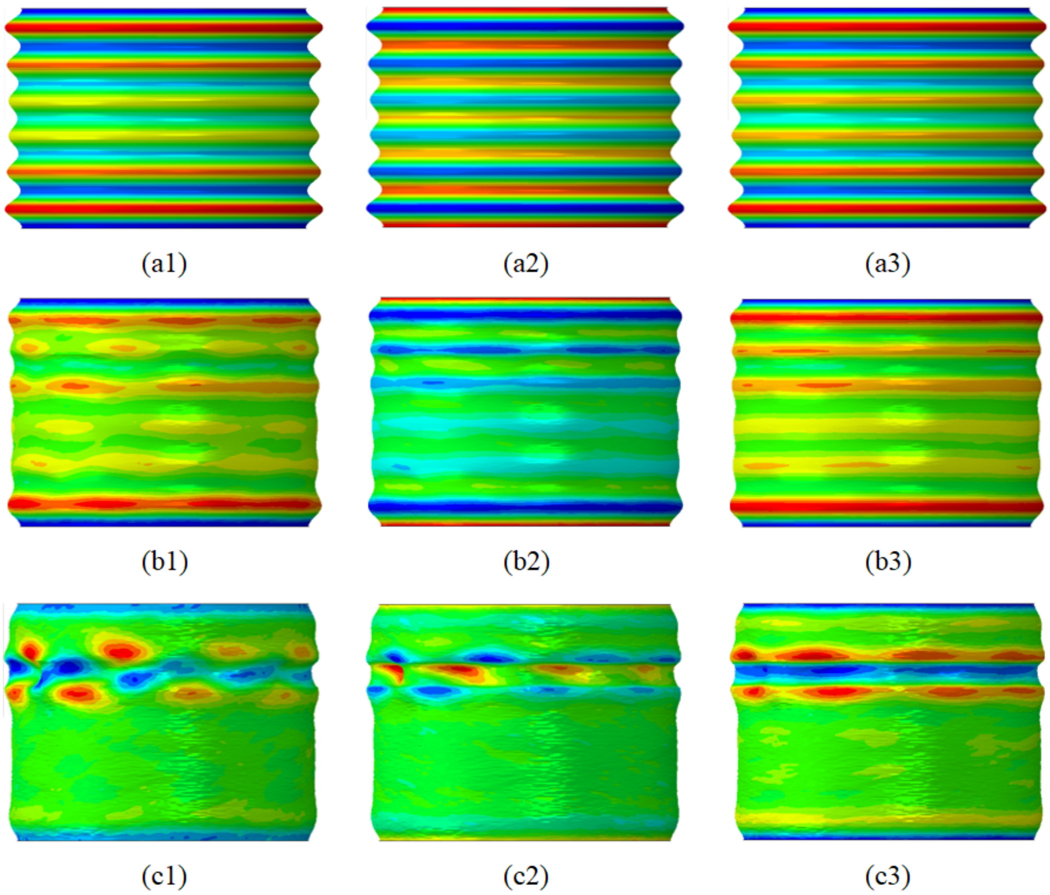

Figure 5.9: Contour plots of the scaled sandwich cylindrical shell, with a scaling factor of 30, for the strain of the first ply. Each row is one type of imperfection: a = without imperfection ; b = mandrel imperfection 4.1% ; c = mandrel imperfection 20%. The number notation: 1,2 and 3 are ε_{11},ε_{22} and ε_{12} respectively.

5.3 Element Comparison

For the element comparison, four different element configuration were used. A single SC8R and S4R through the thickness, 3 SC8R elements through the thickness and a SC8R element as facesheet combined with a CSS8 element for the core. The combination of the S4R and C3D8R element, which was shown in the tensile specimen section, is not used for this comparison as the C3D8R element showed inaccurate results when used for a cylindrical shell in subsection 3.1.3 and was therefore discarded to be used for a shell. The configuration with three SC8R elements through the thickness was not yet tested, but is seen as an interesting option due to the great results seen from the SC8R and CSS8 combination and the SC8R element itself. The element comparison will only be executed using the 4.1% amplitude mandrel imperfection. Comparing the elements for the cylindrical shell without imperfection and the two imperfection amplitudes would require considerable more computational time, while the 4.1% amplitude mandrel imperfection is seen as most realistic case and therefore most important to test. The results of the dynamic implicit analyses using the different element configurations can be seen in Figure 5.10 with the corresponding buckling loads reported in Table 5.10.

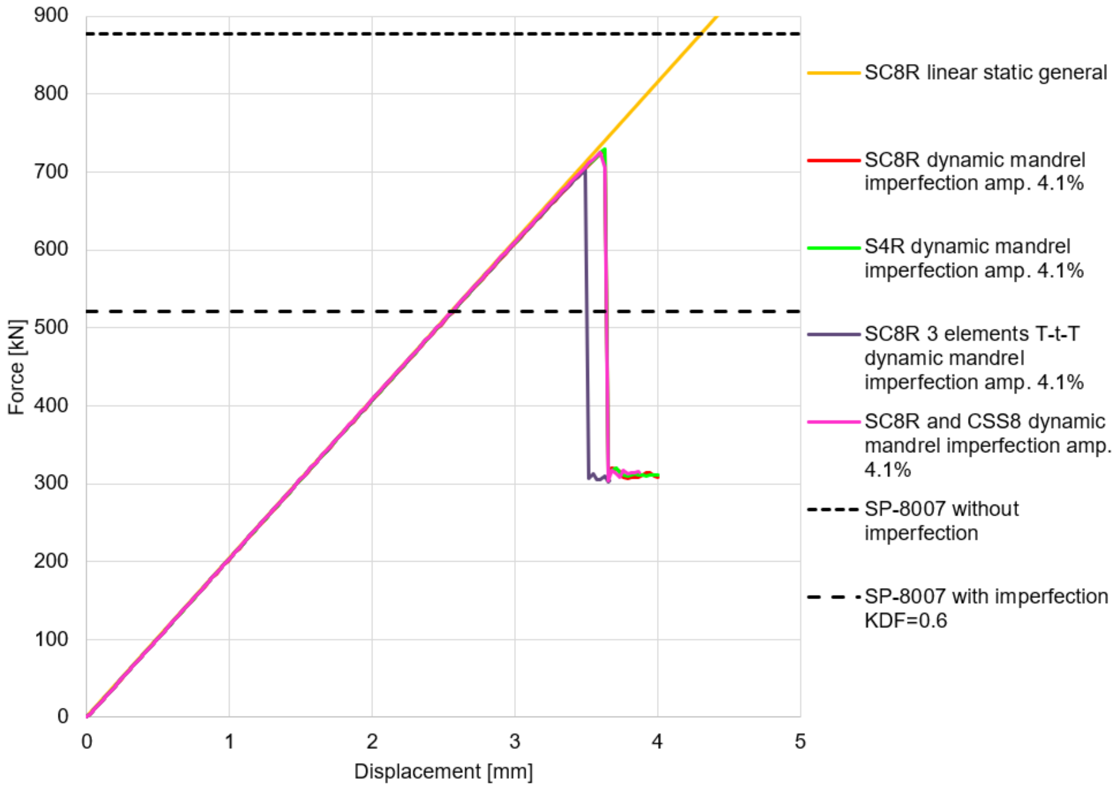

Figure 5.10: Element comparison using the scaled sandwich cylindrical shell with mandrel imperfection.

Table 5.10: Element comparison for the scaled sandwich cylindrical shell with mandrel imperfection.

Element	Buckling load [kN]
SC8R	727.8
S4R	728.9
SC8R 3 T-t-T	703.0
SC8R - CSS8 - SC8R	725.7

Three of the four element configurations show buckling loads within 0.5%. The only configuration showing a small difference is the three SC8R elements through the thickness, with a 3.5% lower buckling load in comparison to the single SC8R element through the thickness. This can be considered unexpected, as the single SC8R element through the thickness does match with the other element configuration. This might be caused by the fact that the core is modelled as a separate shell in between the shell facesheets, while the configuration with the CSS8 element models the core as a solid shell and thus a 3D material model. The configurations using one element through the thickness might not be affected by this difference, as the sandwich panel is modelled as one laminate. The result of the three SC8R elements through the thickness can still be considered accurate as it is a minimal difference.

5.4 Discussion and Outcome

The scaled sandwich cylindrical shell has been analysed for several configurations, which has lead to a set of results which were used for a comparison w.r.t. the full scale cylindrical shell later on. The sandwich cylindrical shell shows similar KDFs as seen for the scaled solid laminate cylindrical shell, and thus also showing a higher KDF than the KDF retrieved from SP-8007. This could confirm that SP-8007 can result in conservative KDFs, but the mandrel imperfection only accounts for the mandrel and not imperfections caused by the manufacturing. This could mean the mandrel imperfection is conservative. The exaggerated imperfection still shows a higher KDF in comparison to SP-8007, which ensures a higher degree of certainty for the claim that SP-8007 is conservative. The sandwich cylindrical shell does not show failure pre-buckling, but the strain values are considerably high at the last pre-buckling increment. An investigation is needed if pad-ups can lower the strains, to be able to ensure that this scaled configuration is a valid option for experimental testing. Three out four element configurations showed buckling loads within 0.5%, with the three SC8R elements through the thickness showing a 3.5% lower buckling load compared to a single SC8R element through the thickness. When the main goal of an analyses is to determine the buckling behaviour, a single SC8R or S4R element through the thickness is still recommended. It saves both time to model as computational time, while the results for the buckling behaviour are as accurate or better than other configurations. When damage analysis or facesheet core separation are of interest, the SC8R facesheet and CSS8 core combination is recommended, as it combines efficient modelling of the facesheets combined with a 3D material model for the core.

5.5 Summary

The scaled sandwich cylindrical shell offers a few new aspects. As it's the first cylindrical shell of this thesis using a sandwich panel design, which offers new possibilities for the FE model. To first get acquainted with the modelling of a sandwich panel, the first sandwich panel to be modelled consisted of a tensile specimen. The tensile specimen was modelled using two different structural configurations and two mesh sizes. A finer mesh saw the results of all element configurations converge, where it was seen that the S4R element is less sensitive to mesh size. The CSS8 element again showed the highest CPU time, even higher than using multiple elements through the thickness with two different combinations. The chapter then continued with the modelling of the sandwich cylindrical shell. The sandwich cylindrical shell has a diameter of 800 mm and a length of 730 mm. It has a core thickness of 1.9 mm, which is why a foam material core is used instead of a honeycomb core. A honeycomb core would be difficult, if not impossible, to manufacture for such a thin core thickness. Three types of this sandwich cylindrical shell were modelled: a cylindrical shell without imperfection, with a 4.1% mandrel imperfection and with a 20% mandrel imperfection. Due to the different thickness, the original mandrel imperfection has a higher amplitude with respect to the thickness compared to the scaled solid laminate cylindrical shell. These three cylindrical shells were modelled, and showed comparable behaviour to the scaled solid laminate cylindrical shell when looking at the load-displacement graph. The cylindrical shell without imperfection did however show a lower buckling load compared to the SP-8007 analytical solution, while the Reese and Bert analytical solution did show better agreement with the FE results. This was to be expected, as this difference is most likely caused by the assumption of using the SP-8007 method, that the core is thin enough to consider the sandwich as a single laminate. All failure criteria showed failure after buckling. The mandrel imperfection showed higher knockdown factors compared to the analytical solution. Strains in the pre-buckling last increment were checked, and were considered high. The cylindrical shell without imperfection showing shear strains close to failure. All contour plots in pre-buckling showed similar behaviour, both in radial displacement and failure criteria values. The largest difference in strain values was between the cylindrical shell without imperfection and the cylindrical shell with 4.1% mandrel imperfection.

An element comparison was executed. Two single element through the thickness configurations were used, with a SC8R and S4R element. Furthermore, two configurations with three elements through the thickness were used: SC8R facesheet and CSS8 core and SC8R facesheet and core. Three out of four configurations showed exact overlap, with only the three SC8R elements through the thickness showed a 4% lower buckling load which can still be considered accurate enough. It is discussed that the sandwich cylindrical shell shows higher KDFs from the FE analyses in comparison to the KDF received from SP-8007. It's also recommended to investigate if the strains can be lowered by adding pad-ups, as values close to material failure were seen. This would ensure the sandwich cylindrical shell would be a valid option for experimental testing.

Chapter 6

Full Scale Cylinder

This chapter focusses on the analyses of the CTA 8.1 cylindrical shell and the comparison with the scaled cylindrical shells which are based on the CTA 8.1. The analyses of the CTA 8.1 provide results which were compared to the results from the scaled cylindrical shells. The CTA 8.1 is a test cylindrical shell designed and manufactured by NASA. The cylindrical shell is manufactured from a sandwich composite which utilizes a honeycomb core. A imperfection sensitivity investigation was executed, and two types of imperfections were compared. The first type is an axisymmetric imperfection, and the second type is an imperfection which is based on measurements of the actual CTA 8.1 cylindrical shell. For this comparison, dynamic implicit analyses was used, next to a linear eigenvalue analysis to determine the axisymmetric modeshape. A linear static analysis was executed, to determine the linear stiffness as a reference case. The last section of the chapter focussed on the comparison between the CTA 8.1 cylindrical shell, and the two scaled configurations which are based on the CTA 8.1. The comparison utilized nondimensional equations, to be able to compare the load-displacement graphs in a nondimensional form. Furthermore, a comparison of the strain contour plots was executed, and lastly a relation between the resulting KDF and imperfection amplitude was established.

6.1 CTA 8.1

The CTA 8.1 cylindrical shell was designed and manufactured by NASA for experimental testing purposes. It has a length of 2286 mm and a diameter of 2402 mm, and is thus considerably larger in comparison to the other cylindrical shells included in this thesis. The full structural properties are shown in Table 6.1. It uses a different composite material for the facesheets, named IM7/MTM45, for which the material properties are shown in Table 6.2. The core material used is a honeycomb core, for which the material properties are shown in Table 6.3. As it is a sandwich cylindrical shell, the analytical buckling load was once more be calculated by using two different methods. The first analytical method to be used is SP-8007, the second method is the method by Reese and Bert. The resulting buckling loads of these analytical methods are reported in Table 6.4. The results are similar to what was seen for the scaled sandwich cylindrical shell. The SP-8007 results in a higher buckling load for a cylindrical shell without imperfection compared to the solution by Reese and Bert.

Table 6.1: CTA 8.1 structural properties [13].

Facesheet Layup	$[\pm 45, 0, \overline{90}]_s$
Core Thickness [mm]	6.35
Diameter [mm]	2402
Length [mm]	2286

Table 6.2: IM7/MTM45 Material Properties [13].

E_{11} [MPa]	E_{22} [MPa]	ν [-]	G_{12} [MPa]	ρ [kg/m^3]	t_p [mm]
142816	8618.5	0.36	5309	1580	0.144

Table 6.3: Honeycomb core material properties [13].

E_{11} [MPa]	E_{22} [MPa]	E_{33} [MPa]	ν_{12} [-]	ν_{13} [-]	ν_{23} [-]	G_{12} [MPa]	G_{13} [MPa]	G_{23} [MPa]	ρ [kg/m^3]
0.345	0.262	413.7	0.45	0.0001	0.0001	0.12	203.4	82.7	72

Table 6.4: Buckling loads for the CTA 8.1 cylindrical shell, SP-8007 [2] and Reese and Bert [58].

Analysis	Buckling load [kN]
SP-8007 without imperfection	5023.2
SP-8007 with imperfection	2985.4
Reese and Bert without imperfection	4519.3

6.2 Preliminary Analysis of the CTA 8.1 Cylindrical Shell

This section focusses on the preliminary analyses of the CTA 8.1 cylindrical shell. Three types of analyses were executed, an eigenvalue analyses which provided a axisymmetric imperfection, a linear static analysis as a reference case for the stiffness of the cylindrical shell, and dynamic implicit analyses. The dynamic implicit analyses that were executed, used a cylindrical shell without imperfections and a cylindrical shell including an axisymmetric imperfection. The axisymmetric imperfection was used for three different amplitudes w.r.t. the thickness, which are: 10%, 20% and 50%. These are similar amplitudes as used in the analyses which were previously executed. The modelling technique used is similar to previous chapter, which is explained in subsection 3.1.1, and results in the FE model shown in Figure 6.1. In previous analyses, a mesh size of 5 mm was used. Due to this cylindrical shell being a different scale and thus considerably larger, a mesh size of 10 mm was used. This results in the same order of magnitude for the number of nodes as previous analyses. The S4R element was used for the analyses of this chapter. Most of these models were build early during the thesis, when the S4R element was the element of choice. Due to the S4R element showing excellent results for the scaled sandwich cylindrical shell in the element comparison, rebuilding the model of the CTA 8.1 cylindrical shell with another element was deemed unnecessary.

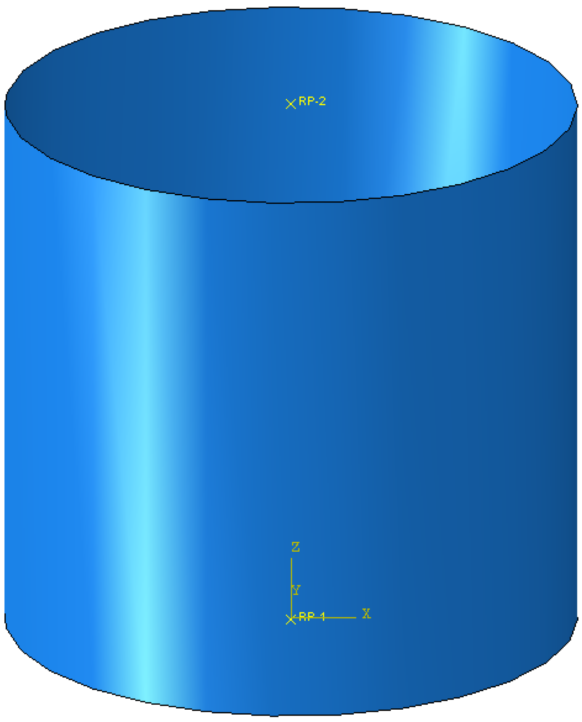

Figure 6.1: FE model of the CTA 8.1 cylindrical shell.

The first results to be shown consists of the first four eigenmodes of the CTA 8.1 cylindrical shell, which are retrieved from the eigenvalue analyses. The first two eigenmodes show a typical axisymmetric modeshape, while the third and fourth eigenmodes show a asymmetric modeshape, see Figure 6.2. The first eigenmode was used as the axisymmetric imperfection for the dynamic implicit analyses. The reasoning for using the axisymmetric modeshape as an imperfection is similar to previous cases. The diamond modeshape is only retrieved when a higher amount of eigenvalues is requested, which resulted in a higher amount of computational time. The dynamic analyses that were executed resulted in a load-displacement graph, which is combined with the analytical buckling loads calculated by using SP-8007. The load-displacement graph for these analyses is shown in"Figure 6.3.

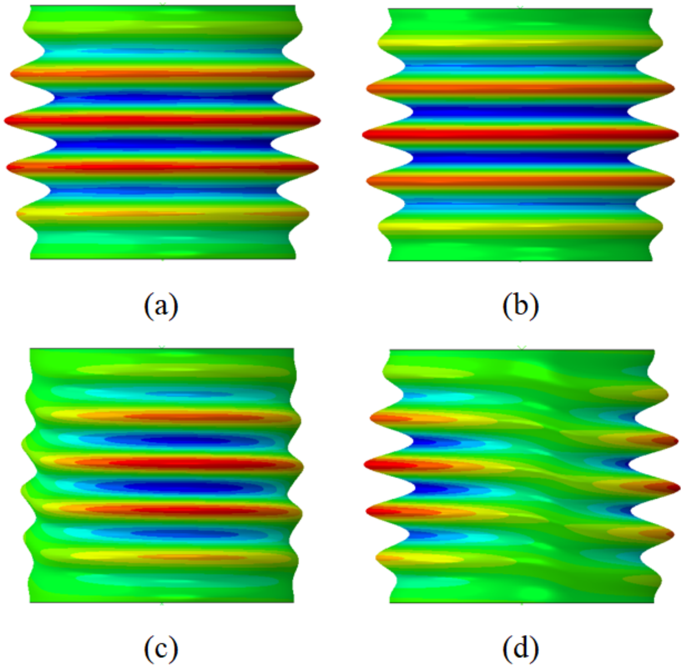

Figure 6.2: First four eigenmodes, showing radial displacement of the CTA 8.1 cylindrical shell: (a) first, (b) second, (c) third and (d) fourth.

The first thing to notice from the results shown in the load-displacement graph is the long loading plateau shown by the cylindrical shell without imperfection. Previous chapters have shown similar occurrences, but the loading plateaus that were encountered never showed a length as is seen for this cylindrical shell. This is a purely numerical problem and its occurrence is linked to a axisymmetric shape forming before buckling. Fine tuning the settings of the dynamic implicit analyses could shorten the loading plateau, or even prevent it from happening. This would however be time consuming, and the cylindrical shell without imperfection is only used to provide a reference buckling load in comparison to cylindrical shells with imperfection. The loading plateau does not seem to increase the buckling load by a considerable margin, and does still serve its purpose.

When the results of the cylindrical shell with axisymmetric imperfection are compared with the cylindrical shell without imperfection, it can be seen that the buckling load drops considerably and that the stiffness is also reduced. The cylindrical shells with the 10% and 20% axisymmetric imperfection converged towards each other in the post-buckling field, which is most likely caused by the modeshape being similar in the post-buckling field. This type of behaviour due to a axisymmetric imperfection was also observed for the scaled solid laminate cylindrical shell.

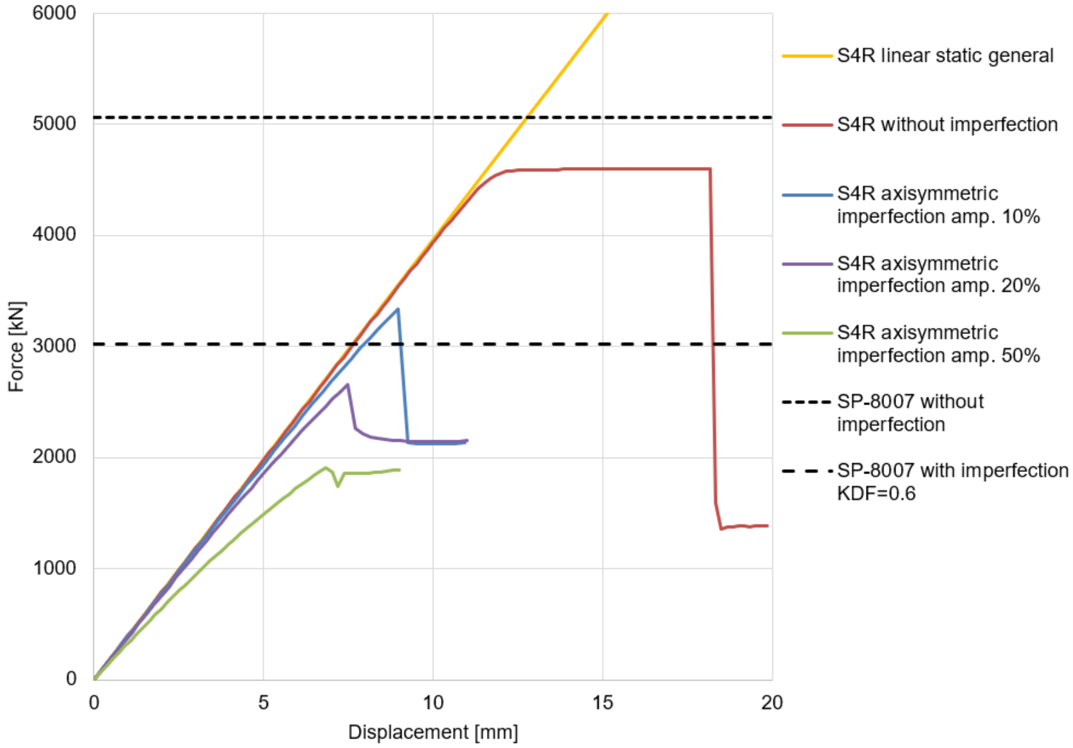

Figure 6.3: Load-displacement graph for the CTA 8.1 cylindrical shell and axisymmetric imperfection.

When comparing the buckling loads for the cylindrical shell without imperfection, the buckling load resulting from the cylindrical shell without imperfection is 10% lower compared to the corresponding SP-8007 analytical buckling load, see Table 6.5. When the analytical solution from Reese and Bert is compared to the FE solutions, the analytical buckling load is very close to the buckling load as received from the eigenvalue and dynamic implicit analyses. With the difference being 1.4% w.r.t. to the FE buckling loads which can be considered very accurate.

Table 6.5: Buckling loads for the CTA 8.1 cylindrical shell, SP-8007 [2].

Analysis	Buckling load [kN]
FE eigenvalue analysis	4584.61
FE dynamic without imperfection	4586.45
FE dynamic with axisymmetric imperfection 10%	3335.35
FE dynamic with axisymmetric imperfection 20%	2645.80
FE dynamic with axisymmetric imperfection 50%	1871.01

6.3 Measured Imperfections of the CTA 8.1 Cylindrical Shell

Measurements that were executed on the manufactured CTA 8.1 cylindrical shells at NASA resulted in several data sets for the imperfection. Measurements were executed both on the inside and outside of the cylindrical shell, from which both a mid-plane was determined and the thickness imperfection. Although this mid-plane and thickness imperfection data was available, only using the inside measurements would result in a more comparable situation w.r.t. the scaled cylindrical shells using mandrel imperfections. No thickness imperfections were used before, and the determined mid-lane might have a different effect on the behaviour of the cylindrical shell as it is based on inside and outside measurements.

The steps that had to be taken to process the inside measurements are similar to the steps that were explained in subsection 4.3.4. The main difference with previous processes, is that this measurement includes the pad-ups of that were used for the CTA 8.1 cylindrical shell, and thus requires extra steps. These pad-ups results in a lower radius in the edge regions, which would distort the imperfection signature. The total imperfection signature, including these pad-up regions, is shown in Figure 6.4.

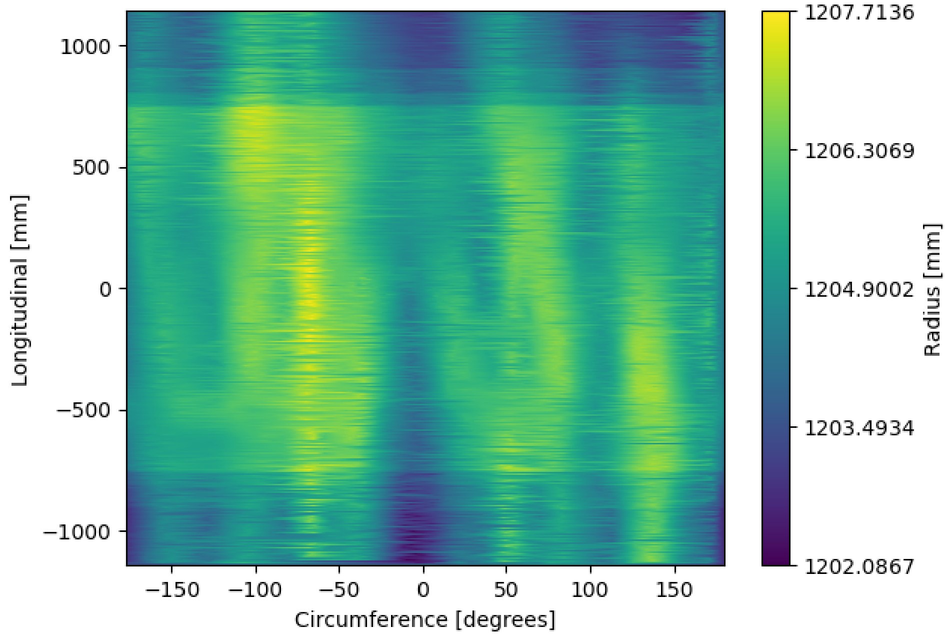

Figure 6.4: 2D representation of the radial coordinates for the inside imperfection of the CTA 8.1 cylindrical shell.

To create a imperfection signature which can be used for further analyses, these pad-ups were compensated for in the imperfection signature. The pad-up layups, and the length of the pad-up regions are described in the publication by Schultz et al. [13] which focusses on the CTA 8.1 cylindrical shell. From this publication, the thickness and length of the pad-ups was determined, and compensated for in the imperfection signature. This results in the imperfection signature as shown in Figure 6.5.

The pad-ups can still be seen when the imperfection is looked at in detail, but only for a few locations and minor radial differences. The current imperfection signature was deemed sufficiently accurate, as the imperfection signature itself shows higher radial variations compared to these few regions still showing influences of the pad-ups. In previous analyses that were executed, a imperfection with a amplitude of 20% w.r.t. to the thickness was used as a reference case. Therefore the imperfection signature of the CTA 8.1 cylindrical shell was scaled to match 20% w.r.t. the thickness. Firstly the mid-plane has to be determined, which is determined by using a histogram plot showing the number of occurrences of the radial coordinates, as shown in Figure 6.6. From this histogram plot the mid-plane radius of the inside measurement was determined to be 1201.1 mm. This mid-plane radius is than used to scale the imperfection amplitude, which results in the imperfection signature as showed in Figure 6.7.

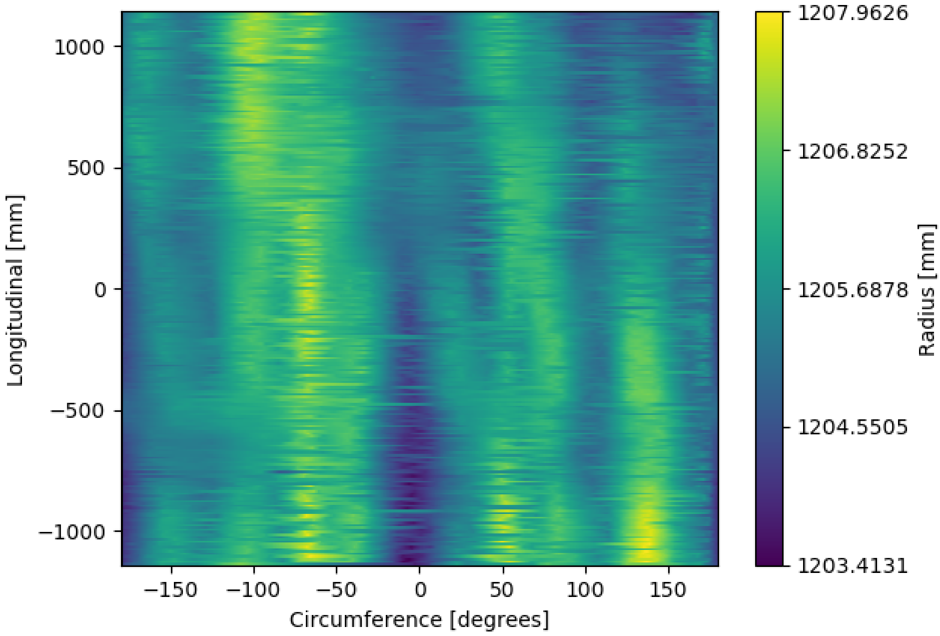

Figure 6.5: 2D representation of the radial coordinates for the CTA 8.1 cylindrical shell imperfection using a 10 mm mesh size.

When the two imperfection signatures are compared, it can be seen that the imperfection signature using the measured amplitude has a larger amplitude compared to the 20% amplitude imperfection. The measured imperfection amplitude is 31.6% w.r.t. to the thickness, and the scaling of the 20% amplitude imperfection is thus the other way around as compared to previous imperfection signatures of the mandrel imperfection. The next step is to use these imperfection signatures in a dynamic implicit analyses, which can then be compared to the results of the cylindrical shell without imperfection. This results in the load-displacement graph as shown in Figure 6.8, with the corresponding buckling loads reported in Table 6.6.

Table 6.6: Buckling loads for the CTA 8.1 cylindrical shell, SP-8007 [2].

Analysis	Buckling load [kN]
FE dynamic without imperfection	4586.45
FE dynamic with measured imperfection 20%	4032.84
FE dynamic with measured imperfection 31.6%	3730.78

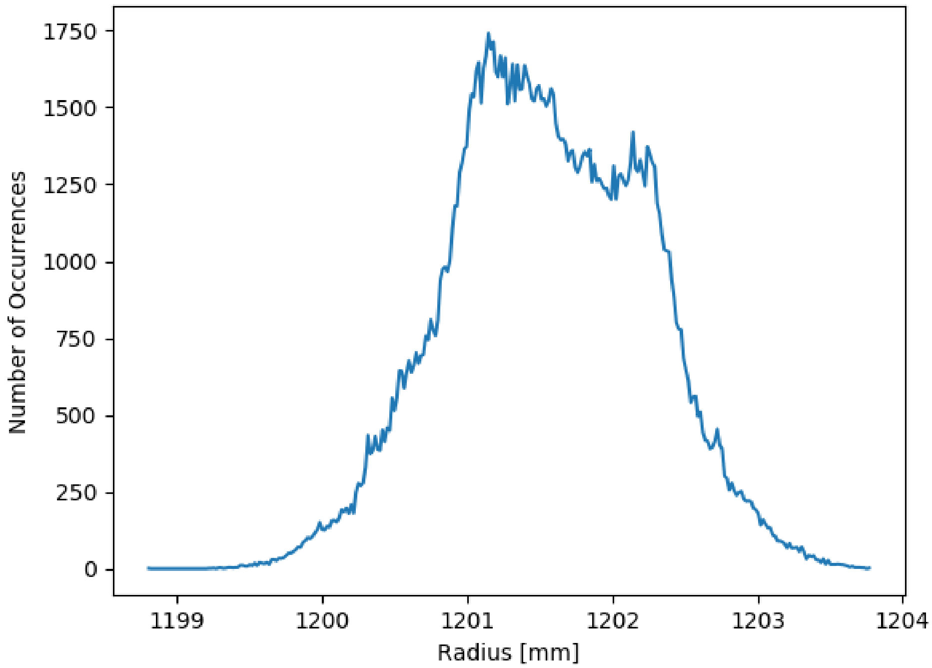

Figure 6.6: Histogram plot for the number of occurrences of the radial coordinates of the imperfection measurement.

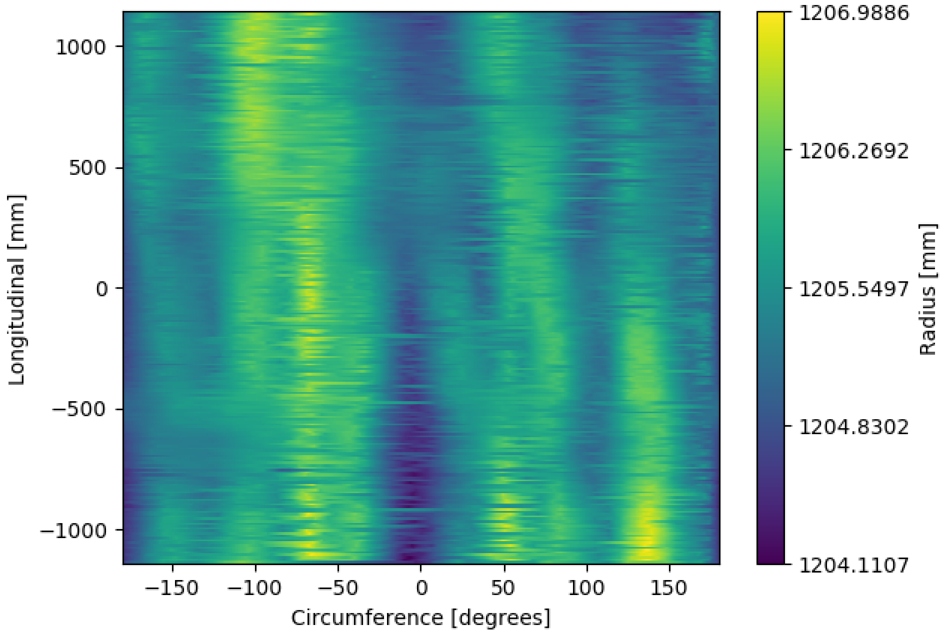

Figure 6.7: 2D representation of the radial coordinates for the CTA 8.1 cylindrical shell imperfection with an amplitude of 20% w.r.t. to the thickness.

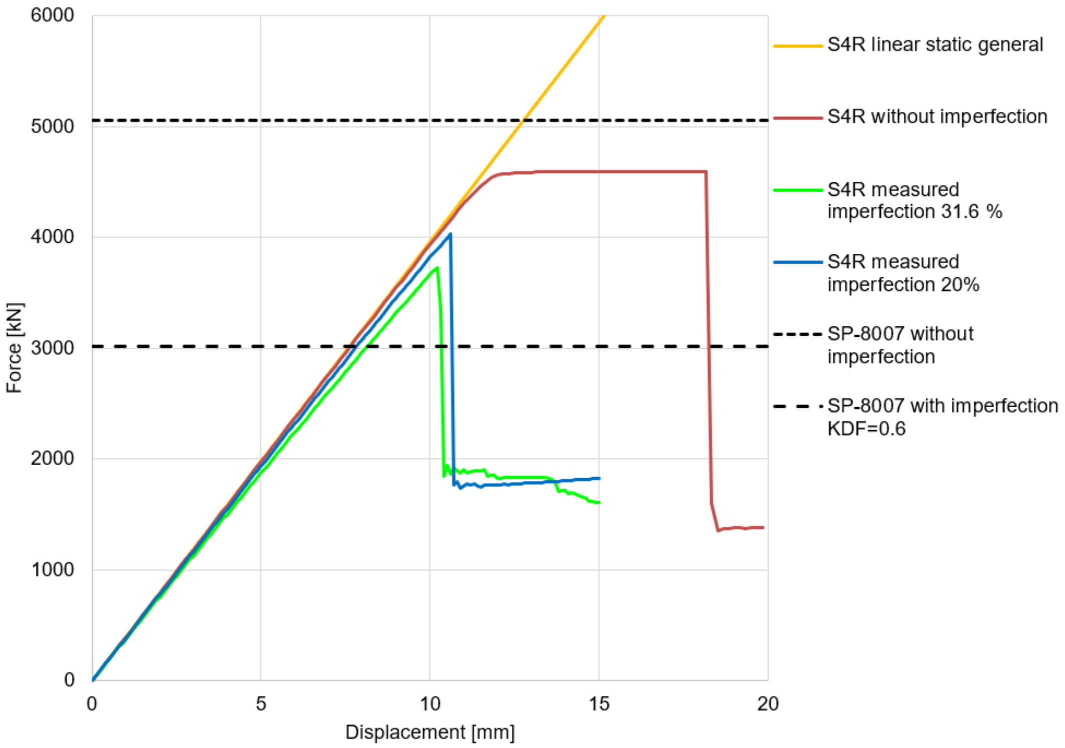

Figure 6.8: Load-displacement graph of the CTA 8.1 cylindrical shell with measured imperfections.

The behaviour in these load-displacement graphs is similar to what was seen for the scaled configurations using the mandrel imperfections. The stiffness does show a decrease, but not in the same order of magnitude as seen for a axisymmetric imperfection. Both imperfection amplitudes show higher KDFs in comparison to the SP-8007 analytical solution, with a KDF of 0.88 and 0.81 for the 20% and 31.6% amplitude respectively. The influence of the amplitude of the measured imperfection seems to have a higher influence on the stiffness, than it does on the buckling load. The relative difference between the buckling loads of the cylindrical shells using an imperfection in comparison to the buckling load of the cylindrical shell without imperfection, is lower in comparison to the stiffness differences. The next step is to compare the strain values of the outer facesheet of the CTA 8.1 cylindrical shell, which contain the most critical strain values. The strain values are reported in Table 6.7.

When comparing the strain values of the three cylindrical shells, all show that the first ply is the most critical. The first and second ply both show high shear strains, where the first ply shows slightly higher shear strains. The third ply shows the highest tensional strain in the 2nd material direction, but does not seem to be as critical as the shear strains. The difference in strain values between the two cylindrical shells including imperfections is minimal, while the difference with the cylindrical shell without imperfection is higher. To determine the location of the critical strain values, the strain values of the first ply are shown in a contour plot in Figure 6.9.

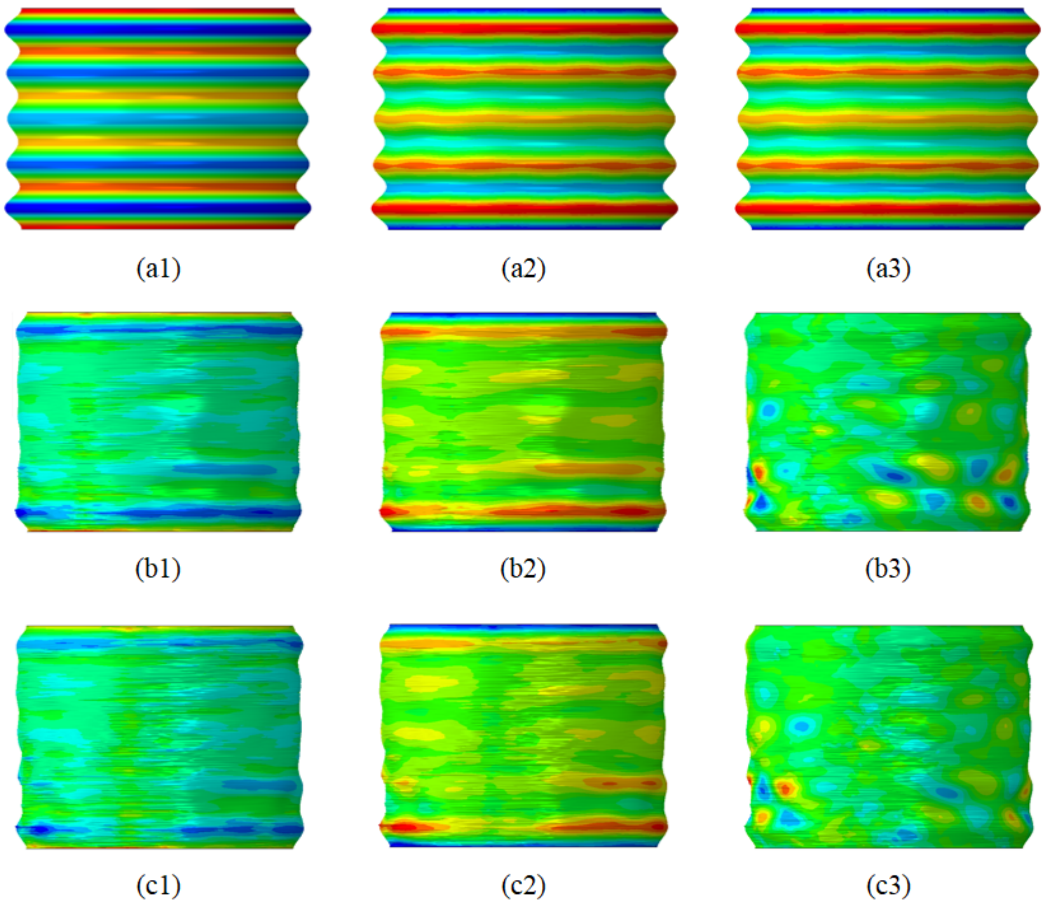

Figure 6.9: Strain contour plots of the first ply of the CTA 8.1 cylindrical shell with a deformation scale of 30. Each row is one type of imperfection: a = without imperfection ; b = measured imperfection 20%; c = measured imperfection 31.6%. The number notation: 1,2 and 3 are ε_{11},ε_{22},ε_{12} respectively.

Table 6.7: Maximum strains ($\mu\varepsilon$) of the inner facesheet of the CTA 8.1 cylindrical shell.

Without imperfection	ε_{11}	ε_{22}	ε_{12}
Ply 1	-1578	-1579	11420
Ply 2	-1552	-1552	-11370
Ply 3	-7168	4142	-1
Ply 4	4142	-7111	1
Ply 5	-7054	4142	-1
Ply 6	-1486	-1495	-2928
Ply 7	-1512	-1512	11080
Mandrel imperfection 20%	ε_{11}	ε_{22}	ε_{12}
Ply 1	-1839	-1901	9582
Ply 2	-1882	-1819	-9527
Ply 3	-6320	3223	820
Ply 4	3223	-6264	-805
Ply 5	-6209	3222	789
Ply 6	-1809	-1740	-9310
Ply 7	-1732	-1790	9255
Mandrel imperfection 31.6%	ε_{11}	ε_{22}	ε_{12}
Ply 1	-1917	-2086	9472
Ply 2	-2062	-1906	-9410
Ply 3	-6288	3111	1118
Ply 4	3110	-6225	-1096
Ply 5	-6161	3108	1082
Ply 6	-1968	-1863	-9163
Ply 7	-1853	-1944	9101

The location of the highest strain values are similar, with the exception of the shear strain of the cylindrical shell without imperfection in comparison to the two cylindrical shells with measured imperfection. The location of the maximum strains in the first and second material direction are close to the edge for all three cylindrical shells. While the maximum shear strain of the two cylindrical shells with imperfections show maximum strain locations which are a bit spread out, and the cylindrical shell without imperfection shows the maximum strain at locations close to the edges. The cylindrical shell without imperfection showed the highest strain values, combined with the strain values occurring in the whole circumferential direction at the edges, it combines into a more critical situation.

6.4 Comparison between the Scaled and Full Scale Cylindrical Shells

This section focusses on the comparison between the three main cylindrical shells of this thesis. These comparisons utilized the results of the three cylindrical shells from the dynamic implicit analyses which were executed. From the scaled solid laminate cylindrical shell, the test article version was used both with and without mandrel imperfection. The scaled sandwich cylindrical shell was used with and without mandrel imperfection. The CTA 8.1 cylindrical shell was used with and without the measured imperfection. This in total provides 9 cylindrical shell configurations to be compared.

6.4.1 Nondimensional Load-Displacement Comparison

The first comparison was executed by using two nondimensional equations to characterize the load-displacement curve of the three cylindrical shells. The nondimensional equations consist of the nondimensional load as shown in Equation 6.1, which is included in the scaling procedure published by Uriol Balbin et al. [4], and the nondimensional displacement as shown in Equation 6.2, which is included in a publication by Schultz and Nemeth [26]. Two comparisons were made using the nondimensional equations. The first comparison included the cylindrical shells without imperfections and with the measured amplitude imperfection. The second comparison included the cylindrical shells without imperfections and with the measured imperfections which are scaled to have an amplitude of 20% w.r.t. to the thickness. The load-displacement results of all cylindrical shells were converted to the nondimensional load-displacement graphs using previously mentioned equations, which results in the first comparison being shown in Figure 6.10, with the corresponding nondimensional buckling loads shown in Table 6.8.

$$K = \frac{PR}{2\pi\sqrt{D_{11}D_{22}}} \tag{6.1}$$

$$U = \frac{uL}{\sqrt{a_{11}a_{22}D_{11}D_{22}}} \tag{6.2}$$

Two properties can be distinguished from this load-displacement graph which are important for the comparison. The first property is the buckling load of each configuration, which can be observed just before the drop in load in each graph. The second property are the stiffnesses, which is the curve of each slope during the increase in loading. When the nondimensional buckling loads of the cylindrical shells without imperfection are compared, it can be seen that the scaled solid laminate cylindrical sh ell shows the highest nondimensional buckling load, 10.2% higher w.r.t. to the CTA 8.1 cylindrical shell. While the buckling loads of the scaled sandwich cylindrical shell and the CTA 8.1 cylindrical shell are quite close, with a difference of 3.3%. The nondimensional stiffnesses of the three cylindrical shells show the similar relation as the nondimensional buckling load, the scaled solid laminate cylindrical shell shows the highest stiffness, while the scaled sandwich cylindrical shell and the CTA 8.1 cylindrical shell show nondimensional stiffnesses which are equal.

The comparison of the cylindrical shell with imperfection using the measured imperfection amplitude shows a different relation between the results. The two scaled cylindrical shells show a drop in nondimensional buckling load, which is less severe in comparison to the drop in nondimensional buckling load of the CTA 8.1 cylindrical shell. The scaled solid laminate cylindrical shell shows a buckling load which is 28.7% higher compared to the CTA

8.1 cylindrical shell, while the scaled sandwich cylindrical shell shows a 12.2% higher buckling load. The two scaled cylindrical shells also show almost no drop in nondimensional stiffness due to the imperfection, while the CTA 8.1 cylindrical shell does show a drop in nondimensional stiffness. These behaviour differences can however be explained, by looking at the amplitudes of the imperfection. The scaled cylindrical shells have a imperfection amplitude of 2.85% and 4.1% w.r.t. to the thickness for the scaled solid laminate and scaled sandwich cylindrical shell respectively. The CTA 8.1 cylindrical shell shows a imperfection amplitude which is 31.6% w.r.t. to the thickness. Relatively speaking, this is a considerable difference in imperfection amplitude from which the effect can be directly seen in the nondimensional load-displacement graphs. The next step is to compare the nondimensional load-displacement graphs of the cylindrical shells with the scaled imperfection amplitude of 20%. These load-displacement graphs are shown in Figure 6.11,with the corresponding buckling loads shown in Table 6.8.

Table 6.8: Nondimensional buckling loads of the three cylindrical shells, with and without imperfections.

	CTA 8.1	Scaled solid laminate		Scaled sandwich	
Without imperfection	556.0	612.8	10.2%	537.9	-3.3%
With imperfection measured amplitude	451.9	579.4	28.7%	507.2	12.2%
With imperfection 20% amplitude	488.5	448.7	-8.1%	408.6	-16.3%

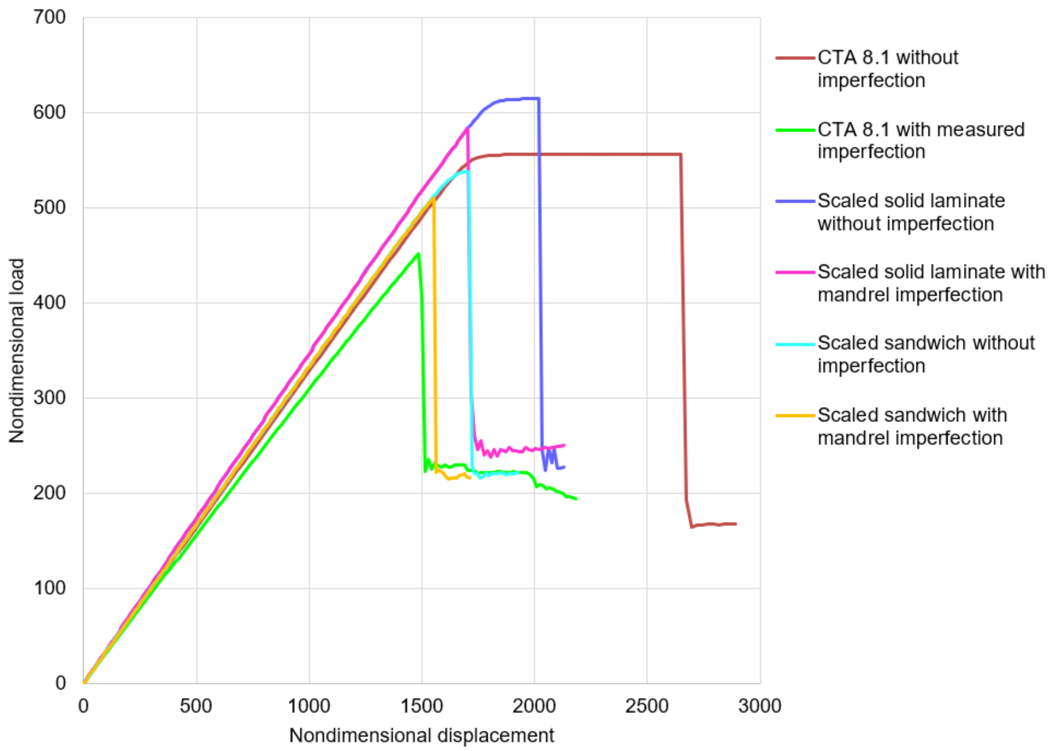

Figure 6.10: Nondimensional load-displacement graph for the cylindrical shells with and without measured and mandrel imperfection.

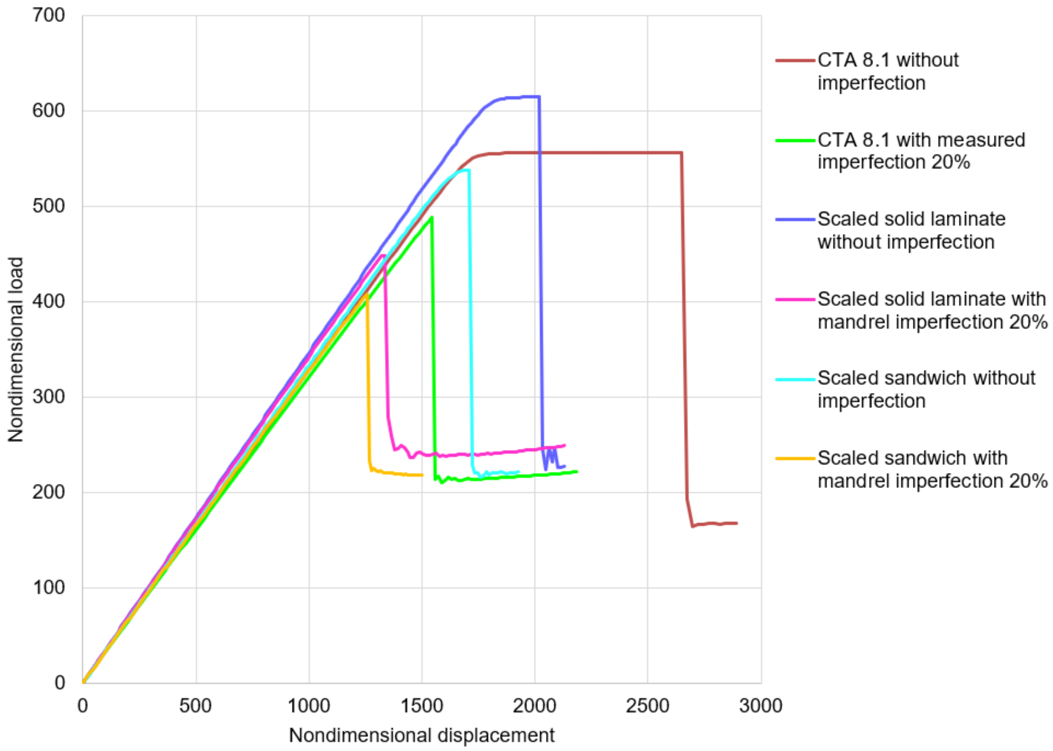

Figure 6.11: Nondimensional load-displacement graph for the cylindrical shells with and without 20% measured and mandrel imperfection.

When comparing the nondimensional buckling loads of the cylindrical shells using the 20% amplitude imperfection, the CTA 8.1 cylindrical shell shows the highest load. The scaled solid laminate cylindrical shell has a 8.1% lower buckling load and the scaled sandwich cylindrical shell has a 16.3% lower buckling load, both in comparison to the CTA 8.1 cylindrical shell. The relation between the two scaled configurations is similar to the previous comparison, but the relation with respect to the CTA 8.1 cylindrical shell is the opposite. The change of this relative relation can have multiple causes:

- Difference in shape and smoothness of the imperfection signature: The shape of the mandrel imperfection and the CTA 8.1 measured imperfection do show differences when the imperfection signatures are compared in Figure 4.13 and Figure 6.4. The mandrel imperfection seems to be smoother in comparison to the CTA 8.1 measured imperfection. This might be due to different objects being measured, one being a mandrel and the other being a actual cylindrical shell. The shape of the mandrel imperfection also seems more constant in the axial direction, but this is a minimal difference. The mandrel imperfection also shows the imperfection band, of which the effect increases when the imperfection is scaled, judging from previous results.

- Difference in scale of the cylindrical shell: It might be that the scale of the cylindrical shell affects the relation between imperfection amplitude and decrease of the buckling load.

- The method of scaling the imperfection, or relating the imperfection to the thickness of the shell: The imperfection has been scaled w.r.t. the thickness of the shell. This type of scaling, or relating the imperfection to the thickness of the shell, might not lead to realistic behaviour. It might also lead to an unrealistic effect of the imperfection amplitude on the behaviour of the cylindrical shell.

These bullet points actually describe the main problem of using scaled structures, as the comparison between different scales remains difficult. The differences seen in this comparison should however not be exaggerated, as the differences in nondimensional stiffness and nondimensional buckling load are relatively small.

6.4.2 Comparison of Strain Contour Plots

The next comparison used the strain contour plots of the cylindrical shells with the measured and mandrel imperfections using the measured amplitude. Using these cylindrical shells for this comparison showed the most realistic case for each cylindrical shell that was analysed. All plots show the most critical ply of the cylindrical shells at the pre-buckling increment, which were previously used to check for material failure before buckling. The strain contour plots are shown in Figure 6.12.

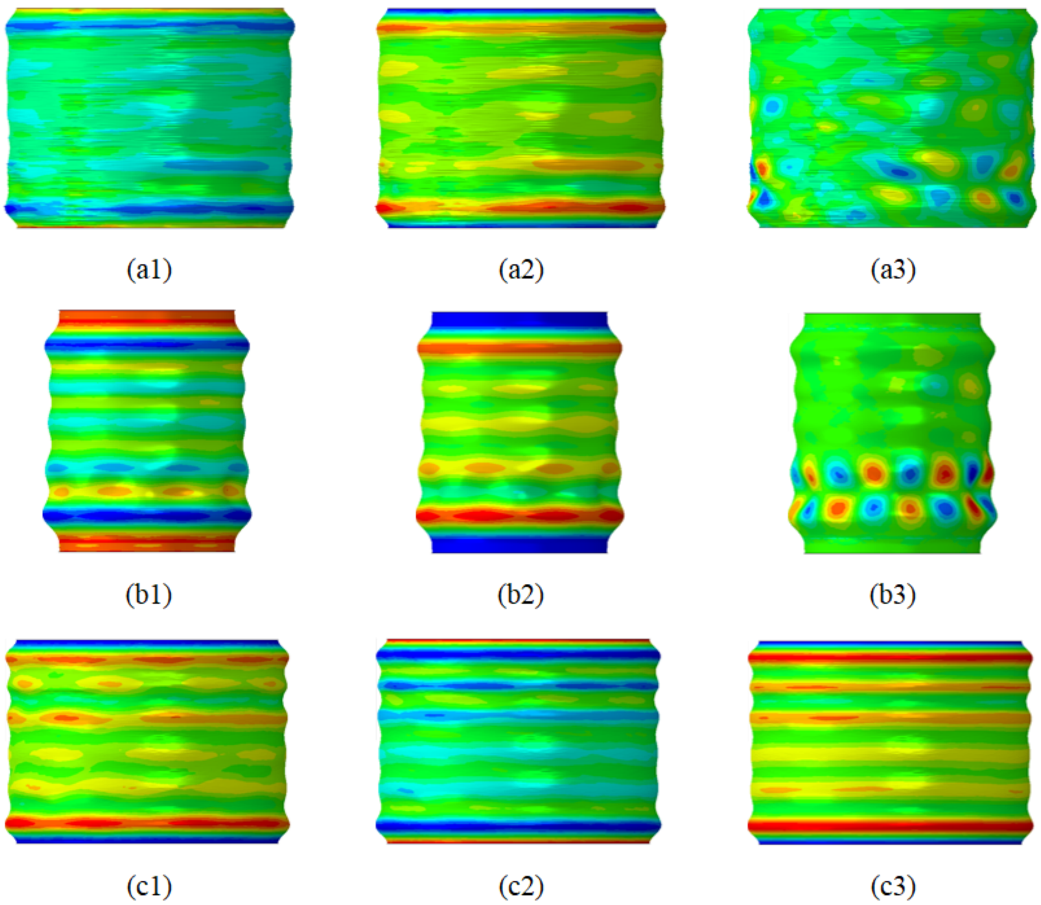

Figure 6.12: Strain contour plots of the three cylindrical shells using the measured and mandrel imperfections. Each row is one cylindrical shell configuration: a = CTA 8.1 (deformation scale of 30) ; b = scaled solid laminate (deformation scale of 50); c = scaled sandwich (deformation scale of 30). The number notation: 1,2 and 3 are ε_{11},ε_{22},ε_{12} respectively.

When comparing the contour plots of the three cylindrical shells, it can be seen that very similar colour patterns are seen next to similar displacement fields. It should be noted that the general deformation shape and relative colour pattern differences should be judged, as the scaled solid laminate cylindrical shape has a different radius to length ratio it might give a slight distorted image while it does show comparable behaviour. The relative location of the maximum strain values and radial displacement is similar. Furthermore, the ratio between the amplitudes of the half waves close to the edges and at the mid section are similar between the cylindrical shells as well. The largest difference is seen between the shear strains, for which the CTA 8.1 cylindrical shell and solid laminate cylindrical shell show some similarities, while the scaled sandwich cylindrical shell shows a different colour pattern.

6.4.3 Relation between KDF and Imperfection Amplitude

The last step of the comparison between the three cylindrical shells focussed on relating the KDF of each cylindrical shell and imperfection combination to the amplitude of the imperfection. A similar approach is seen in SP-8007, where the knockdown factor is related to the radius over thickness and not the imperfection itself, as seen in Figure 2.1. To be able to base this relation on a larger dataset than is available from previous analyses, a few additional dynamic implicit analyses with scaled imperfections were executed. The CTA 8.1 cylindrical shell and the solid laminate cylindrical shell were both used for one additional analyses, while the scaled sandwich cylindrical shell was used for three additional analyses. The scaled sandwich cylindrical shell was used for more analyses as it is the most efficient to analyse. This is due to a combination of relative element size and length of the cylindrical shell, which is why it has the lowest number of elements. Only the buckling load of these analyses was used for the comparison. First, a basic comparison of the geometry of the three cylindrical shells was compared, which was used to determine the relation between KDF and imperfection amplitude later on. The geometry of each cylindrical shell is reported in Table 6.9.

Table 6.9: Dimentions of the three cylindrical shells of the comparison.

	Radius [mm]	Length [mm]	Thickness [mm]
CTA 8.1	1205.3	2286	8.37
Scaled solid laminate	402.2	1220	4.21
Scaled sandwich	401.6	730	2.95

The radius differences that can be seen between the two scaled configurations, is due to difference in thickness. As in the inside diameter is determined by the radius of the mandrel, which results in different mid-plane radii for the scaled configurations. The next step of this last comparison is to combine the results of the dynamic implicit analyses of all cylindrical shell configurations. The imperfection w.r.t. to the thickness was reported, as it was used throughout the thesis as a reference towards the imperfections, next to the actual imperfection amplitude in mm. The buckling loads of each cylindrical shell configuration with imperfection is compared to the buckling load of the corresponding cylindrical shell without imperfection, which leads to a knockdown factor. The last step of the comparison would be to actually relate the knockdown factor to the imperfection amplitude in mm and to a set of properties of each cylindrical shell. Several combinations of structural properties were investigated to determine if a trend could be established, where it was seen that relating the imperfection amplitude to the radius and length of the cylindrical shell saw the most consistent results. The imperfection amplitude was divided by the radius and length, from which the resulting data is reported in Table 6.10.

Table 6.10: The 11 cylindrical shell configurations for the imperfection versus knockdown factor comparison.

CTA 8.1	Imp. w.r.t. to thickness	Imp. amp. (i_a) [mm]	KDF	i_a/(R*L)
1	12.80	1.08	0.91	3.9E-07
2	20.00	1.67	0.88	6.1E-07
3	31.60	2.64	0.81	9.6E-07
Scaled solid laminate	Imp. w.r.t. to thickness	Imp. amp. (i_a) [mm]	KDF	i_a/(R*L)
4	2.85	0.12	0.95	2.4E-07
5	6.90	0.29	0.89	5.9E-07
6	20.00	0.84	0.73	1.7E-06
Scaled sandwich	Imp. w.r.t. to thickness	Imp. amp. (i_a) [mm]	KDF	i_a/(R*L)
7	4.10	0.12	0.95	4.1E-07
8	6.30	0.19	0.88	6.5E-07
9	10.00	0.29	0.83	9.9E-07
10	20.00	0.59	0.76	2.0E-06
11	28.40	0.84	0.67	2.9E-06

The comparison used 11 configurations in total, with the majority using scaled imperfections. The high amplitude imperfections w.r.t. to the radius and length were only used for the scaled configuration, as it was not deemed to be an accurate representation to up-scale the imperfection of the CTA 8.1. The imperfection of the CTA 8.1 already showed large deviations, and the FE model would most likely require a finer mesh to be able to represent a higher imperfection amplitude accurately. When the KDFs are compared to the imperfection w.r.t. to the thickness, it can be seen that this relation is quite different between the CTA 8.1 cylindrical shell and the scaled cylindrical shells. To create a more clear idea why the imperfection amplitude over radius times length is chosen, the KDFs was plotted against this relation. The plot showing this relation is shown in Figure 6.13.

It can be seen that the highest level of agreement is achieved at lower imperfection amplitudes w.r.t. to the radius and length of the cylindrical shell. This could be caused by the scaling factor that was used for the mandrel imperfection for some of these configurations. The scaling factor for the extreme cases ranged from 5 to 7, which is a significant exaggeration of the imperfection. This could already be seen for the strain contour plots from the scaled cylindrical shell using the 20% w.r.t to the thickness imperfections, where the imperfection band caused high strain values. When the results for each cylindrical shell are compared, the CTA 8.1 and the scaled solid laminate cylindrical shells seem to follow a linear relation. While the scaled sandwich cylindrical shell shows less consistent behaviour, which might be due to the imperfection band having a larger influence on the sandwich in comparison to the solid laminate configurations.

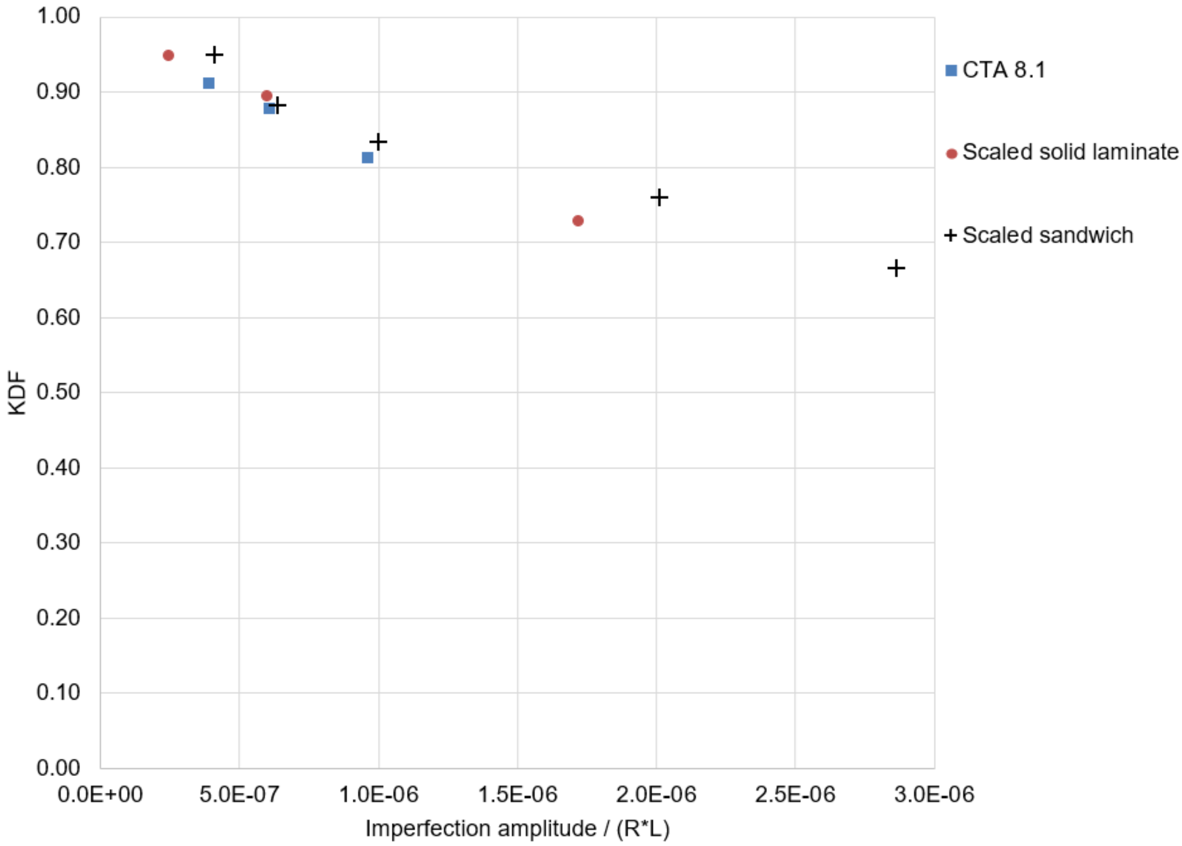

Figure 6.13: Graphical representation of the relation between the KDF and imperfection amplitude over radius and length.

6.5 Discussion and Outcome

The CTA 8.1 cylindrical shell was analysed for two different imperfection types, next to a configuration without imperfections. The imperfection sensitivity to the axisymmetric imperfection is high, which is thus similar to what was seen for the solid laminate cylindrical shell. When comparing the two imperfection types, the imperfection sensitivity for the measured imperfection is much lower compared to the axisymmetric imperfection. When both imperfection types are used with a amplitude of 20% w.r.t. to the thickness, the difference in buckling load is 35%. The axisymmetric imperfection does not result in realistic behaviour of a cylindrical shell, when it is compared with a measured imperfection. If measured imperfections are not available, a diamond modeshape would be a better choice in most cases, but this option was not explored for the CTA 8.1 cylindrical shell due to the main focus being on the comparison between cylindrical shells using measured imperfections.

The three main cylindrical shells of the thesis were compared in the nondimensional load-displacement graphs. Although differences were seen, the cylindrical shells do show very similar behaviour, both for the buckling loads and stiffnesses of the cylindrical shells. The maximum buckling load difference for the cylindrical shells without imperfection was 10.2%, while the cylindrical shells with imperfections showed a maximum difference of 28.7%. This difference for the cylindrical shells with imperfection is most likely caused by the difference in imperfection amplitude and imperfection signature, due to the CTA 8.1 cylindrical shell also including manufacturing imperfections. The comparison of the strain contour plots strengthen the conclusion of the nondimensional load-displacement graphs. The strain contour plots showed good agreement in general, with the largest difference seen between the shear strain plots. This difference in shear strain contour plots is most likely caused by the differences in orientation of the ply used for these plots.

This level of agreement between scaled and full-scale structures was not seen during the literature review, even when structures with more properties in common were compared by authors [31]. The current scaled configurations have a lot of distortions w.r.t. to the properties of the full-scale cylinder, when properties such as dimensions and layup are compared, and still show representative behaviour. This leads to the conclusion that the scaling procedure results in representative scaled structures judging from these results, even when a combination of distorted properties are used. The scaled structures should always be checked if they are valid options for experimental testing, to ensure that no material failure happens in pre-buckling and the design can then be adapted when needed.

The last step of the comparison was to investigate if a relation could be determined between the KDFs resulting from the three cylindrical shells using different imperfection amplitudes. Such a relation was presented, but it requires more research if such a relation can result in accurate predictions for KDFs of other cylindrical shells. The relation that was found consisted of relating the imperfection to the radius and length of the cylindrical shell. It did show slight divergence for higher imperfection amplitudes, but the higher imperfection amplitudes are scaled imperfections with a high scaling factor which might cause the divergence behaviour. It would be ideal if this relation could be expanded by using full scale and scaled cylindrical shells which are based on existing launch vehicle cylindrical shell designs.

6.6 Summary

The CTA 8.1 cylindrical shell is a test article of the SBKF project. This cylindrical shell was a basis for which two scaled cylindrical shells were designed, which were analysed in previous chapters. This chapter therefore focused on analysing the CTA 8.1 cylindrical shell, to provide a set of results for the comparison with the scaled cylindrical shells. A preliminary analysis was done on the CTA 8.1 cylindrical shell. A linear eigenvalue analysis and a linear static analysis were executed, to provide a axisymmetric modeshape and reference stiffness of the cylindrical shell. In the next step dynamic analyses were executed. For both a cylindrical shell without imperfection, and three cylindrical shells using the axisymmetric imperfection at different amplitudes. A similar imperfection sensitivity to the axisymmetric imperfection was seen as for the scaled solid laminate cylindrical shell. As the axisymmetric imperfection resulted in both a drop in stiffness and a drop buckling load.

The next step was to incorporate measured imperfections. These measured imperfections were processed similar to previous chapters, but an extra processing step was required. The measurement included padups, which would not be included into the FE model. To compensate for the radial difference, the padup thicknesses were compensated for, which resulted in a imperfection signature without padups. A scaled imperfection of this imperfection signature was also created, to stay consistent with previous analyses of the scaled cylindrical shells. Due to the measured amplitude of the imperfection being 31.6% w.r.t. to the thickness, the imperfection was scaled down to 20% w.r.t. to the thickness. The two imperfection signatures were used in dynamic implicit analyses which resulted in relatively high buckling loads, as the imperfection seems large when it is compared to the thickness. The strain values of the CTA 8.1 cylindrical shell were reported, from which could be seen that there were rather high shear strains. The contour plots for the strain were shown for the cylindrical shell without imperfection and with the two measured imperfection cases.

A comparison of the three cylindrical shells was executed. The first step consisted of determining the nondimensional load-displacement graphs, for which a nondimensional load and nondimensional displacement equation were shown and used. From this comparison it was seen that there was general agreement. With the scaled sandwich cylindrical shell showing the highest level of agreement with the CTA 8.1 cylindrical shell, while the scaled solid laminate cylindrical shell showed higher buckling loads and stiffnesses. The CTA 8.1 cylindrical shell including the measured imperfection was a slight outlier, as the measured amplitude resulted in a imperfection which caused the buckling load to drop more in comparison to the scaled cylindrical shells with imperfection. The cylindrical shells including 20% imperfection amplitude w.r.t. to the thickness were then compared, which showed the opposite relation in comparison to the measured imperfection amplitude comparison.

Next the strain contour plots of the three cylindrical shells were compared, all cylindrical shells using the measured imperfection amplitude. A high level of agreement was seen, with the shear strain contour plots showing different colour patterns. The last step of the comparison consisted of establishing a relation between the KDF and the corresponding imperfection amplitude used for the cylindrical shells. To slightly enlarge the dataset on which this relation would be based on, a few extra analyses of the cylindrical shells using different imperfection amplitudes were executed. This resulted in the comparison including 11 cases in total. From these results a relationship was determined and shown, but it requires more research to establish a relationship with a higher certainty.

Chapter 7

Conclusions

A buckling analysis and imperfection sensitivity study of scaled launch-vehicle cylindrical shells have been executed, with the emphasis on scaled cylindrical shells due to the expensive nature of full-scale launch-vehicle cylindrical shells. The work as presented in this thesis is in a framework of a collaboration with NASA Langley. A literature review on the buckling of cylindrical shells showed that it is considered a structural problem which is yet to be fully understood. The cylindrical shells show a high imperfection sensitivity, but the exact influence of imperfections caused by different manufacturing processes is a source of uncertainty. The second subject of the literature review was the scaling of structures. The need for scaled structures is due to the size constraints of experimental testing equipment, next to the financial benefits compared to testing full scale launch-vehicle cylindrical shells. However, the scaling of structures can be a challenging process, as a scaled model which shows full scale representative behaviour is difficult to design due to constraints such as manufacturability.

The main objective of this thesis was to investigate if a scaling method results in representative scaled cylindrical composite shells, which will be validated by experimental tests at NASA Langley. The investigation started with a preliminary analysis of a 800 mm x 800 mm cylindrical shell, which focussed on an element comparison and a mesh sensitivity study. The knowledge gained during the preliminary analyses will be used for the following analyses on the two scaled and full scale cylindrical shells .

The first scaled cylindrical shell to be analysed was a solid laminate cylindrical shell. The focus was on an element comparison, next to a study on different imperfection types and the corresponding imperfection sensitivity. The scaled solid laminate cylindrical shell is then modelled as a test article including mandrel imperfections, padups and potting.

Hereafter, the analyses of a scaled sandwich cylindrical shell was executed, which includes the mandrel imperfections. The scaled sandwich cylindrical shell was used for an element comparison, where different element configurations are compared while using the mandrel imperfection.

Finally, the full scale structure which was the basis of the two scaled cylindrical shells, named the CTA 8.1, was analysed using both an axisymmetric and measured imperfection. The CTA 8.1 cylindrical shell, both without and with measured imperfection, was then used for a comparison with the two scaled cylindrical shells. This comparison was executed by comparing the nondimensional load and displacement of each cylindrical shell, next to comparing the strain contour plots. Then a relation was established between the knockdown factors of the cylindrical shells with respect to the imperfection amplitude and structural properties of each cylindrical shell.

The mesh sensitivity analysis showed that a 5 mm mesh should be used. It should also be kept in mind, that the mesh size can also be a point of discussion when imperfections are to be used in the FE model. For example, when measured imperfections are included, with a finer mesh size the imperfection signature can be approximated more accurately, depending on the resolution of the measurements.

From the element comparison during the preliminary analysis it was concluded that the S4R element shows good results, is less sensitive to mesh size and is computational efficient. The SC8R element showed to be more sensitive to mesh size, but still showed good results and is also computational efficient. Although the results of the CSS8 element were in line with the S4R and SC8R element for finer meshes, its computational efficiency makes it the less obvious choice. Therefore, the CSS8 element should only be used when its 3D material model is necessary. The C3D8R element showed inaccuracies when modelling a shell. Using three elements through the thickness improved its results, but the results were still not on par with the S4R, SC8R and CSS8 elements. The accuracy of the results obtained when using the C3D8R element can most likely be improved by using an element per ply, but this increases the computational time and cause the modelling of the composite structure to be inconvenient. From the preliminary analyses it was concluded that the C3D8R was not a valid option for subsequent analyses.

The element comparison of the scaled solid laminate cylindrical shell showed agreement between the SC8R and CSS8 element, while the S4R element showed 5% higher buckling loads on average. Therefore, for the remaining analysis of the scaled solid laminate cylindrical shell, the SC8R element was preferred. The scaled sandwich cylindrical shell was used to compare different element configurations, with single and multiple elements through the thickness where the facesheets and core were a separate layer of elements. All configurations, except for the three SC8R elements through the thickness, showed very close agreement. The three SC8R elements through the thickness showed a 3.5% lower buckling load compared to other element configurations. Judging from these results, a sandwich cylindrical shell has many options which can be used to accurately model its behaviour. When a single element through the thickness is sufficient, as the modelling of damage or separation is not of interest, a S4R or SC8R element is recommended. When damage or separation is of interest, the SC8R facesheet and CSS8 core is recommended. This configuration provides a 3D material model for the core, in combination with efficient modelling of the facesheets.

The dynamic implicit analyses of cylindrical shells without imperfection showed loading plateaus. The effect of numerical damping on the loading plateau was investigated, where it was concluded that it does affect the loading plateau but it is not a quick fix and requires case specific fine tuning.

The scaled solid laminate cylindrical shell was used to investigate the effect of several types of imperfection, next to the investigation into the imperfection sensitivity with respect to the amplitude of the imperfection. It was shown that an axisymmetric modeshape imperfection causes a considerable reduction in stiffness and buckling load, while a diamond modeshape imperfection only causes a minor reduction of the stiffness and a drop in buckling load, with a 18% higher buckling load compared to the axisymmetric imperfection. A loading imperfection was investigated as well, and showed that it did not affect the stiffness of the shell even at high imperfection amplitudes for which the buckling load did show a considerable drop. However, the amplitude of a loading imperfection is not comparable to a geometrical imperfection. This makes the imperfection sensitivity comparison between a loading imperfection and a geometrical imperfection difficult as there is no relationship. Mandrel imperfections were introduced, to which the scaled solid laminate cylindrical shell showed a lower imperfection sensitivity in comparison to the diamond modeshape imperfection. With 10% and 19% higher buckling loads when using a mandrel imperfection for a 2.85% and 20% imperfection amplitude with respect to the thickness respectively. When measured imperfections are not available, it is recommended to use a diamond modeshape imperfection and not an axisymmetric imperfection, as the diamond modeshape imperfection showed behaviour closer to the mandrel imperfection. It is however always recommended to use measured imperfections, as the shape of the imperfection showed to have a large impact on the deformation behaviour, both in pre-buckling and post-buckling, which will also have a considerable effect on strain field.

The CTA 8.1 cylindrical shell was also used for a investigation into the effect of two different geometrical imperfections. The axisymmetric modeshape imperfection was used, next to a measured imperfection. Similar behaviour differences as with the scaled solid laminate cylindrical shell was seen. The axisymmetric modeshape causes a considerable drop in stiffness, which is not seen for the measured imperfection. The drop in buckling load due to the axisymmetric imperfection is considerably higher in comparison the drop in buckling load seen for the measured imperfection, with a 35% difference in buckling loads for an imperfection amplitude of 20% with respect to the thickness.

A sensitivity study of the laminate thickness and cylindrical shell radius was executed, which showed that an increase of the radius should not cause problems for experimental testing. An increase in thickness can cause problems due to an increase of the buckling load, but only when an increase of 7-8% is seen in laminate thickness, which is unlikely to happen.

The maximum strains of the three cylindrical shells at the last increment pre-buckling were investigated to check for material failure. The maximum strains of the CTA 8.1 are high, the maximum strains of the scaled sandwich cylindrical shells are close to material failure, while the scaled solid laminate cylindrical shell has a higher margin with respect to material failure. The scaled cylindrical shells were also used for a failure analysis, for which both cylindrical shells saw failure after buckling.

The general comparison of the CTA 8.1 cylindrical shell and the scaled cylindrical shells saw good agreement, with both scaled configurations resulting as valid options. The first comparison used nondimensional load and displacement. Which showed for the cylindrical shells without imperfection, that the scaled solid laminate cylindrical shell has the highest nondimensional stiffness and a 10.2% higher nondimensional buckling load compared to the CTA 8.1 cylindrical shell, while the stiffness of the scaled sandwich cylindrical shell shows close agreement with the CTA 8.1 cylindrical shell and only a 3.3% difference in buckling load. When the effect of the measured imperfections are compared, the scaled solid laminate cylindrical shell shows the highest stiffness and a nondimensional buckling load which is 28.7% higher compared to the CTA 8.1 cylindrical shell. The scaled sandwich cylindrical shell shows a 12.2% higher nondimensional buckling load in comparison to the CTA 8.1 cylindrical shell, with a stiffness which is in between the scaled solid laminate and CTA 8.1 cylindrical shell. The scaled cylindrical shells using the mandrel imperfection have a knockdown factor of 0.95, which can be expected due to the imperfection being equal. The measured imperfection of the CTA 8.1 cylindrical shell did however show a lower knockdown factor of 0.81. This is most likely due to the larger measured amplitude of the imperfection. The relation between imperfection amplitude and the scale of the cylindrical shell also seems to have an effect. This effect was magnified when the measured imperfections were scaled to 20% with respect to the thickness and compared by nondimensional load and displacement. This comparison showed the opposite in terms of buckling loads with respect to the previous comparison. The CTA 8.1 cylindrical shell showed the highest buckling load, followed by the buckling load of the scaled solid laminate cylindrical shell, which was 8.1% lower, and the buckling load of the scaled sandwich cylindrical shell, which was 16.3% lower. The knockdown factor of the scaled sandwich cylindrical shell was 0.73, while the knockdown factor of the scaled solid laminate cylindrical shell was 0.76. The scaled mandrel imperfection had a larger influence on the scaled solid laminate cylindrical shell than on the scaled sandwich cylindrical shell, while the scaled cylindrical shells showed equal knockdown factors for the measured amplitude.

When the strain contour plots are compared, similarities are seen between the ε_{11} and ε_{22} colour patterns in the contour plots between all three cylindrical shells, while the ε_{12} contour plots show differences in the patterns. The differences are most likely due to the difference in ply orientation of the most critical ply at pre-buckling, which were shown in these contour plots.

The last part of the comparison between the cylindrical shells investigated if a relation could be determined between the structural properties with respect to the imperfection amplitude and the knockdown factor of all cylindrical shell configurations. A trend was seen when the imperfection amplitude was related to the radius and length of the cylindrical shells. It however does require more research into more types of cylindrical shells to determine if the trend is a local trend for these cylindrical shells or not.

The scaled cylindrical shells that were studied in this thesis do show behaviour that is representative of the full scale they were based on. Although differences were observed, the level of similarity that was seen between these scaled structure and their full scale counterpart, was not found in literature. There is still research to be done, as some of the similarities that are seen are not quantified, such as the strain patterns that were compared and the relation between imperfection amplitude and knockdown factor. The certainty behind these conclusions can be strengthened, by adding more full scale and scaled cylindrical shells to the comparison. This would increase the dataset which the conclusions and found relations are based on, next to providing more experience on the analyses of scaled cylindrical shells. This experience can be a valuable asset when these scaled cylindrical shells are used during the design process of launch-vehicle cylindrical shells.

A recommended next step of the research of these scaled cylindrical shells, is to investigate if the results of the scaled cylindrical shells can be used to predict behaviour of the full scale cylindrical shell. This prediction method can then be compared with both the experimental and numerical results of the CTA 8.1 cylindrical shell. This capability of predicting behaviour of full scale cylindrical shell is the major remaining part which will increase the usefulness of knowledge gained by testing scaled cylindrical shells. If such prediction method is developed successfully, it will further increase the certainty of results based on scaled structures and increase the amount of possibilities to use these methods for the design process of launch-vehicle cylindrical shells.

References

[1] Bisagni C. Numerical analysis and experimental correlation of composite shell buckling and post-buckling. *Composites Part B: Engineering*, 2000, 31(8):655–667.

[2] Peterson J.P., Seide P., and Weingarten V.I. Buckling of thin-walled circular cylinders. Technical Report NASA SP-8007, 1968.

[3] Hilburger M. Developing the next generation shell buckling design factors and technologies. In *53rd AIAA/ASME/ASCE/AHS/ASC Structures, Structural Dynamics and Materials Conference 20th AIAA/ASME/AHS Adaptive Structures Conference 14th AIAA*, paper number 1686, 2012.

[4] Uriol Balbin I., Bisagni C., Schultz M.R., and Hilburger M.W. Scaling methodology for buckling of sandwich composite cylindrical structures. In *2018 AIAA/ASCE/AHS/ASC Structures, Structural Dynamics, and Materials Conference*, paper number 1988, 2018.

[5] Schultz M.R., Sleight D.W., Myers D.E., Waters Jr W.A., Chunchu P.B., Lovejoy A.W., and Hilburger M.W. Buckling design and imperfection sensitivity of sandwich composite launch-vehicle shell structures. In *American Society For Composites 2016 Thirty-First Technical Conference*, paper number 3505, 2016.

[6] Degenhardt R. New robust design guideline for imperfection sensitive composite launcher structures. In *3rd CEAS and 21st AIAA Congress*, 2011.

[7] Degenhardt R., Kling A., Bethge A., Orf J., Kärger L., Zimmermann R., Rohwer K., and Calvi A. Investigations on imperfection sensitivity and deduction of improved knock-down factors for unstiffened CFRP cylindrical shells. *Composite Structures*, 2010, 92(8): 1939–1946.

[8] Kepple J., Herath M.T., Pearce G., Gangadhara Prusty B., Thomson R., and Degenhardt R. Stochastic analysis of imperfection sensitive unstiffened composite cylinders using realistic imperfection models. *Composite Structures*, 2015, 126:159–173.

[9] Takano A. Statistical knockdown factors of buckling anisotropic cylinders under axial compression. *Journal of Applied Mechanics*, 2012, 79(5):051004.

[10] Bisagni C. and Alfano M. Probabilistic buckling analysis of sandwich composite cylindrical shells based on measured imperfections. In *58th AIAA/ASCE/AHS/ASC Structures, Structural Dynamics, and Materials Conference*, paper number 0886, 2017.

[11] Cha G. and Schultz M.R. Buckling analysis of a honeycomb-core composite cylinder with initial geometric imperfections. In *51st AIAA/ASME/ASCE/AHS/ASC Structures, Structural Dynamics, and Materials Conference, Structures, Structural Dynamics, and Materials and Co-located Conferences*, paper number 2531, 2013.

[12] Haynie W. and Hilburger M. Comparison of methods to predict lower bound buckling loads of cylinders under axial compression. In *51st AIAA/ASME/ASCE/AHS/ASC Structures, Structural Dynamics, and Materials Conference 18th AIAA/ASME/AHS Adaptive Structures Conference 12th*, paper number 2532, 2010.

[13] Schultz M.R., Sleight D.W., Gardner N.W., Rudd M.T., Hilburger M.W., Palm T., and Oldfield N.J. Test and analysis of a buckling-critical large-scale sandwich composite cylinder. In *2018 AIAA/ASCE/AHS/ASC Structures, Structural Dynamics, and Materials Conference*, paper number 1693, 2018.

[14] Orifici A.C. and Bisagni C. Perturbation-based imperfection analysis for composite cylindrical shells buckling in compression. *Composite Structures*, 2013, 106:520–528.

[15] Castro S.G.P., Zimmermann R., Arbelo M.A., Khakimova R., Hilburger M.W., and Degenhardt R. Geometric imperfections and lower-bound methods used to calculate knock-down factors for axially compressed composite cylindrical shells. *Thin-Walled Structures*, 2014, 74:118–132.

[16] Wagner H.N.R., Hühne C., and Niemann S. Robust knockdown factors for the design of axially loaded cylindrical and conical composite shells − development and validation. *Composite Structures*, 2017, 173:281–303.

[17] Hilburger M.W. and Starnes J.H. Effects of imperfections of the buckling response of composite shells. *Thin-Walled Structures*, 2004, 42(3):369–397.

[18] Hilburger M.W., Nemeth M.P., and Starnes J.H. Shell buckling design criteria based on manufacturing imperfection signatures. *AIAA Journal*, 2006, 44(3):654–663.

[19] Bisagni C. Composite cylindrical shells under static and dynamic axial loading: An experimental campaign. *Progress in Aerospace Sciences*, 2015, 78:107–115.

[20] Bisagni C. Dynamic buckling of fiber composite shells under impulsive axial compression. *Thin-Walled Structures*, 2005, 43(3):499–514.

[21] Bisagni C. and Cordisco P. An experimental investigation into the buckling and post-buckling of CFRP shells under combined axial and torsion loading. *Composite Structures*, 2003, 60(4):391–402.

[22] Bisagni C. and Cordisco P. Testing of stiffened composite cylindrical shells in the post-buckling range until failure. *AIAA Journal*, 2004, 42(9):1806–1817.

[23] Bisagni C. and Cordisco P. Post-buckling and collapse experiments of stiffened composite cylindrical shells subjected to axial loading and torque. *Composite Structures*, 2006, 73 (2):138–149.

[24] Nemeth M.P. *Nondimensional parameters and equations for buckling of symmetrically laminated thin elastic shallow shells.* National Aeronautics and Space Administration, Langley Research Center, 1991.

[25] Nemeth M.P. Nondimensional parameters and equations for nonlinear and bifurcation analyses of thin anisotropic quasi-shallow shells. Technical Publication NASA/TP-2010-216726, 2010.

[26] Schultz M.R. and Nemeth M.P. Buckling imperfection sensitivity of axially compressed orthotropic cylinders. In *Proceedings of the 51st AIAA/ASME/ASCE/AHS/ASC structures, structural dynamics and materials conference. Orlando, FL*, paper number 2531, 2010.

[27] Simitses G.J. and Rezaeepazhand J. Structural similitude for laminated structures. *Composites Engineering*, 1993, 3(7-8):751–765.

[28] Coutinho C.P., Baptista A.J., and Dias Rodrigues J. Reduced scale models based on similitude theory: A review up to 2015. *Engineering Structures*, 2016, 119:81–94.

[29] Rezaeepazhand J. and Simitses G.J. Design of scaled down models for stability and vibration studies. In *Proceedings of 35th AIAA, Structures, Structural Dynamics, and Materials Conference, AIAA paper*, pages 1990–1997, 1993.

[30] Simitses G.J. and Rezaeepazhand J. Structural similitude and scaling laws for buckling of cross-ply laminated plates. *Journal of Thermoplastic Composite Materials*, 1995, 8 (3):240–251.

[31] Rezaeepazhand J., Simitses G.J., and Starnes J.H. Scale models for laminated cylindrical shells subjected to axial compression. *Composite Structures*, 1996, 34(4):371–379.

[32] Tabiei A. and Simitses G.J. Scaled down imperfection sensitive composite cylindrical shells under axial compression and lateral pressure. In *38th Structures, Structural Dynamics, and Materials Conference*, pages 2502–2509, 1998.

[33] Frostig Y. and Simitses G.J. Structural similitude and scaling laws for sandwich beams. *AIAA Journal*, 2002, 40(4):765–773.

[34] Frostig Y. and Simitses G.J. Similitude of sandwich panels with a 'soft' core in buckling. *Composites Part B: Engineering*, 2004, 35(6):599–608.

[35] Rezaeepazhand J. and Yazdi A.A. Similitude requirements and scaling laws for flutter prediction of angle-ply composite plates. *Composites Part B: Engineering*, 2011, 42(1): 51–56.

[36] Coutinho C.P., Baptista A.J., and Dias Rodriges J. Modular approach to structural similitude. *International Journal of Mechanical Sciences*, 2018, 135:294–312.

[37] Luo Z., Zhu Y.P., Zhao X.Y., and Wang D.Y. Determination method of dynamic distorted scaling laws and applicable structure size intervals of a rotating thin-wall short cylindrical shell. 2014, 229(5):806–817.

[38] Zhu Y., Luo Z., Zhao X., and Wang D. The dynamic similitude design of a thin-walled cylindrical shell by considering the strength requirement. *Proceedings of the Institution of Mechanical Engineers, Part G: Journal of Aerospace Engineering*, 2016, 230(2):234–243.

[39] Zhu Y., Wang Y., Luo Z., Han Q., and Wang D. Similitude design for the vibration problems of plates and shells: A review. *Frontiers of Mechanical Engineering*, 2017, 12 (2):253–264.

[40] Luo Z., Zhu Y., Han Q., and Wang D. The dynamic similitude design of a thin-wall cylindrical shell with sealing teeth and its geometrically distorted model. *Advances in Mechanical Engineering*, 2015, 7(2):234–243.

[41] Luo Z., Wang Y., Zhu Y., and Wang D. The dynamic similitude design method of thin walled structures and experimental validation. *Shock and Vibration*, 2016, 2016 (6836183).

[42] Eydani Asl M., Niezrecki C., Sherwood J., and Avitabile P. Vibration prediction of thin-walled composite I-beams using scaled models. *Thin-Walled Structures*, 2017, 113: 151–161.

[43] Asl M.E., Niezrecki C., Sherwood J., and Avitabile P. Experimental and theoretical similitude analysis for flexural bending of scaled-down laminated I-beams. *Composite Structures*, 2017, 176:812–822.

[44] Morton J. Scaling of impact-loaded carbon-fiber composites. *AIAA Journal*, 1988, 26 (8):989–994.

[45] Simitses G.J. and Rezaeepazhand J. Structural similitude and scaling laws for laminated beam-plates. Technical Publication NASA-CR-190585, 1992.

[46] Mixson J.S. and Catherine J.J. *Comparison of Experimental Vibration Characteristics Obtained from a 1/5-scale Model and from a Full-scale Saturn SA-1.* National Aeronautics and Space Administration, 1964.

[47] Brock Jr E.J., Leadbetter S.A., and Leonard H.W. Design and fabrication considerations for a 1/10-scale replica model of the Apollo/Saturn V. Technical Report NASA-TN-D-4138, 1967.

[48] Leadbetter S.A. Application of analysis and models to structural dynamic problems related to the Apollo-Saturn 5 launch vehicle. Technical report NASA TN D-5831, 1970.

[49] Catherines J.J. Experimental vibration characteristics of a 1/40-scale dynamic model of the Saturn 5 launch umbilical tower configuration. Technical Report NASA TN D-4870, 1968.

[50] Levy A., Zalesak J., Bernstein M., and Mason P.W. Development of technology for modeling of a 1/8-scale dynamic model of the shuttle solid rocket booster (SRB). Technical Report NASA-CR-132492, 1974.

[51] Leadbetter S.A., Stephens W., Sewall J.L., Majka J.W., and Barret J.R. Vibration characteristics of 1/8-scale dynamic models of the space-shuttle solid-rocket boosters. Technical Report NASA TN D-8158, 1976.

[52] Blanchard U.J. Experimental investigation of the vibration characteristics of a model of an asymmetric multielement space shuttle. Technical Report NASA TN D-8448, 1977.

[53] Hilburger M., Rose C., and Starnes , Jr J.H. Nonlinear analysis and scaling laws for noncircular composite structures subjected to combined loads. In *19th AIAA Applied Aerodynamics Conference*, paper number 1335, 2001.

[54] Przekop A., Schultz M.R., and Hilburger M.W. Design of buckling-critical large-scale sandwich composite cylinder test articles. In *2018 AIAA/ASCE/AHS/ASC Structures, Structural Dynamics, and Materials Conference*, paper number 1694, 2018.

[55] Kassapoglou C. *Design and analysis of composite structures: with applications to aerospace structures*. John Wiley & Sons, 2013. ISBN 9781118401606.

[56] Hexcel 8552 IM7 Unidirectional Prepreg 190 gsm and 35 percent RC, Qualification Material Property Data Report. *National Institute for Aviation Research, Wichita State University*, 2017.

[57] Abaqus 2017 documentation. *Dassault Systemes Simulia Corp.*, 2017.

[58] Bert C. W. and Reese C. D. Simplified design equations for buckling of axially compressed sandwich cylinders with orthotropic facings and core. *Journal of Aircraft*, 1969, 6(6): 515–519.